

MONDRAGON UNIBERTSITATEA



DOCTORAL THESIS

**SLENDER WORKPIECE CUTTING PROCESS
STABILITY PREDICTION AND MONITORING
BASED ON INTERNAL SIGNALS**

Author:

Xabier Badiola Aiestaran

Supervisors:

Dr. Pedro J. Arrazola Arriola

Dr. Aitzol Iturrospe Iregui

Mondragon Unibertsitatea
Mechanical and Manufacturing Department

December 16, 2019

"A goal without a plan is just a wish."

Antoine de Saint-Exupéry

Abstract

Chatter is commonly found when machining slender components on a lathe due to the low stiffness and damping. Aspects such as accuracy and roughness are usually compromised owing to large variation in stiffness along the length of the workpiece, which is a problem for the machining industry.

The main contributions of this thesis are the proposal of (I) models for determine the chatter-free cutting conditions in slender workpiece machining and (II) a process monitoring system to detect chatter using available internal signals from the regulator.

The clamping of a workpiece in the spindle of a lathe is not completely stiff, so the classical boundary conditions such as clamped-free, are not enough. The natural frequencies of the machine-workpiece system are usually lower than the theoretical ones obtained with classical boundary conditions. As the system is different for each machine and clamping method, it is necessary to characterize them. In order to be industrially feasible, a experimental method based on models with elastic boundary conditions is proposed to identify the system parameters. A exciter tool prototype based on a piezo actuator is developed to excite the system and natural frequencies have been measured by an accelerometer. The system parameters for a specific clamping and machine tool have been identified by means of model updating method. Once the system parameters have been identified, the effective stiffness of the system at each tool position of the workpiece is obtained.

In slender workpieces, two nearby local modes appear due to the clamping, so workpiece chatter may occur by mode coupling in addition to regenerative. The stability of the process for a facing operation has been modelled in the state space

taking into account both phenomena. An eigenvalue analysis is carried out by freezing the physical parameters of the time varying system at each time instant. The stability of the process is determined for certain cutting conditions. The theoretical results are validated by experimental tests.

As the system is variant periodically in time due to the workpiece rotation, a Linear Time Periodic (LTP) stability model for slender workpiece machining has been proposed in order to define the process stability for each cutting condition. The stability is analysed by Floquet theory and the Stability Lobe Diagram (SLD) are obtained.

Finally, the development and validation of a process monitoring system using internal signals available in the Computer Numerical Control (CNC) is presented. The feasibility of different internal signals for chatter monitoring are evaluated. An internal signal based monitoring system is implemented on a fast prototyping generic hardware and the monitoring system is experimentally evaluated in a CNC lathe.

Resumen

El *chatter* se encuentra comúnmente cuando se mecanizan componentes esbeltos en un torno debido a su baja rigidez y amortiguación. Aspectos como la precisión y la rugosidad suelen verse comprometidos debido a la gran variación de la rigidez a lo largo de la pieza de trabajo, lo que constituye un problema para la industria del mecanizado.

Las principales contribuciones de esta tesis son el desarrollo de (I) modelos para determinar las condiciones de corte sin vibraciones en el mecanizado de piezas esbeltas y (II) un sistema de monitorización del proceso para detectar *chatter* utilizando las señales internas disponibles del regulador.

La sujeción de una pieza de trabajo en el husillo de un torno no es completamente rígida, por lo que las condiciones de contorno clásicas, como por ejemplo, viga empotrada-libre, no son suficientes. Las frecuencias naturales son generalmente más bajas que las teóricas obtenidas con las condiciones de contorno clásicas. Como el sistema varía para cada máquina y método de amarre, es necesario caracterizarlos. Para que sea industrialmente viable, se propone un método experimental basado en modelos con condiciones de contorno elásticas para identificar los parámetros del sistema. El sistema ha sido excitado mediante un prototipo de herramienta excitadora basado en un actuador piezoeléctrico y las frecuencias naturales han sido medidas por un acelerómetro. Los parámetros del sistema para un amarre y una máquina herramienta específica han sido identificados mediante el método de *model updating*. Una vez identificados los parámetros del sistema, se ha obtenido la rigidez efectiva del sistema en cada posición de la pieza.

En piezas esbeltas, aparecen dos modos locales cercanos debido al amarre, por lo que el *chatter* de pieza puede ocurrir por acoplamiento de modos además del efecto regenerativo. La estabilidad del proceso para una operación de refrentado ha sido modelada en el espacio de estado teniendo en cuenta ambos fenómenos. El análisis de los valores propios se lleva a cabo congelando los parámetros físicos del sistema en cada instante de tiempo. La estabilidad del proceso ha sido determinada para ciertas condiciones de corte. Los resultados teóricos han sido validados por medio de pruebas experimentales.

Como el sistema es variante periódicamente en el tiempo debido a la rotación de la pieza, se ha propuesto un modelo de estabilidad lineal periódica en el tiempo para el mecanizado de piezas esbeltas, con el fin de definir la estabilidad del proceso para cada condición de corte. La estabilidad ha sido analizada con la teoría de Floquet y ha sido obtenido el diagrama de lóbulos de estabilidad.

Finalmente, se presenta el desarrollo y validación de un sistema de monitorizado de proceso utilizando señales internas disponibles en el regulador. Se evalúa la viabilidad de diferentes señales internas para la monitorización del *chatter*. El sistema de monitorizado ha sido implementado en hardware genérico de prototipado rápido y el sistema de monitorización ha sido validada experimentalmente en un torno.

Laburpena

Oso ohikoa da *chatterra* aurkitzea tornu batean pieza lirainak mekanizatzen direnean, sistemaren zurruntasun eta amortiguazio txikiagatik. Mekanizatzean zehaztasuna oso txikia izan ohi da piezaren zurruntasunaren aldakortasun handiagatik luzeran zehar, eta hori arazo bat da mekanizatu industrian.

Tesi honen ekarpen nagusiak (I) pieza lirainak mekanizatzeako *chatterrik* gabeko ebaketa baldintzak zehazteko modeloak eta (II) erregulatzailan eskuragarri dauden barne seinaleak erabiliz mekanizazio prozesua monitorizatzeko sistema dira.

Tornu baten pieza amarratze sistema ez da erabat zurruna, beraz, gainazaleko baldintza klasikoak, ez dira nahikoak. Maiztasun naturalak orokorrean maiztasun teorikoak baino baxuagoak izan ohi dira. Makina eta amarratze metodo bakoitzerako sistema aldatzen denez, beharrezkoa da horiek identifikatzea. Industrialki bideragarria izan dadin, gainazaleko baldintza elastikoak dituen modeloetan oinarritutako metodo esperimental bat proposatzen da, sistemaren parametroak identifikatzeko. Sistema kitzikatzeko, eragingailu piezoelektriko batean oinarritutako erremienta kitzikagailu prototipo bat garatu da, eta maiztasun naturalak azelerometro baten bidez neurtzen dira. Amarre baterako eta makina-erremienta espezifiko baterako sistemaren parametroak identifikatu dira *model updating* metodoaren bidez. Sistemaren parametroak ezagutu ondoren, sistemaren zurruntasun eraginkorra lortu da piezaren luzeran zehar.

Pieza lirainetan, hurbileko bi modu lokal agertzen dira amarratzearen ondorioz. Beraz, *chatterra*, moduen akoplamenduaren bidez gerta daiteke, birsorkuntza efektuaz gain. Errefrentatze operazio baterako, prozesuaren egonkortasuna modelatu da egoera-eremuan, bi fenomenoak kontuan hartuta. Balio propioak aztertzeke, sistemaren parametro fisikoak izoztu dira une bakoitzean. Ebaketa baldintza jakin

batzuetarako prozesuaren egonkortasuna zehaztu da eta emaitza teorikoak proba esperimentalen bidez baliozkotu dira.

Sistema denboran zehar aldakorra da periodikoki piezaren errotazioarengatik. Horregatik, denboran zehar periodikoa den egonkortasun modelo bat garatu da pieza liraintzako eta haren egonkortasuna Floquet teoriaren bidez aztertu da. Ebaketa baldintza bakoitzerako prozesuaren egonkortasuna zehazteko, egonkortasun lobuluaren diagrama lortu da.

Azkenik, erregulatzailan eskuragarri dauden barne seinaleak erabiliz prozesua monitorizatzeko sistema bat garatu da. *Chatterra* monitorizatzeko barne seinale desberdinen bideragarritasuna ebaluatu da. Barne seinaleetan oinarritutako monitorizazio sistema implementatu da *hardware* generiko batean eta monitorizazio sistema esperimentalki balioztatu da tornu batean.

Acknowledgements

I would like to express my sincere gratitude to my supervisors Pedro Arrazola and Aitzol Iturrospe for the continuous support of my thesis. Their guidance helped me during my research.

I would also like to mention Jose Manuel Abete, for the support during the thesis and Ouyang, for receiving me in Liverpool and sharing his knowledge.

I also express my gratitude to the committee members for accepting to review this dissertation.

I thank my fellow labmates for all the support and fun we have had in the last four years.

Last but not the least, I would like to thank my family and especially to Oihana for supporting me throughout this thesis.

Contents

Abstract	v
Resumen	vii
Laburpena	ix
Acknowledgements	xi
1 Introduction	1
1.1 Motivation	1
1.2 Literature review	4
1.2.1 Machining	4
1.2.2 Process monitoring	5
1.2.3 Chatter vibrations	6
1.2.4 Chatter prediction methods	10
1.2.5 Chatter monitoring strategies	15
1.2.6 Chatter control methods	20
1.3 Conclusions of the literature review	27
1.4 Hypothesis	28
1.5 Objectives	28
1.6 Structure of the document	29
2 Dynamic model of slender workpiece turning operation	31
2.1 Introduction	31
2.2 System model and boundary conditions	34
2.3 Turning operation dynamic model	39
2.3.1 System parameter identification	39

2.3.2	Turning dynamic model	44
2.3.3	Numerical simulation	53
3	Slender workpiece cutting process stability analysis	57
3.1	Introduction	57
3.2	State-Space Model	57
3.3	Stability analysis of the system	61
3.3.1	Analysis of system stability, as a function of cutting speed and tool relative angular position	62
3.4	Experimental results	65
3.4.1	System parameters identification	66
3.4.2	Model Simulation	69
3.4.3	Machining tests	73
4	Stability prediction by LTP model	81
4.1	Introduction	81
4.2	State-Space LTP Model	81
4.3	Stability of a LTP system	84
4.4	Stability limits prediction	88
4.5	Experimental results	92
5	Internal signals based chatter monitoring	95
5.1	Introduction	95
5.2	Feasibility of internal signals	96
5.3	Experimental signal acquisition and comparison	97
5.4	Internal signals based chatter monitoring and control system devel- opment	103
5.4.1	Monitoring system hardware	103
5.4.2	Monitoring system software	104
5.4.3	Human Machine Interface (HMI)	109
5.5	Monitoring system experimental validation	111
5.5.1	Setup	111
5.5.2	Experimental validation test	112

6	Conclusions	119
6.1	Conclusions of the dissertation	119
6.2	Suggestions for future research	120
7	Main contributions and publications	123
	Bibliography	125

List of Figures

1.1	Orthogonal cutting geometry	4
1.2	Artis' process monitoring system (Artis, 2019b)	6
1.3	Okuma's harmonic spindle speed control method (Okuma, 2015)	6
1.4	Primary chatter mechanism for (I) Single Degree of Freedom (SDoF) flexible tool and rigid workpiece, (II) rigid tool and SDoF flexible workpiece, (III) Two Degrees of Freedom (2DoF) flexible tool and workpiece	8
1.5	Chatter regeneration mechanism	9
1.6	Stability lobes diagram	11
1.7	Estimation of cutting forces based on current and position signals (Kakinuma and Kamigochi, 2012)	19
1.8	Estimation of cutting forces based on accelerometer signals and tool displacement Albertelli et al. (2015)	20
1.9	Passive chatter suppression by Tuned Mass Damper (TMD) (Yang et al., 2010)	21
1.10	Passive chatter suppression by TMD (Wang et al., 2010)	22
1.11	Active chatter suppression by Spindle Speed Variation (SSV) (Al-Regib et al., 2003)	23
1.12	Active chatter suppression by limited band force control (Kakinuma et al., 2014)	25
1.13	Active suppression of structural chatter (Munoa et al., 2015)	25
1.14	Chatter suppression methods	26
2.1	Natural frequencies of single-span beams (Blevins, 2015)	33
2.2	Spindle-workpiece model	34
2.3	Spindle-workpiece model with exciter tool support	37

2.4	Prototype description	40
2.5	Prototipo	40
2.6	Accelerometer measurements comparison between exciter tool and impact hammer	41
2.7	Experimental test set-up	42
2.8	Experimental modes frequency vs theoretical model modes frequency	43
2.9	Workpiece model	45
2.10	Workpiece deflection in v direction in a turning operation	54
2.11	Workpiece deflection in w direction in a turning operation	55
2.12	Effective stiffness along the workpiece	55
3.1	2 Degrees of Freedom (DoF) model in orthogonal metal cutting	58
3.2	Surface of function $g(V_c, \alpha)$	62
3.3	A C_1 and C_2 curves, B $g(V_c)_{\min}$ for C_2 curve	63
3.4	A Natural frequencies evolution as a function of V_c for the stable interval, B Natural frequencies evolution as a function of V_c for the unstable interval	65
3.5	Danobat Danumerik CNC lathe	66
3.6	Frequency response function of the workpiece in different angular positions obtained by a hammer impact test	67
3.7	Workpiece mode directions	67
3.8	Evolution of cutting constants with V_c	69
3.9	Natural frequencies as a function of V_c without damping	71
3.10	Natural frequencies as a function of V_c with damping	72
3.11	Time domain simulation considering the regenerative effect	73
3.12	CNC experimental set-up	74
3.13	CNC experimental set-up	75
3.14	Radial and tangential cutting forces	76
3.15	A Tangential cutting forces and B machine-tool accelerations in the frequency domain during unstable/stable machining	76
3.16	Workpiece vibration velocity in the time domain	77
3.17	Workpiece vibration velocity spectrogram	77

3.18	Radial and tangential cutting forces of case study 1	78
3.19	Radial and tangential cutting forces of case study 2	79
4.1	2 DoF model in orthogonal metal cutting	82
4.2	Critical characteristic multipliers for periodic systems: (a) secondary Hopf bifurcation, (b) cyclic-fold bifurcation, and (c) period-doubling bifurcation.(Insperger and Stepen, 2011)	85
4.3	Comparison of SLD obtained from the Linear Time Invariant (LTI) model and the LTP model	89
4.4	Stability lobe obtained from LTP model considering the cutting speed influence	90
4.5	SLD obtained from LTP model considering both cutting speed and rotation speed	90
4.6	Time domain simulation of LTP model	92
4.7	Radial and tangential cutting forces	93
5.1	Sin-Cos and Transistor-Transistor Logic (TTL) encoders	97
5.2	Electrical panel installed signal conditioners	98
5.3	Natural frequency identification with Montronix WLAN BoxNG Kit.	99
5.4	Acceleration signal in frequency domain.	100
5.5	Cutting force signal in frequency domain.	100
5.6	X axis current signal in frequency domain.	101
5.7	X axis voltage signal in frequency domain.	101
5.8	Sin-Cos encoder signal processing.	102
5.9	Encoder signal in frequency domain.	102
5.10	Monitoring system architecture.	103
5.11	cRIO-9039 and I/O modules.	104
5.12	Detection algorithm flow diagram.	106
5.13	Control algorithm flow diagram.	108
5.14	Monitoring system HMI.	111
5.15	Monitoring system validation experimental setup.	112
5.16	Frequency Response Function (FRF) of the experimental set up.	113
5.17	Surface of the workpiece after the test.	114

5.18 Monitoring system validation test. Area . Chatter frequency detected at 283.97 Hz, unstable machining. 115

5.19 Monitoring system validation test. Area B. Chatter frequency detected at 286.84 Hz, unstable machining. 116

5.20 Monitoring system validation test. Area C. Chatter frequency detected at 290,47 Hz, unstable machining. 116

5.21 Monitoring system validation test. Area D. No chatter frequency detected, stable machining. 117

List of Tables

1.1	Chatter stability prediction by SLD proposed in the literature	15
1.2	Chatter monitoring in the literature	17
2.1	Workpiece specifications	42
2.2	Experimentally identified modes with different support positions	42
2.3	Simulation parameters	53
2.4	Simulation parameters	54
3.1	Stability cases	63
3.2	Workpiece parameters	66
3.3	Workpiece modal parameters	68
3.4	Parameters and measuring instruments	69
3.5	Simulation parameters	70
3.6	Test parameters, cutting conditions and measuring instruments	74
4.1	Workpiece parameters	88
4.2	Simulation parameters	91
5.1	Workpiece specifications	112
5.2	Monitoring system configuration	113

Acronyms

2DoF Two Degrees of Freedom

3DoF Three Degrees of Freedom

ADC Analog-to-Digital Converter

AE Acoustic Emissions

BIBO Bounded Input Bounded Output

CNC Computer Numerical Control

DC Direct Current

DDE Delay Differential Equation

DOB Disturbance Observer

DoF Degrees of Freedom

FDM Full Discretization Method

FFT Fast Fourier Transform

FPGA Field-Programmable Gate Array

FRF Frequency Response Function

FTF Frozen Transfer Function

HMI Human Machine Interface

KF Kalman Filter

LPTV Linear Periodic Time Variant

LTI Linear Time Invariant

LTP Linear Time Periodic

LTV Linear Time Variant

MFS Multi-Frequency Solution

MMR Material Removal Rate

MRR Material Removal Rate

OS Operating System

RPM Revolutions per minute

RT Real Time

SDM Semi Discretization Method

SDoF Single Degree of Freedom

SLD Stability Lobe Diagram

SSV Spindle Speed Variation

TMD Tuned Mass Damper

TTL Transistor-Transistor Logic

VSM Variable Speed Machining

WT Wavelet Transform

ZOA Zero Order Approximation

Nomenclature

Symbols

a_i Fitting constant

b Depth of cut (mm)

b_i Fitting constant

c_i Viscous damping (N·s/m)

d Workpiece diameter (mm)

E Young's Modulus (MPa)

F Force (N)

f Natural frequency (Hz)

f_r Workpiece rotation frequency (Hz)

F_a Axial force (N)

F_r Radial force (N)

F_t Tangential force (N)

h Chip thickness (mm)

I Moment of inertia (kg·m²)

J Moment of inertia (kg·m²)

k_c Clamping translational spring (N/m)

k_e Exciter translational spring (N/m)

k_i Stiffness (N/m)

k_s Spindle translational spring (N/m)

K_a Axial cutting constant (N/mm²)

K_c Clamping rotational spring (N·m/rad)

K_r Radial cutting constant (N/mm²)

K_s Spindle rotational spring (N·m/rad)

K_t Tangential cutting constant (N/mm²)

l Workpiece length (mm)

m Mass per unit length (kg)

m_i Effective mass (kg)

m_m Spindle mass (kg)

M Mass (kg)

M_z Workpiece bending moment (N·m)

n Workpiece rotation speed (RPM)

r Workpiece radius (mm)

$u(t)$ Workpiece displacement (m)

V_c Cutting speed (m/min)

x_i Workpiece mode displacement (m)

Vectors

\mathbf{v} Workpiece deformation in x direction (m)

\mathbf{w} Workpiece deformation in y direction (m)

\mathbf{x} Workpiece mode displacement vector (m)

$\boldsymbol{\alpha}$ Modal coordinate vector of x direction

β Modal coordinate vector of y direction

φ Spatial function vector that satisfies the boundary conditions

Matrices

C Viscous damping matrix (N·s/m)

I Identity matrix

K Stiffness matrix (N/m)

O Null matrix

Σ_m Workpiece matrix

Σ_p Cutting process matrix

Φ_p Monodromy matrix or Floquet transition matrix

Greek Symbols

α Tool relative angular position (rad)

α_i Modal coordinate for i th mode of x direction

β Mode direction angle (rad)

β_i Modal coordinate for i th mode of y direction

λ Nondimensional parameter

λ_j Characteristic exponents

μ_j Characteristic multiplier

ω Natural frequency (rad)

ω_r Workpiece angular velocity (rad/s)

Ω Workpiece rotation speed (rad/s)

ρ Material density (kg/m³)

σ Nondimensional parameter

φ_i Spatial function that satisfies the boundary conditions for i th mode

ζ Damping ratio

Chapter 1

Introduction

1.1 Motivation

Machining is the most prevalent manufacturing operation in terms of volume. Machined components are used in almost every type of manufactured product. It has been estimated that machining contributes to approximately 5% of the GDP in developed countries. Spain is the third largest producer and exporter of machine tools in the European Union and the ninth largest in the world. The machine tool sector managed to increase its production by 2.4% in 2018, reaching a turnover of 1731 million euros.

The machine tool industry has evolved over time with the aim of increasing the competitiveness of its machines by reducing costs and increasing the quality of manufactured components (Byrne et al., 1995). The monitoring and automation have been one of the keys to this goal.

In machining, certain dimensional (tolerances) and surface requirements (roughness, material damage, residual stresses) must be fulfilled. Process stability is an important factor in meeting these requirements. Despite the great advances made in the last decades in terms of machining process knowledge, the reality is that in many cases the selection of suitable initial cutting conditions is not achieved on the first attempt. This is due to many reasons, such as the fact that the hypotheses established to determine the cutting conditions are not valid, the influence of machine dynamics or the wear or damage of the tool as it is machined is not contemplated

(Balaji et al., 2006). In addition, optimal conditions may change during machining. Tool wear, generated by thermo-mechanical loads produced during the chip formation process, causes variations in cutting forces, which can contribute to destabilize the process and cause vibrations, that affects the finish of the machined workpiece (Lu and Li, 2013).

When it comes to slender workpieces, the selection of cutting conditions becomes even more complicated. Chatter develops easily when turning slender parts on a lathe because of low stiffness and damping of the system. Also, due to a great variation of the stiffness along the workpiece, the machining accuracy is usually very poor (Rivin and Kang, 1989). In fact, the clamping system for the component is not totally stiff and the consideration of as clamped-free, is not right. Thus, when the relationship between the length and diameter of the workpiece is high, the tailstock is used to improve the stiffness and avoid instability problems. This implies limitations in the geometry of the part and increases machining times. By predicting stability limits, together with process monitoring, machining processes could be optimized, reducing costs and time.

The monitoring of machining processes is a field of research in which intensive work has been carried out in recent decades. The interest in monitoring arises from the advantages of its application:

- Stand-alone production is only possible if there is a method available for monitoring and detecting faults or anomalies in production.
- Monitor tool wear and vibrations to fulfil dimensional tolerances and surface finish requirements.
- Stand-alone production ensures the quality of the components manufactured, reducing labour costs.
- The premature identification of anomalies in the process to prevent unscheduled downtimes, avoiding loss of production time and saving money.

Therefore, the need for supervision of the cutting process arises. To respond to this need, this thesis focuses on (I) the development of models to predict system stability and (II) the real-time monitoring of the process stability using available signals from the regulator.

1.2 Literature review

1.2.1 Machining

Machining is a manufacturing process that includes a set of operations for shaping workpieces by removing material. In machining by chip removal, the material is pulled out with a tool resulting in a chip. The tool generally consists of one or more cutting edges that separate the chip from the workpiece in each revolution. Schematic representations of orthogonal cutting process is shown in Figure 1.1 where V_c is the cutting velocity, b is the depth of cut and h is the chip thickness. F_t and F_f are tangential and feed forces respectively.

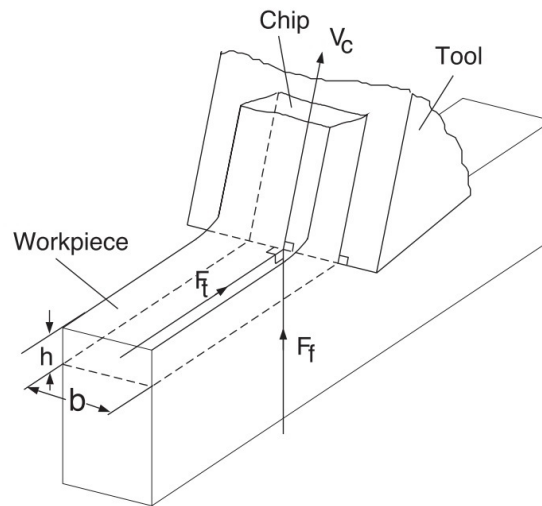


FIGURE 1.1: Orthogonal cutting geometry

Nowadays, Computer Numerical Control (CNC) machine tool are used in machining. These numerically controlled machines offer versatility, high production and preparation capacities, offering the highest precision in the order of microns. The classic machine tools are lathe, drilling machine, broaching machine and milling machine/machining centre.

1.2.2 Process monitoring

The automation of the machining process has been the focus of attention for decades for both the industrial sector and the scientific community due to the competitive advantages it brings. Industrial solutions focus on increasing productivity, improving product quality and reducing costs (Liang et al., 2004). The aim of automating the machining process is twofold: on the one hand, to improve productivity in large batches of work, and on the other hand, to manufacture components with less labour costs, but ensuring the demanded component quality. To achieve these objectives, it is necessary to monitor the machining process. The two main phenomena that destabilize a machining process are tool wear and chatter vibrations. As tool wear increases, cutting forces, vibrations and temperature increase, deteriorating the surface integrity and dimensional finish of the workpiece. Chatter is defined as self-regenerating mechanical vibrations which are caused by (I) tool-to-workpiece friction, (II) thermo-mechanical effects or (III) mode coupling (Siddhpura and Paurobally, 2012).

There are available industrial solutions for monitoring the machining process in real time. Artis (2019a), Montronix (2019a), Okuma (2019) or Omative (2019c) are some of the best-known manufacturers of machining monitoring systems. Most of them focus on tool condition monitoring (Artis, 2019b; Montronix, 2019c; Omative, 2019b). They are versatile systems that allow to add sensors of acoustic emissions, vibrations, power, torque or forces according to the client's needs. The interface of monitoring systems are usually integrated in the CNC. The main function is to monitor the power consumed by spindle. After a few iterations generates a profile with upper and lower limits for a specific workpiece operation protecting the tool from overloads. As tool wear increases, the power consumed by the spindle rises, generating a warning or stop warning in the event of breakage (see Figure 1.2). Montronix (2019b) allow to add accelerometers to detect collisions. Artis (2019b) and Omative (2019a) also have adaptive control functions to improve the performance and shorten cycle times. Okuma (2015) is able to detect chatter and adapt cutting conditions using different sensors as an accelerometer or a microphone (see Figure

1.3). Nevertheless, the integration of sensors in the cutting area often interferes negatively with the process due to the hostile environment.

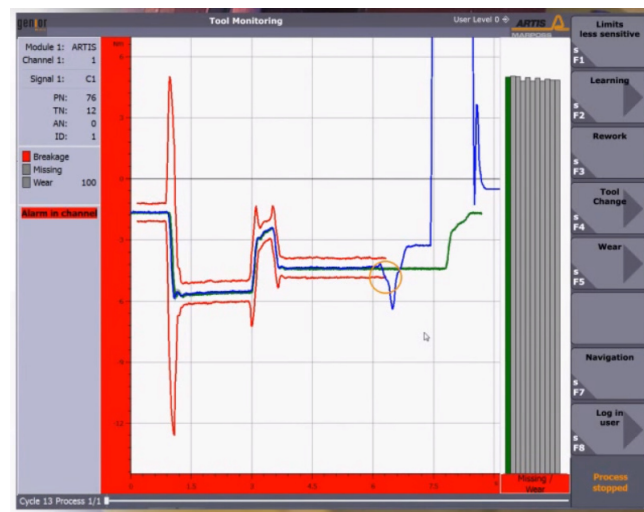


FIGURE 1.2: Artis' process monitoring system (Artis, 2019b)

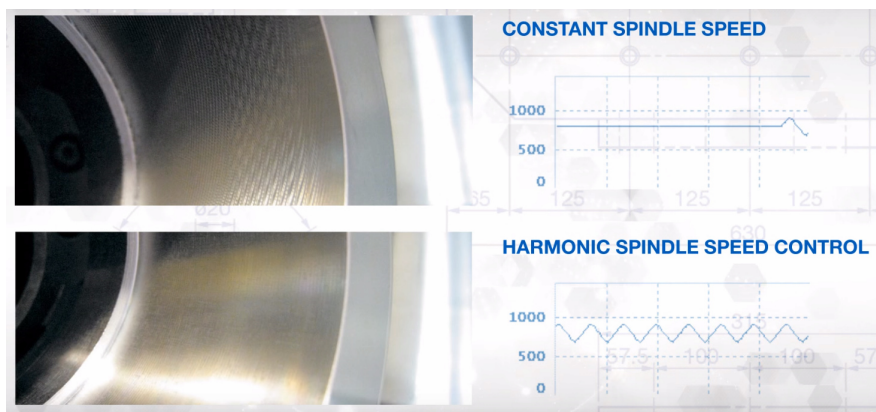


FIGURE 1.3: Okuma's harmonic spindle speed control method (Okuma, 2015)

1.2.3 Chatter vibrations

One of the major challenges for the automating of the machining process are chatter vibrations (Siddhpura and Paurobally, 2012). Chatter vibration arises due to interaction between the machining process and the machine tool structure. Chatter was first identified as a productivity limitation of machining by Taylor (1907). Tobias and Fishwick (1958) and Tlustý and Poláček (1963) found that chatter is caused by instability in the metal cutting processes. It was observed that the modulation of chip

thickness due to vibrations affects the cutting forces dynamically, which in turn increases the amplitude of the vibrations producing a process known as regenerative chatter. They concluded that depth of cut was the key parameter in the stability of the cutting process. Stability limits were proposed based on the dynamics of the system for orthogonal cutting. Analytically demonstrated that, for cutting depths greater than predicted stability limits, the magnitude of the dynamic forces and oscillations increased, producing instability and therefore chatter.

Most research have focused on avoiding chatter by predicting or detecting it early. Research prior to 1990 focused primarily on process parameters such as speed, feed rate and depth of cut in the dynamic models of the cutting process. However, over the last few decades, the influence of process damping, tool wear, tool geometry, machine component stiffness have been incorporated into dynamic machine tool models. Results obtained with these models proved to be more accurate in predicting the stability / instability of the cutting process (Siddhpura and Paurobally, 2012).

In machining processes, three main types of chatter are present: tool chatter, workpiece chatter or machine tool chatter (Tobias, 1961). The tool chatter is the most studied because in most cases the tool is the least stiff part. When the workpiece is the least stiff part, for example in turning slender workpieces, the phenomenon of workpiece chatter arises. Little attention has been paid to chatter vibrations in slender workpiece. Chatter vibrations are also commonly classified into primary and secondary chatter (Wiercigroch and Budak, 2001). The primary is originated by friction between tool and workpiece, thermo-mechanical effects or by coupling of modes. The secondary chatter is caused by the regeneration of the surface waves in the workpiece.

The cutting force can cause deflections in the cutting tool, in the workpiece or both. If the workpiece or the tool is vibrating as it is removing material, these vibrations are imprinted on the workpiece surface as a wavy profile. Figure 1.4 shows different cases ((I) Single Degree of Freedom (SDoF) flexible tool and rigid workpiece, (II) rigid tool and SDoF flexible workpiece, (III) Two Degrees of Freedom (2DoF) flexible tool and workpiece), where the initial impact with the workpiece surface causes to

begin vibrations and the oscillations. The parameters m_i , k_i and c_i are mass, stiffness and damping coefficient respectively.

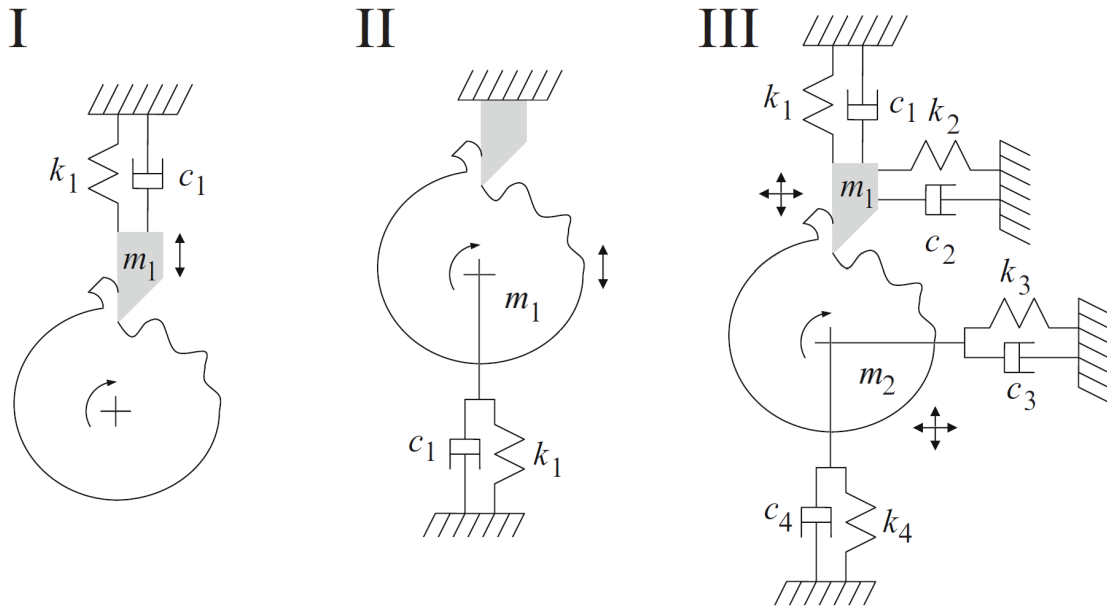


FIGURE 1.4: Primary chatter mechanism for (I) SDoF flexible tool and rigid workpiece, (II) rigid tool and SDoF flexible workpiece, (III) 2DoF flexible tool and workpiece

The regenerative chatter occurs at the frequency of the dominant mode (Altintas, 2012). Excitation in this way causes a relative movement between the machine tool and the workpiece. The time dependent, instantaneous chip thickness, $h(t)$, is determined using Ec 1.1. It is seen that larger positive vibration during the previous revolution, $y(t - \tau)$, where τ is the time for one rotation, gives an increased chip thickness (i.e., less material was removed so the current chip is thicker). Larger positive current vibration, $y(t)$, on the other hand, yields a thinner chip.

$$h(t) = h_m + y(t - \tau) - y(t) \quad (1.1)$$

Figure 1.5 shows the regeneration mechanism between a flexible SDoF tool and a rigid workpiece in orthogonal cutting. The relative phasing between the surface waviness from one pass to the next determines the level of force variation and whether the operation is stable or unstable (chatter). Figure 1.5 show the regeneration mechanism with two possibilities. When $h_1(t) = h_2(t)$, the wavy surfaces

between two revolutions are in phase. Therefore, although vibration is present during material removal, the chip thickness variation (vertical distance between the two curves) is negligible and there is no appreciable force variation. This enables stable cutting at larger chip widths. Considering that the tool tends to vibrate at its natural frequency, it is intuitive that matching the workpiece rotating frequency (spindle speed) to the tool's natural frequency will lead to this preferred "in phase" situation. However, this is counter intuitive based on our traditional understanding of resonance where we avoid driving the system at its natural frequency. When $h_1(t) \neq h_2(t)$, shows a less favorable phase relationship where there is significant variation in the chip thickness. This leads to unstable cutting at smaller chip widths than the previous case due to the force variations and subsequent tool deflections (Schmitz and Smith, 2008).

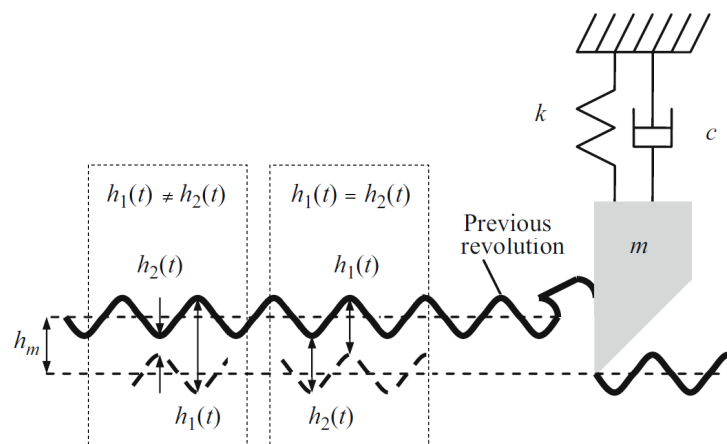


FIGURE 1.5: Chatter regeneration mechanism

While extensive research on regenerative machining chatter has been reported, work on mode coupling chatter is limited (Cen et al., 2018). When a modal coupling occurs, the system vibrates in at least two different directions, and therefore a system with several Degrees of Freedom (DoF) must be analysed (Case III of Figure 1.4). Gasparetto (2001) and Gallina and Trevisani (2003), carried out an analytical study of stability in state space for a wood milling process. They focused on analysing coupled system damping, to improve process stability. Pan et al. (2006) focused on chatter vibrations due to mode coupling in robotic machining process. The research

conclude that if the structure stiffness is not significantly higher than process stiffness, mode coupling chatter occurs previous to the regenerative chatter. Iturrospe et al. (2007) analyzed mode-coupling in the state-space domain for an orthogonal turning process. System stability was analysed and variations of natural frequencies were proposed for monitoring stability, forces and indirectly tool condition. However, the research was focused on tool vibrations. Zhang et al. (2012) and Ji et al. (2018) considered structural mode coupling, regenerative effect and process damping. They concluded that multiple phenomena coexist in the practical milling cases.

The chatter can be recognized by the noise generated by these vibrations and by the tool marks on the cut surface. This has a negative effect on the surface finish of the workpiece. On the other hand, variations in the cutting force due to chatter can lead to tool breakage (Huang 2006). The chatter is often a limiting factor in the Material Removal Rate (MRR), which reduces the productivity of the machine.

1.2.4 Chatter prediction methods

Several analytical methods are proposed in the literature for the prediction and analysis of chatter stability conditions. In most of the cases the stability of the process is represented by Stability Lobe Diagram (SLD) (Siddhpura and Paurobally, 2012).

The most relevant cutting parameter, which is decisive for the generation of chatter in the cutting process, is the depth of cut b (chip width). The cutting process is more stable for lower depth of cut. Above a certain depth, chatter phenomenon occurs. The value of b_{lim} depends on the dynamic characteristics of the structure, the material of the workpiece, the cutting speed, the feed rate, and the geometry of the tool (Tlustý, 1986).

The SLD method can be used for determine chatter free conditions in a turning process. b_{lim} is represented versus rotational speed (N) in the SLD as shown in Figure 1.6.

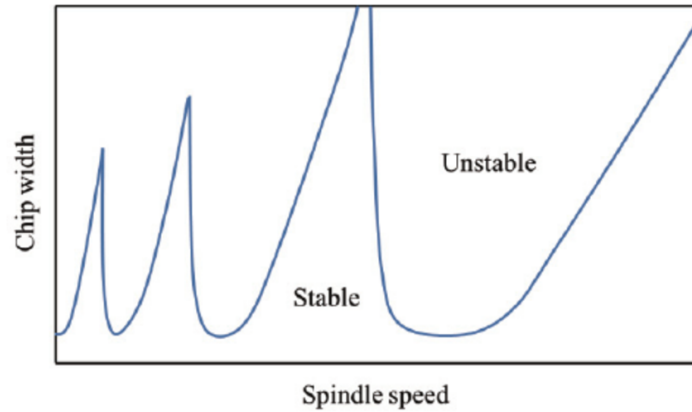


FIGURE 1.6: Stability lobes diagram

Any combination of cutting depth and speed that is below these lobes results in a stable operation (no vibrations) and above these lobes in an unstable operation (chatter). A turning process can be modelled as SDoF, 2DoF or more DoF. In the case of Figure 1.5, this is a flexible SDoF tool in orthogonal cut that is cutting a rigid workpiece. The equation of motion of the dynamic system can be modelled in the feed direction as:

$$m\ddot{x}(t) + c\dot{x}(t) + kx(t) = F_f(t) \quad (1.2)$$

where $F_f(t)$ is the cutting force in feed direction.

To obtain chatter-free cutting parameters, analytical prediction of stability limits is necessary. In most research, the tool is represented by a SDoF mass-spring system that is cutting a rigid part where the cutting force is linear with the process parameters (Case I of Figure 1.4).

Suzuki et al. (2010) compared an analytical SDoF model with another 2DoF model obtaining the same results for regenerative chatter. It was concluded that the 2DoF model is redundant and not useful in understanding the cutting process.

Dombovari et al. (2011) also noted that it is not necessary to create models with two or more DoF as it does not provide better predictions than SDoF models. A simple one degree freedom model provides a fairly accurate prediction of chatter stability for the turning process.

Benardos et al. (2006), Chen and Tsao (2006a), Vela-Martinez et al. (2008), Sekar et al. (2009), and Siddhpura et al. (2017) have considered both the flexibility of the tool and the workpiece in the analysis and prediction of chatter stability. The authors affirm that it is convenient to consider in order to obtain more realistic models that best represent the real system.

Some publications also consider tool wear and process damping in their models. It should be taken into account that tool wear changes the geometry of the tool resulting in a drastic change in the dynamics of the cutting process. Various types of wear occur during the cutting process. The most important are crater wear, flank wear and notch wear (Tlustý, 2000). On the other hand, process damping is a phenomenon that occurs at low speed. Process damping is believed to be influenced by the interference of the relief face of the cutting tool with the waveform traced on the cut surface, with material properties and the relief geometry of the tool. It is important to take into account in the modelling phase, as it significantly affects the stability limit predictions (Siddhpura and Paurobally, 2012).

In most of the above mentioned works, the dynamics of the machine tool structure are described using Linear Time Invariant (LTI) systems, and the effect of vibrations on chip thickness modulation are represented by a delay term in the cutting force model. In this case, the modal parameters of the system can be obtained by experimental modal analysis. As a result, chatter dynamics are formulated using autonomous Delay Differential Equation (DDE).

Lu et al. (2018) presented a chatter prediction model for tailstock supported slender workpiece turning. The model includes the effect of the travelling tool position along the longitudinal direction of the workpiece during machining. The chatter stability was analysed as a Linear Time Variant (LTV) cutting system due the stiffness along the workpiece was location-dependent.

In some cases, as tool chatter in milling or workpiece chatter in turning, the magnitude and direction of cutting forces vary periodically as the tool/workpiece rotates during the process. The self-excited vibrations are described by DDEs with time periodic coefficients that appear in the cutting force model. When coefficients vary

periodically over time, the system is called Linear Time Periodic (LTP). In order to avoid the complexity caused by the periodicity of forces, some strategies were presented. Tlustý and Koenigsberger (2016) approximated the periodic coefficients in the DDE with constants with average values of the periodic coefficients. Others concluded that when the dynamics of a system are slowly varying, the concept of a frozen system makes sense. The frozen system is obtained by freezing the physical parameters of the time varying system at a time instant. The Frozen Transfer Function (FTF) is then defined as the transfer function of the frozen system (Zadeh, 1951; Louarroudi et al., 2012).

According to Floquet theorem for LTP systems, the system is stable if all of its characteristic multipliers are located inside the unit circle on the complex plane (Insperger and Stepan, 2011). However, delayed systems have infinite number of characteristic multipliers, and generally the characteristic equation cannot be expressed in closed-form. Therefore, determining the stability of the periodic delayed systems analytically is challenging. Numerical and semi-analytic methods, both in time and frequency domain, have been presented to determine system stability.

Time domain methods use various approaches to obtain a finite dimensional approximation of the state transition matrix of the system, the eigenvalues of which determine the stability of the system. For example, Insperger et al. (2003) and Bayly et al. (2003) used Temporal Finite Element Approximation, Butcher et al. (2004) used Chebychev polynomial expansion, Semi Discretization Method (SDM) was used in Insperger and Stépán (2002) and Insperger et al. (2003), and Ding et al. (2010) used Full Discretization Method (FDM) to approximate the state transition matrix.

Frequency domain approaches use Hill's infinite determinant method to approximate the characteristic equation of the system (Magnus and Winkler, 1976). Minis and Yanushevsky (1993) were among the first researchers to implement Hill's infinite determinant method to approximate the characteristic equation of a 2DoF model of milling dynamics. Having obtained the characteristic equation, they used the Nyquist criterion to determine the stability of vibrations.

Budak and Altintas (1998) also used a similar approach to present a frequency domain method known as the Multi-Frequency Solution (MFS) for chatter in milling. They modelled the tool and the workpiece using multiple DoF LTI systems and consequently used the Frequency Response Function (FRF) matrices of the tool and the workpiece to represent their dynamics in the DDE. The periodic coefficients associated with milling forces were approximated using Fourier series. They showed that in most practical applications, the average term in Fourier series is enough to obtain accurate estimations of the stability of the system. When only the average term is used in MFS, the method is referred to as Zero Order Approximation (ZOA).

The Table 1.1 summarizes the researches on chatter stability prediction by SLD proposed in the literature.

The main disadvantage of the SLD method is that the slightest variation in machine tool, workpiece or tool geometry changes the results so it is difficult to apply in industry.

Apart from model-based analytical methods, experimental methods can be used for both predicting chatter stability and detecting chatter in-process. Some experimental methods are used to predict chatter stability by producing system SLD by repeating tests in each condition. This method is very time consuming because it is necessary to perform a large number of experimental tests with different conditions and several repetitions to obtain a reliable SLD.

TABLE 1.1: Chatter stability prediction by SLD proposed in the literature

Models	References
Based on number of DoF	Tobias and Fishwick (1958); Tobias (1961); Merritt (1965); Hanna and Tobias (1974); Tlusty (2000); Altintas and Weck (2004); Chandiramani and Pothala (2006); Budak and Ozlu (2007); Ozlu and Budak (2007); Dassanayake and Suh (2008); Suzuki et al. (2010); Dombovari et al. (2011)
Considering tool and workpiece flexibility	Benardos et al. (2006); Chen and Tsao (2006a); Chen and Tsao (2006b); Vela-Martinez et al. (2008); Sekar et al. (2009); Budak et al. (2012); Yue et al. (2017); Siddhpura et al. (2017)
Considering tool wear / process damping	Sisson (1969); Wu (1989); Elbestawi et al. (1994); Lee et al. (1995); Chiou and Liang (1998); Clancy and Shin (2002); Fofana et al. (2003); Altintas et al. (2008b); Budak and Tunc (2010); Kurata et al. (2010); Ahmadi and Ismail (2011); Tunc and Budak (2012); Ahmadi and Ismail (2012b); Tyler and Schmitz (2013); Jin and Altintas (2013); Ahmadi and Altintas (2014); Wan et al. (2015); Yaser et al. (2017); Li et al. (2017)
LTP system	Minis and Yanushevsky (1993); Budak and Altintas (1998); Bayly et al. (2003); Insperger et al. (2003); Altintas et al. (2008a); Ding et al. (2010); Ahmadi and Ismail (2012a); Guo et al. (2014); Urbikain et al. (2015); Mohammadi and Ahmadi (2019)

1.2.5 Chatter monitoring strategies

Technically, chatter stability prediction cannot completely eliminate chatter occurrence in practice. Hence, machining process monitoring becomes necessary. Chatter monitoring by experimental methods has been proposed by signals of force, displacement, acceleration, sound, motor currents or Acoustic Emissions (AE) generated in the machining process. In most investigations these signals come from external sensors. The internal signals provided by the machine's regulators, such as

encoders and head consumptions, present advantages fundamentally in terms of cost and can provide useful information for monitoring. In addition, any new sensors installed may also be subject to sensor failure (Jun et al., 2002; Iturrospe et al., 2012).

Thusty and Andrews (1983) reviewed several sensors and their capabilities for chatter detection and tool breakage detection in machining processes in order to develop an autonomous machining centre. Forces, vibrations and acoustic sensors were used in turning and milling tests. It is concluded that force signals are the most suitable for chatter detection compared to vibration signals.

In the respect of signal processing techniques for detecting chatter, Heyns (2007) analysed different processing methods and concluded that, usually, the most used method is to determine a magnitude threshold value in the time domain or the frequency domain. It was concluded that time-frequency domain methods such as Wavelet Transform (WT) have greater capabilities that have not yet been fully exploited. Zhu et al. (2009) argue that time domain methods are the most commonly used in monitoring, but that through these methods some of the information is lost. They claim that WT has great potential in detecting abrupt changes in tool conditions because it is robust and insensitive to changes in working conditions.

In the Table 1.2 it can be observed that most scientific publications are based on cutting forces and vibrations for chatter monitoring.

TABLE 1.2: Chatter monitoring in the literature

References	Forces	Vibrations	AE	Current	Sound	Displacement
Soliman and Ismail (1997)				x		
Chiou and Liang (2000)			x			
Dimla and Lister (2000)	x	x				
Clancy and Shin (2002)		x				
Altintas and Weck (2004)	x	x				x
Budak and Ozlu (2007)		x	x			
Ozlu and Budak (2007)		x				
Altintas et al. (2008a)	x	x				
Kebdani et al. (2008)	x	x				
Sekar et al. (2009)	x	x				
Eynian and Altintas (2009)		x			x	
Suzuki et al. (2010)						x
Kurata et al. (2010)					x	
Liu et al. (2011)				x		
Bhuiyan et al. (2012)			x			
Siddhpura and Paurobally (2013)	x	x			x	
Hynynen et al. (2014)		x			x	x
Lamraoui et al. (2014)		x			x	
Urbikain et al. (2015)		x			x	
Zhang et al. (2016)	x					
Cao et al. (2017)					x	
Aslan and Altintas (2018)				x		
Caliskan et al. (2018)		x				

It should be noted that force and vibration measurements require relatively expensive instrumentation, such as dynamometers and accelerometers, which sometimes makes it difficult to implement them in an industrial environment. Dynamometers, for example, are sensitive to overloads and shocks. In addition, they need to be calibrated periodically. Other less used signals, such as motor currents, are available at the CNC and make them more suitable to implement in the industry as neither interfere with machining nor require additional cost.

Due to the cost and limitations of the sensors, scientific publications propose virtual sensing techniques, also called soft sensing. Virtual sensors are used to provide feasible and economical alternatives to costly or impractical physical measurement instruments. Accuracy is usually lower than in direct methods, but they are more flexible for industrial solutions. They require more complex post-processing of signals and extraction of features to correlate the information of interest in the process. These methods make it possible to avoid additional sensors and propose a solution in cases where it is not possible to install them. The application of observers for the estimation of cutting forces has been proposed in several recent publications.

Shinno et al. (2003) presented a cutting force monitoring system based on a Disturbance Observer (DOB), for ultra-precision micro machining. It is based on power consumption signals and head position for the estimation of cutting forces. The prototype in which the system was validated consisted of a linear brushless Direct Current (DC) motor with aerostatic guides and a laser interferometer with a resolution of 0.63nm. In industrial environments the motors are not usually linear and the position accuracy is more limited.

Kurihara et al. (2009) propose a robust cutting force control system. They applied a DOB based on consumed currents and head speed for force estimation. The system was validated in a prototype milling laboratory consisting of a small DC motor, an encoder and two guides. Forces in the range of 0-5N were used in the experimental tests.

Kakinuma and Kamigochi (2012) proposed force estimation using DOB in micro machining. They obtain a sensitivity of 0.1 N (see Figure 1.7) in their estimates based on current signals and head position.

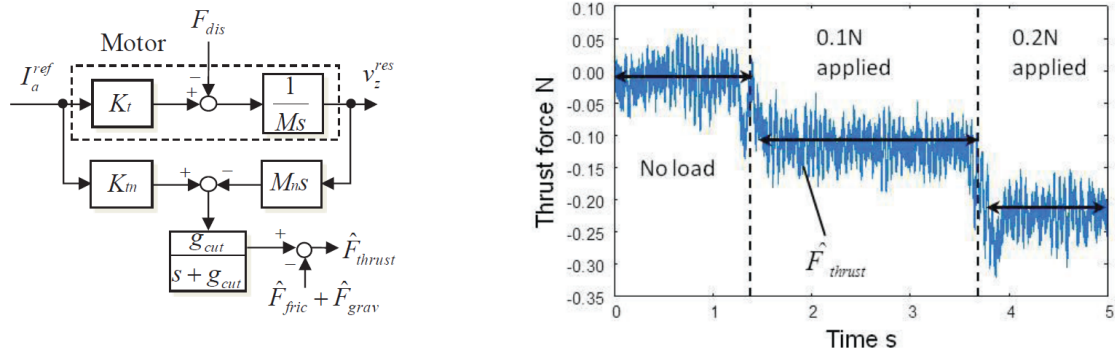


FIGURE 1.7: Estimation of cutting forces based on current and position signals (Kakinuma and Kamigochi, 2012)

Annotated publications are based on laboratory set-up with linear and low power motors in specific conditions far from industrial conditions. Albertelli et al. (2015) proposed the Kalman Filter (KF) as an observer to estimate cutting forces in milling. To carry out the force estimation, they use accelerometer sensors and displacement of the tool in its development (see Figure 1.8).

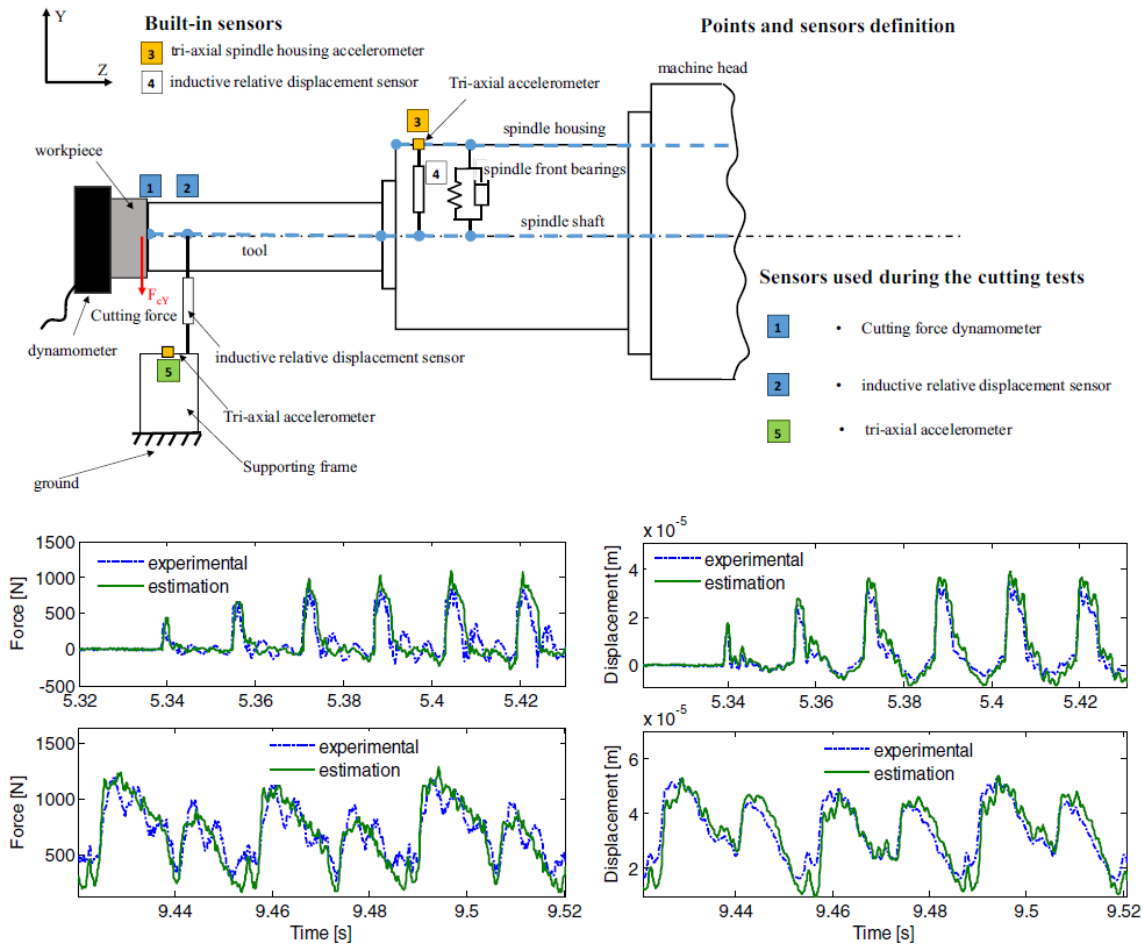


FIGURE 1.8: Estimation of cutting forces based on accelerometer signals and tool displacement Albertelli et al. (2015)

Revised publications above propose the use of observers to estimate cutting forces. The application of observers requires prior knowledge of the system. The robustness of the observer will depend on the model of the system used. An observer can be used to estimate system parameters, status variables or disturbances. The condition for its application is that the system is observable (Jalali et al., 2006).

1.2.6 Chatter control methods

The potential of adaptive control goes beyond improving productivity. Adaptive control is a control method used to adapt parameters according to system behaviour. Adaptive capability can be used to correct phenomena such as chatter. In the literature, chatter suppression methods are classified as passive and active.

In passive methods, the goal is to suppress chatter by changing the behaviour of the system. The behaviour of the system can be changed or modified by improving the design of the machine tool or by using additional devices that can absorb extra energy or interrupt the regenerative effect (Quintana and Ciurana, 2011). These additional devices generally have less rigidity and are capable of damping, reducing and controlling the chatter. Vibration dampers, friction dampers, mass dampers or Tuned Mass Damper (TMD) are some of the most common devices added to the machine for passive chatter suppression.

Yang et al. (2010) proposed optimizing the actual negative part of the FRF of the tool-piece by attaching passive mass dampers to the machine structure improving the stability of the turning process (see Figure 1.9).

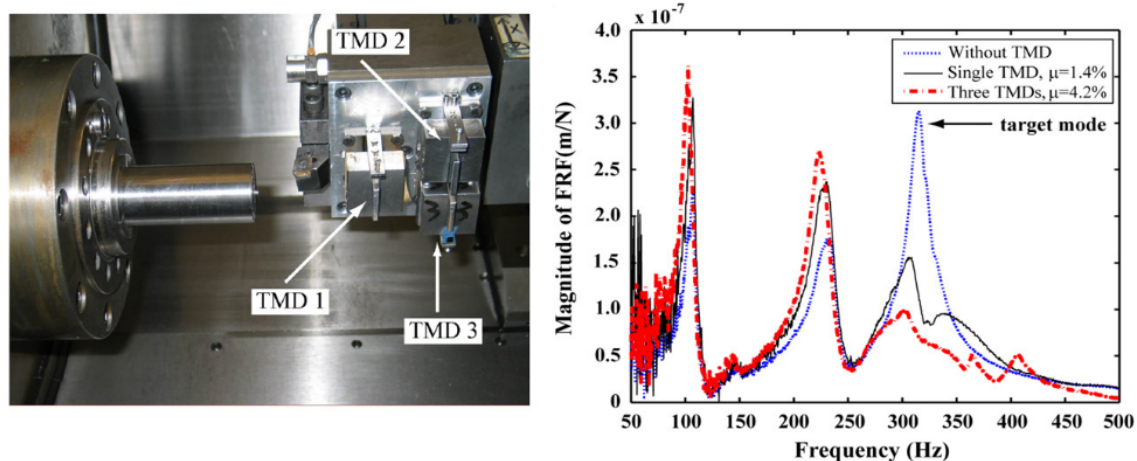


FIGURE 1.9: Passive chatter suppression by TMD (Yang et al., 2010)

Wang et al. (2010) proposed a new non-linear TMD capable of absorbing energy through sliding friction and vibration of its own mass by eliminating the chatter in a turning process. The new non-linear TMD improved the stable limit depth of cut by 150-180 % compared to the non-damped system (see Figure 1.10). The TMD reduces the natural frequency of 300 Hz of the system and increases the limiting cutting depth so that the process is stable.

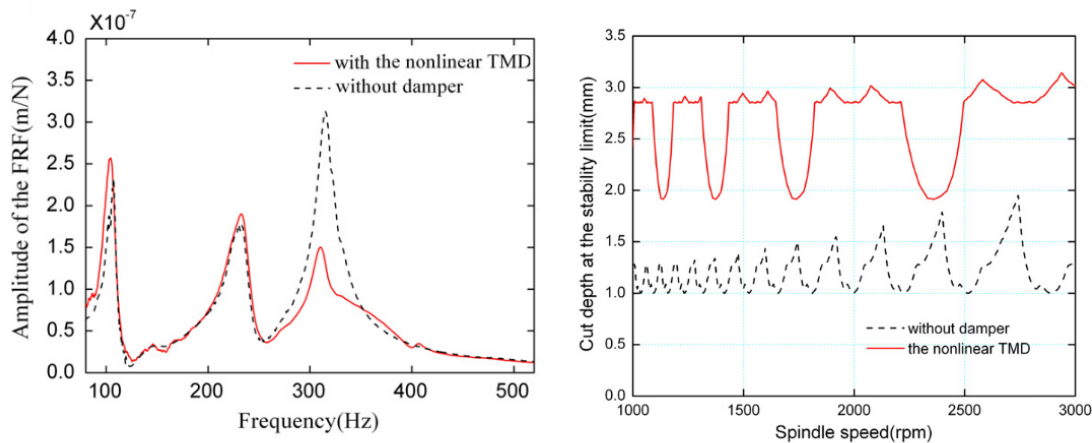


FIGURE 1.10: Passive chatter suppression by TMD (Wang et al., 2010)

Passive vibration suppression methods have numerous advantages, such as easy implementation, low cost and no need for external energy. However, passive dampers require very precise adjustment, which is difficult due to uncertainties in the machine tool structure and in the cutting process. In addition, they require periodic calibration.

In active chatter suppression methods, chatter vibrations are actively eliminated by continuous monitoring and diagnosis of the process and execution of necessary process changes. Adaptive control come into play in these methods. Some researchers use techniques that adapt process parameters such as speed, feed and cutting depth in real time to interrupt the chatter regenerative effect. Lin and Hu (1992) proposed an approach in which the advance and head speed were varied to suppress chatter.

Frumusanu et al. (2013) introduced an intelligent stability control system for turning. This system performed continuous monitoring of the cutting forces while a dedicated control took care of making the right decisions regarding the adjustment of the part's rotational speed. The process chatter was successfully avoided. However, the experiments were conducted in a laboratory environment and the system need to be validated in an industrial environment.

Another active technique for chatter suppression is Spindle Speed Variation (SSV), where the rotational speed is continuously varied, breaking the regenerative effect. This method of continuous modulation of the head speed is attracting more and more attention due to its simplicity and effectiveness in suppressing chatter.

Al-Regib et al. (2003) developed a systematic procedure for the optimal selection of amplitude and frequency for SSV in a turning process. A sinusoidal SSV was used to alter the regenerative vibration mechanism. The proposed criterion for selecting the sinusoidal frequency is based on how fast the regenerative energy is dissipated from the machining system. The Figure 1.11 shows that when SSV is applied the amplitude of the acceleration signal decreases and the surface finish improves.

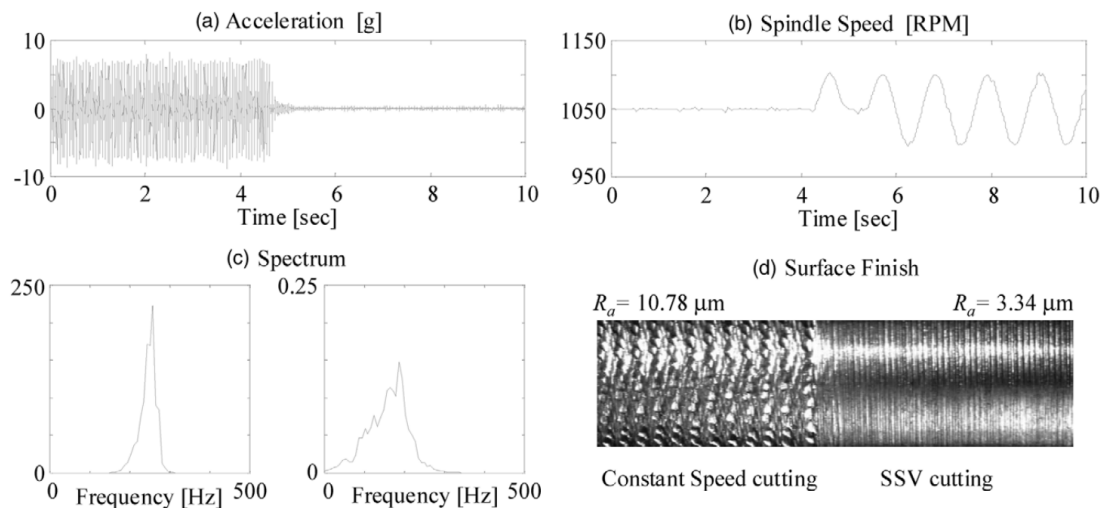


FIGURE 1.11: Active chatter suppression by SSV (Al-Regib et al., 2003)

In industrial applications, SSV method is very effective, but energetically inefficient. This method requires an over sizing of the machine head motor due to the torque needed to overcome the inertia of the spindle.

Wu et al. (2009) applies the Variable Speed Machining (VSM) technique to increase the stability of the non-circular turning process. The cutting tool is driven by a very fast servo that dynamically varies the cutting depth by adaptive control. A closed loop dynamic model involving strong dynamic feedback between the machining process and the fast tool servo was developed.

Pan and Su (2001) introduced a piezoelectric actuator mounted on a tool holder for chatter suppression. The actuator regulates the movement of the tool with a robust adaptive control. It was claimed that the technique significantly reduced chatter phenomena.

Xiao et al. (2002) presented a method for suppressing chatter by applying vibration cutting. Vibratory cutting was found to be more stable than conventional cutting as it suppresses chatter vibration by breaking the regenerative effect.

Chiou et al. (2003) used active electrostatic and piezoelectric spindle bearing support to modify the FRF and modal properties of the structure to suppress chatter.

Ganguli et al. (2005) proposed an active damping strategy with an actuator for the stabilization of regenerative chatter. The effect of active damping on regenerative chatter instability was demonstrated through a mechatronic simulator for a turning operation. It was concluded that the active damping by velocity feedback does not require a very precise model of the structure and can be focused as a broadband vibration control strategy. They observed that different spindle speeds cause changes in the damping system, resulting in different stability limits (Ganguli et al., 2007). For this reason, an active damping strategy was proposed by means of adaptive control with speed feedback.

Chen and Knospe (2007) presented three adaptive control strategies for chatter suppression for the turning process: independent speed control, specified speed control and speed interval control. An active magnetic bearing was used to maximize the damping effect and improve the stability of the cutting process.

Kakinuma et al. (2014) propose a limited band force control system based on DOB to actively suppress chatter vibrations. This system allows a higher chatter free limit cutting depth compared to conventional position control. The authors employ a laboratory prototype under favorable conditions using a DC linear motor and aerostatic bearings, so that there are no frictional forces in the system. The Figure 1.12 shows that the cutting forces are stabilized and the surface finish of the part improves when the control is applied.

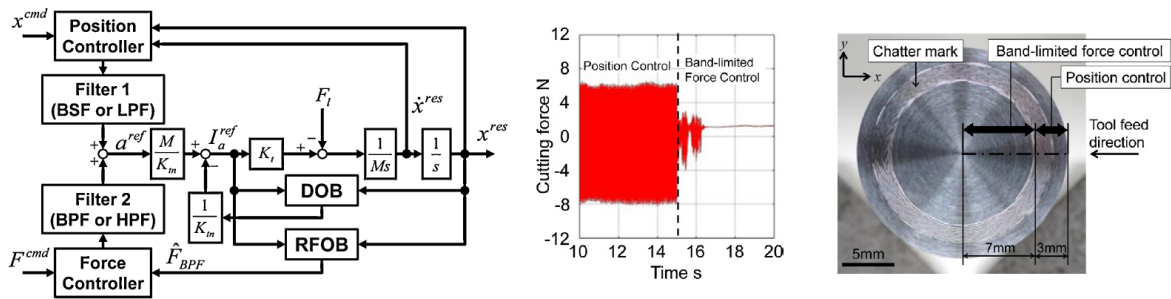


FIGURE 1.12: Active chatter suppression by limited band force control (Kakinuma et al., 2014)

Munoa et al. (2015) proposed a structural chatter suppression method, capable of actively damping the structural modes of a large machining centre using only its own machine advance drives and low-cost accelerometers. A Multiple Input/Output Model (MIMO), based on experimental frequency response measurements, was developed in order to apply active damping by means of a robust controller. Experimental validation shows that the proposed strategy can increase productivity between 85 and 600 % by suppressing structural chatter. Figure 1.13 shows the experimental configuration used and how it reduces the natural frequency of 40 Hz by active damping.

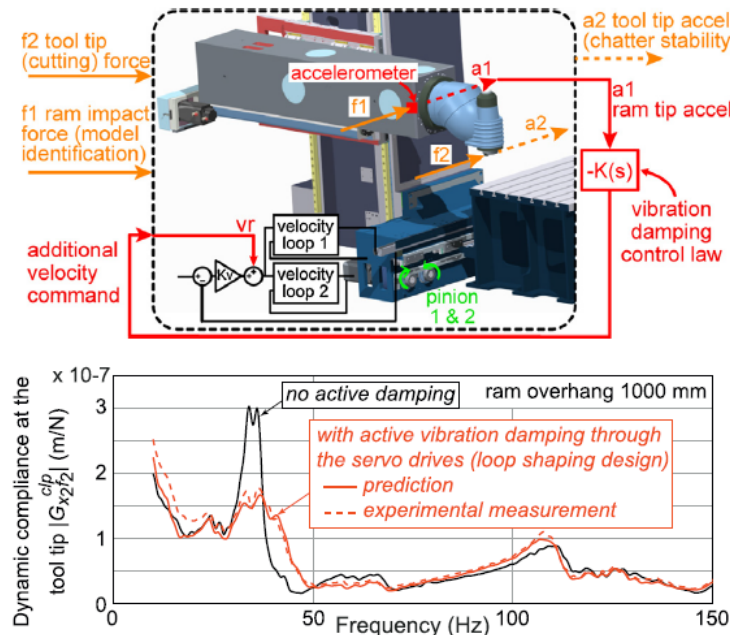


FIGURE 1.13: Active suppression of structural chatter (Munoa et al., 2015)

The reviewed active chatter suppression proposals can be divided into three groups:

- Control methods based on available signals from the regulator and suppress the chatter using the machine actuators. They do not require additional sensors. This approach can only deal with low-frequency structural chatter up to around 50 Hz.
- Control methods based on accelerometers signals and damp the chatter using the machine actuators. This approach allows higher frequency chatter to be detected, but it is limited by the dynamics of the chatter damping system.
- Control methods based on accelerometer signals and using piezoelectric actuators for chatter damping. These methods require installation of sensors and modification of actuators. This approach allows detecting and damping high frequency chatter.

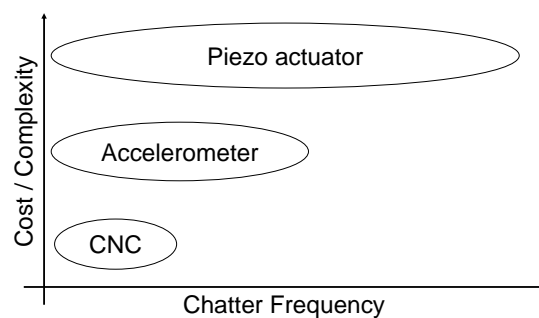


FIGURE 1.14: Chatter suppression methods

The requirements for active chatter control systems hardware (piezo actuators, magnetic bearings...) and software (complex control systems, very fast control loops...) are more expensive compared to passive systems. The performance of both active and passive chatter suppression methods depend above all on the correct tuning of parameters. Passive control methods never lead the controlled system to instability, while active control methods can cause the system to become unstable. Due to significant advances in electronic control, future chatter suppression methods should be a fusion between passive and active methods, where they are applied simultaneously to control the chatter.

1.3 Conclusions of the literature review

Despite the wealth studies in the literature about chatter little attention has been paid to chatter vibrations in slender workpiece turning operations where the workpiece is less rigid than the tool. To the best of my knowledge, the few studies about slender workpiece chatter focus only on regenerative chatter and underestimate the mode coupling effect. A cutting model focused on workpiece chatter considering multiple phenomena has not been proposed yet. This remains a problem today.

On the other hand, most of today's industrial solutions focus on tool monitoring and are based on energy consumption. For other functions, such as chatter detection, industrial solutions are based on accelerometer signals or external microphones that often interfere with machining.

According to the literature, the cutting forces are the most suitable for monitoring due to the extensive information they carry about the process, and therefore they are the most used in investigations. At the same time, the sensors to measure the cutting forces, the dynamometers, are the least indicated to use them in an industrial environment, due to the inconveniences and limitations that they present:

- Assembly limitations
- System stiffness is altered
- Limited measuring ranges
- Fragility against overloads and blows
- Periodic calibration required

Indirect measurement are an effective alternative to this issue. Revised research on indirect measurement techniques has been validated within controlled environments and small-scale prototypes. There is a lack of research focused on implementation and validation in industrial environments. A monitoring system for chatter based on regulator internal signals as currents, voltages or encoder signals has not been proposed yet to the best of our knowledge.

As far as chatter suppression methods are concerned, the SSV method stands out for its effectiveness for turning. On the other hand, piezoelectric actuators or magnetic bearings for chatter compensation are still in the laboratory prototype stage. They are expensive solutions and require complex controls, not suitable for today's industry.

1.4 Hypothesis

The hypothesis of this dissertation is,

Slender workpiece cutting process stability can be (I) predicted by a model and (II) monitored based on available internal signals from the regulator.

1.5 Objectives

The main objective is to (I) predict and (II) monitor the stability of slender workpiece cutting process. The operational objectives to achieve this main objective will be:

- To identify the machine-workpiece-process joint system.
- To analyse the stability of slender workpiece cutting process.
- To predict chatter-free cutting conditions for slender workpiece cutting process based on models.
- To develop a process monitoring system based on available internal signals from the regulator.

1.6 Structure of the document

The rest of the document is organized in four main chapters and a final one with the conclusions, which are detailed below:

Chapter 2 is focused on the identification of the machine-workpiece-process joint system. System parameters are identified by modal updating and turning operation dynamics are simulated.

Chapter 3 presents a slender workpiece cutting state-space model. The cutting process stability and its natural frequencies are analysed. The theoretical results are validated by experimental tests in a CNC lathe.

Chapter 4 proposes a LTP stability model for slender workpiece machining. SLDs are obtained to determine the chatter-free cutting conditions and theoretical results are validated against the experimental results.

Chapter 5 is focused on the development and validation of a process monitoring system. The viability of different internal signals for chatter monitoring are evaluated. Then, a monitoring system is developed on a fast prototyping generic hardware. In addition, the monitoring system is experimentally validated in a CNC lathe.

In **Chapter 6**, the main conclusions of this thesis are presented and some future research guidelines are suggested.

Chapter 2

Dynamic model of slender workpiece turning operation

2.1 Introduction

A lathe with a workpiece attached to the spindle can be modelled using the beam equation of motion. The usual first step is to determine the natural frequencies and mode shapes of the structure. These results characterize the basic dynamic behaviour of the structure and are an indication of how the structure will respond to dynamic loading. The natural frequencies of a structure are the frequencies at which the structure naturally tends to vibrate if it is subjected to a disturbance. Mode shape is the deformed shape of the structure at a specific natural frequency of vibration. Each mode shape is associated with a specific natural frequency.

Natural frequencies and mode shapes are functions of the structural properties and boundary conditions. A cantilever beam has a set of natural frequencies and associated mode shapes. If the structural properties change, the natural frequencies change, but the mode shapes may not necessarily change. For example, if the elastic modulus of cantilever beam is changed, the natural frequencies change but the mode shapes remain the same. If the boundary conditions change, then both the natural frequencies and mode shapes both change.

The four classical boundary conditions at the ends of a beam are (1) free boundary, which bears no load; (2) pinned, which allows rotation but not displacement; (3) guided, also called sliding, which allows displacement but not rotation; and (4) clamped, which allows neither rotation nor displacement.

For a cantilever beam, according to Bernoulli–Euler theory, the system is described as follow for the case of normal modes,

$$\frac{d^4W}{d\bar{x}^4} - \frac{m}{EI}\omega^2W = 0 \quad (2.1)$$

The solution of Eq. (2.1) is:

$$W(x) = A \cos \lambda x + B \sin \lambda x + C \cosh \lambda x + D \sinh \lambda x \quad (2.2)$$

where

$$x = \frac{\bar{x}}{L}, \quad \lambda^2 = \sqrt{\frac{m}{EI}} 2\pi f L^2 \quad (2.3)$$

where E is modulus of elasticity of the beam, f is the natural frequency of the beam, I is the area moment of inertia, L is length of the beam, m is mass per unit length of the beam, x is the axial coordinate, λ is a non dimensional parameter, and A , B , C , and D are constants. The value of λ can be found from any beam boundary conditions.

A workpiece attached to a spindle of a lathe could be modelled as a clamped-free beam or clamped-pinned if the tailstock is used. Based on this assumption, the dominant vibration frequency for a slender workpiece and its mode shape would be obtained as follows (Blevins, 2015):

$$\text{Natural Frequency, } f_i = \frac{\lambda_i^2}{2\pi L^2} \sqrt{\frac{EI}{m}}, \quad i=1,2,3\dots \text{ Hertz}$$

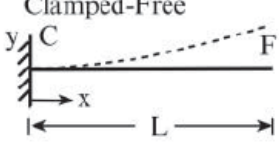
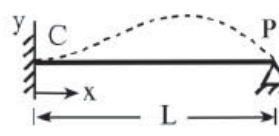
Boundary Conditions	$\lambda_i, i=1,2,3.$	Mode Shape, $\tilde{y}_i(\lambda_i x / L)$	$\sigma_i, i=1,2,3.$
	1.87510407 4.69409113 7.85475744 10.99554073 14.13716839 $(2i-1)\pi/2, i>5$	$\cosh \frac{\lambda_i x}{L} - \cos \frac{\lambda_i x}{L}$ $-\sigma_i \left(\sinh \frac{\lambda_i x}{L} - \sin \frac{\lambda_i x}{L} \right)$ $\approx 2.1[1 - \cos(\pi x / 2L)], i=1$	0.734095514 1.018467319 0.999224497 1.000033553 $\approx 1 \text{ for } i > 5$
	3.92660231 7.06858275 10.21017612 13.35176878 16.49336143 $(4i+1)\pi/4, i>5$	$\cosh \frac{\lambda_i x}{L} - \cos \frac{\lambda_i x}{L}$ $-\sigma_i \left(\sinh \frac{\lambda_i x}{L} - \sin \frac{\lambda_i x}{L} \right)$ $\approx 105^{1/2} \left(\frac{x^2}{L^2} - \frac{x^3}{L^3} \right), \text{ for } i=1$	1.000777304 1.000001445 1.000000000 $\approx 1 \text{ for } i > 3$

FIGURE 2.1: Natural frequencies of single-span beams (Blevins, 2015)

where σ is a non dimensional parameter.

Inevitably, there always exist some differences between a real structure or machine and the theoretical model due to the assumptions used in the development of the mathematical model and inaccurate structural properties used in the model. For analysing the dynamic characteristics of the workpiece which is more or less elastically supported, classical boundaries such as clamped-free, are not enough (Lv et al., 2015). The real structure is a joint system where the machine is involved and should be taken into account. Performing a modal analysis, the first natural frequency will not correspond to the theoretical frequency of a clamp-free beam. The natural frequency is usually lower due to the fact that (I) the clamping is not completely stiff and to (II) the influence of the spindle.

In this chapter a slender workpiece machining process is modelled taking into account the influence of cutting process, the spindle and the workpiece-chuck clamping. System parameters are identified by modal updating and turning operation dynamics are simulated.

2.2 System model and boundary conditions

According to the characteristics of the rotating workpiece system, it can be modeled as shown in Figure 2.2. The workpiece itself is represented by a rotating Rayleigh beam, while the spindle (with chuck) is simplified as one lumped mass connected to the beam with translational springs k_{c_x} , k_{c_y} and rotational springs K_{c_x} , K_{c_y} . As the spindle is also supported by the main body of lathe, two translational springs k_{s_x} , k_{s_y} and two rotational springs K_{s_x} , K_{s_y} are included in the model. The workpiece is allowed to bend in both the xz and yz planes. Torsional vibration of the workpiece is not considered as the first torsional frequency is much higher than the first several bending frequencies. As a result of the complexity of the model, only the parameters contained in one plane are showed in the Figure 2.2.

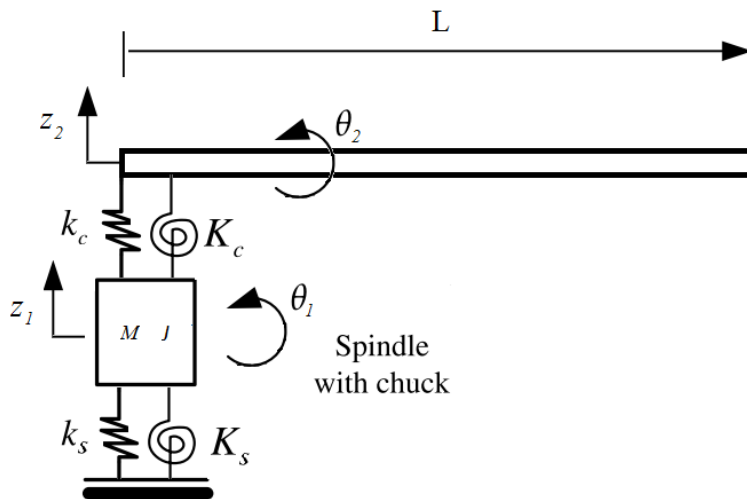


FIGURE 2.2: Spindle-workpiece model

The boundary conditions at $x = L$ are,

$$\begin{aligned} \frac{d^2 W}{dx^2}(L) &= 0 \\ \frac{d^3 W}{dx^3}(L) &= 0 \end{aligned} \quad (2.4)$$

while at $x = 0$ are,

$$\begin{aligned} -EI \frac{d^3 W}{dx^3}(0) &= k_c z \\ EI \frac{d^2 W}{dx^2}(0) &= K_c \theta \end{aligned} \quad (2.5)$$

where E and I are, respectively, the Young's modulus and the moment of area and,

$$z = z_2 - z_1 \quad \theta = \theta_2 - \theta_1 \quad (2.6)$$

According to Figure 2.2, let z_1 be the displacement of the mass M and z_2 the one corresponding to the other end of the spring. Therefore,

$$M \frac{d^2 z_1}{dt^2} = k_c (z_2 - z_1) - k_s z_1 \quad (2.7)$$

Defining,

$$z = z_2 - z_1 \rightarrow z_1 = z_2 - z \quad (2.8)$$

and replacing in Eq. (2.7) obtains,

$$M \frac{d^2 z_2}{dt^2} - M \frac{d^2 z}{dt^2} = k_c z - k_s (z_2 - z) \quad (2.9)$$

and since

$$z_2 = W(0) e^{i\omega t} \quad (2.10)$$

replacing in Eq. (2.9) results in

$$M \frac{d^2 z}{dt^2} + z (k_c + k_s) = (k_s - \omega^2 M) W(0) e^{i\omega t} \quad (2.11)$$

whose particular solution is,

$$z = \frac{(k_s - \omega^2 M) W(0)}{(k_c + k_s - \omega^2 M)} e^{i\omega t} \quad (2.12)$$

and the boundary condition Eq. (2.5a) becomes,

$$-EI \frac{d^3 W}{dx^3}(0) = k_c \frac{(k_s - \omega^2 M) W(0)}{(k_c + k_s - \omega^2 M)} \quad (2.13)$$

In the same way, the boundary condition Eq. (2.5b) becomes,

$$EI \frac{d^2W}{dx^2}(0) = K_c \frac{(K_s - \omega^2 J) W'(0)}{(K_c + K_s - \omega^2 J)} \quad (2.14)$$

Substituting Eq. (2.2) in the governing boundary conditions one obtains the determinant equation,

$$\begin{vmatrix} -\cos \lambda & -\sin \lambda & \cosh \lambda & \sinh \lambda \\ \sin \lambda & -\cos \lambda & \sinh \lambda & \cosh \lambda \\ k & -EI\lambda^3 & k & EI\lambda^3 \\ EI\lambda & K & -EI\lambda & K \end{vmatrix} = 0 \quad (2.15)$$

where

$$k = \frac{k_c (k_s - \omega^2 M)}{(k_c + k_s - \omega^2 M)} \quad K = \frac{K_c (K_s - \omega^2 J)}{(K_c + K_s - \omega^2 J)} \quad (2.16)$$

Expansion of the determinant Eq. (2.15) leads to the following expression,

$$\begin{aligned} & -2\lambda^4 E^2 I^2 (\cosh \lambda \cos \lambda - 1) - 2K\lambda^3 EI (\cosh \lambda \sin \lambda + \sinh \lambda \cos \lambda) \\ & + 2k\lambda EI (\cosh \lambda \sin \lambda - \sinh \lambda \cos \lambda) - 2Kk (\cosh \lambda \cos \lambda + 1) \end{aligned} \quad (2.17)$$

In order to determine λ values and consequently the natural frequencies, system parameters K_s , k_s , M , J , K_c and k_c must be identified. Once their values have been determined, the modal shapes can be obtained.

The values of the parameters can be experimentally obtained by exciting the system using the exciter tool. As the exciter tool acts as a flexible support (k_e), the boundary conditions change. The workpiece has two spans (W_1 and W_2) now. Varying the position of the tool, several equations are obtained in order to identify the required parameters. The new system can be modelled as shown in Figure 2.3.

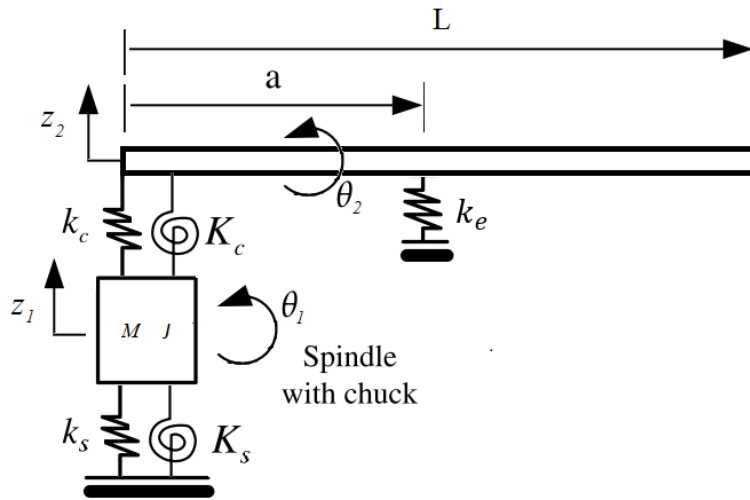


FIGURE 2.3: Spindle-workpiece model with exciter tool support

The boundary conditions at $x = 0$ are,

$$\begin{aligned} -EI \frac{d^3 W_1}{dx^3}(0) &= k_c z \\ EI \frac{d^2 W_1}{dx^2}(0) &= K_c \theta \end{aligned} \quad (2.18)$$

while at flexible support position ($x = a$) are,

$$\begin{aligned} EI \frac{d^3 W_1}{dx^3}(a/L) - EI \frac{d^3 W_2}{dx^3}(0) &= k_e W_2(0) \\ W_1(a/L) &= W_2(0) \\ \frac{dW_1}{dx}(a/L) &= \frac{dW_2}{dx}(0) \\ \frac{d^2 W_1}{dx^2}(a/L) &= \frac{d^2 W_2}{dx^2}(0) \end{aligned} \quad (2.19)$$

while at $x = L$ are,

$$\begin{aligned} \frac{d^2 W_2}{dx^2}(1 - a/L) &= 0 \\ \frac{d^3 W_2}{dx^3}(1 - a/L) &= 0 \end{aligned} \quad (2.20)$$

With these boundary conditions one obtains the following determinant equation,

$$\begin{vmatrix} \lambda EI & K & -\lambda EI & K & 0 & 0 & 0 & 0 \\ k & -EI\lambda^3 & k & EI\lambda^3 & 0 & 0 & 0 & 0 \\ \sin \gamma & -\cos \gamma & \sinh \gamma & \cosh \gamma & -k_e/\lambda^3 EI & 1 & -k_e/\lambda^3 EI & -1 \\ \cos \gamma & \sin \gamma & \cosh \gamma & \sinh \gamma & -1 & 0 & -1 & 0 \\ -\sin \gamma & \cos \gamma & \sinh \gamma & \cosh \gamma & 0 & -1 & 0 & -1 \\ -\cos \gamma & -\sin \gamma & \cosh \gamma & \sinh \gamma & 1 & 0 & -1 & 0 \\ 0 & 0 & 0 & 0 & -\cos \delta & \sin \delta & \cosh \delta & -\sinh \delta \\ 0 & 0 & 0 & 0 & -\sin \delta & -\cos \delta & -\sinh \delta & \cosh \delta \end{vmatrix} = 0 \quad (2.21)$$

where

$$K = \frac{K_c (K_s - \omega^2 J)}{(K_c + K_s - \omega^2 J)} \quad k = \frac{k_c (k_s - \omega^2 M)}{(k_c + k_s - \omega^2 M)} \quad \gamma = \lambda \frac{a}{L} \quad \delta = \lambda \left(\frac{a}{L} - 1 \right) \quad (2.22)$$

Expansion of the determinant Eq. (2.15) leads to the following expression,

$$\begin{aligned} & -8\lambda^7 E^3 I^3 ((\cosh \gamma \cosh \delta - \sinh \gamma \sinh \delta) (\cos \gamma \cos \delta + \sin \gamma \sin \delta) - 1) \\ & + 8K\lambda^6 E^2 I^2 (\cos \gamma \cos \delta + \sin \gamma \sin \delta) (\cosh \gamma \sinh \delta - \cosh \delta \sinh \gamma) \\ & + 8K\lambda^6 E^2 I^2 (\cos \gamma \sin \delta - \cos \delta \sin \gamma) (\cosh \gamma \cosh \delta - \sinh \gamma \sinh \delta) \\ & - 8k\lambda^4 E^2 I^2 (\cos \gamma \cos \delta + \sin \gamma \sin \delta) (\cosh \gamma \sinh \delta - \cosh \delta \sinh \gamma) \\ & + 8k\lambda^4 E^2 I^2 (\cos \gamma \sin \delta - \cos \delta \sin \gamma) (\cosh \gamma \cosh \delta - \sinh \gamma \sinh \delta) \\ & + 4\lambda^4 E^2 I^2 k_e (\cos \delta \cosh \delta + 1) (\cos \gamma \sinh \gamma - \sin \gamma \cosh \gamma) \\ & - 4\lambda^4 E^2 I^2 k_e (\cos \gamma \cosh \gamma + 1) (\cos \delta \sinh \delta - \sin \delta \cosh \delta) \\ & + 8K\lambda^3 E I k_e (\cosh \gamma \cos \gamma) (\cos \delta \cosh \delta + 1) \\ & - 4K\lambda^3 E I k_e (\cos \gamma \sinh \gamma + \sin \gamma \cosh \gamma) (\cos \delta \sinh \delta - \sin \delta \cosh \delta) \\ & + 8Kk\lambda^3 E I ((\cos \gamma \cos \delta + \sin \gamma \sin \delta) (\cosh \gamma \cosh \delta - \sinh \gamma \sinh \delta) + 1) \\ & + 8k\lambda E I k_e (\sin \gamma \sinh \gamma) (\cos \delta \cosh \delta + 1) \\ & + 4k\lambda E I k_e (\cos \gamma \sinh \gamma - \sin \gamma \cosh \gamma) (\cos \delta \sinh \delta - \sin \delta \cosh \delta) \end{aligned} \quad (2.23)$$

λ values, and consequently natural frequencies of the system, can be determined by identifying the system parameters.

2.3 Turning operation dynamic model

The procedure for the evaluation of developed model was divided into three main part: (I) system parameter identification, (II) turning dynamic model and (III) numerical simulation.

First, system parameters were experimentally identified. For this, a piezo actuator based exciter tool was developed to excite the system and modal updating method was used to identify the parameters. Then, a turning operation dynamic model from the literature (Ouyang and Wang, 2007; Han et al., 2012; Lv et al., 2015) was adapted for turning operation of slender workpieces without tailstock. Finally, numerical simulations were carried out with identified parameters to obtain the stability predictions.

2.3.1 System parameter identification

The methodology carried out to identify the parameters K_s , k_s , M , J , K_c , k_c and k_e was as follows:

1. A slender workpiece was clamped to the spindle through a self-centering chuck with hard jaws.
2. Several points were determined along the workpiece to excite the system.
3. The system was excited and the response of the system was measured by means of accelerometers.
4. System parameters are estimated using model updating method.

In order to excite the system, a piezo actuator based exciter tool was designed. A VDI A11 40X100 tool holder and a Sandvik PCLNL 3225P tool holder were modified for this purpose. The prototype integrates a piezo actuator which is controlled by a compact RIO 9039. The developed design allows to excite the joint system by frequency sweeps. The prototype is shown in the Figure 2.4 and Figure 2.5:

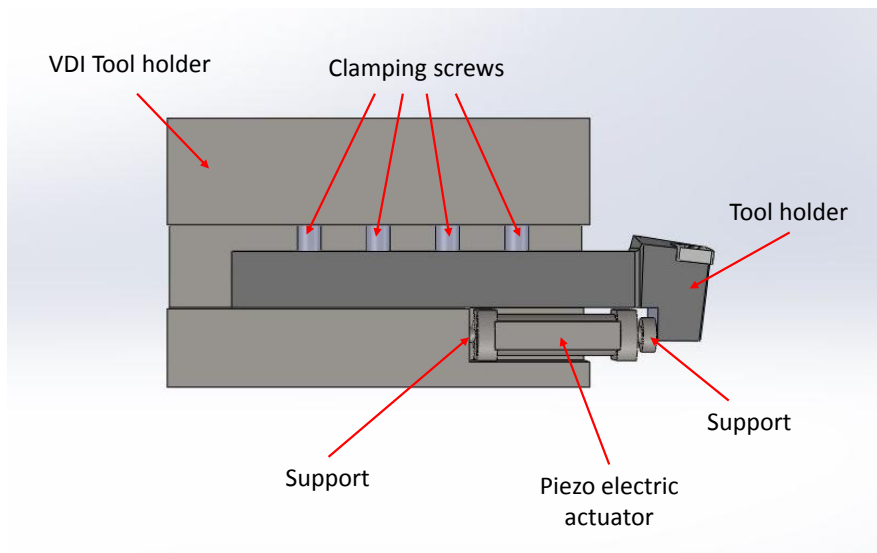


FIGURE 2.4: Prototype description

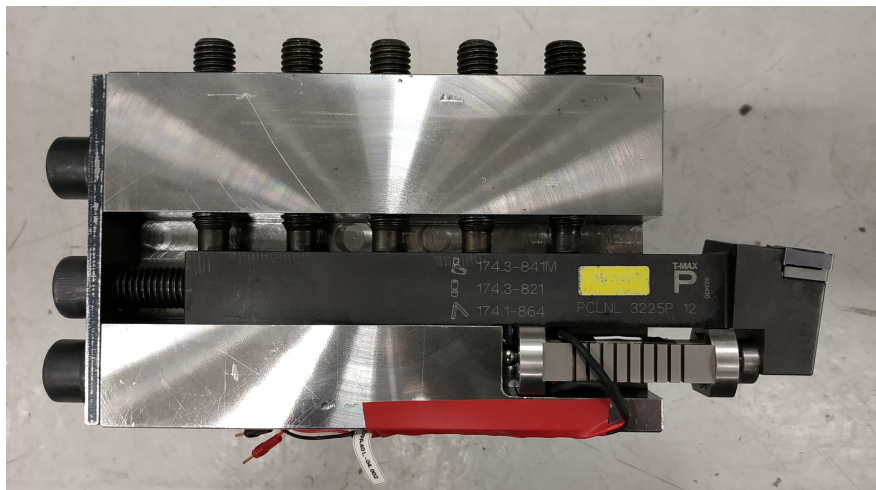


FIGURE 2.5: Prototipo

The performance of the exciter tool has been validated by impact hammer tests. The workpiece clamped in the machine was excited with the prototype by a frequency sweep from 1 to 2000 Hz. The Figure 2.6 shows the response measured by the accelerometer placed on the spindle. It can be observed that both measurement, from

impact hammer and exciter tool tests, shows good agreement. Natural frequencies of 342 Hz and 603 Hz are excited and satisfactorily identified by both excitation methods.

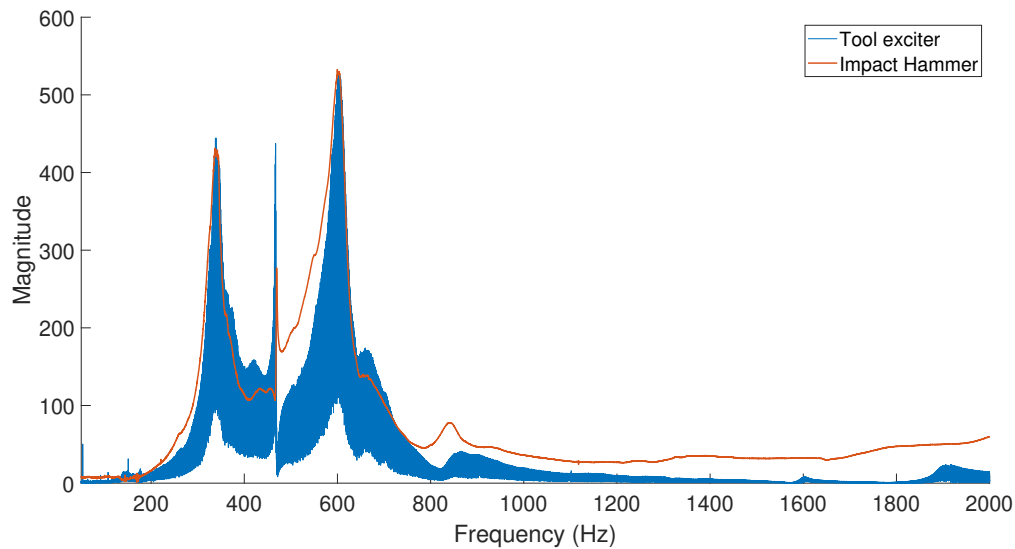


FIGURE 2.6: Accelerometer measurements comparison between exciter tool and impact hammer

In order to determine the values of the parameters, several tests have been carried out by exciting the system using the exciter tool. A slender workpiece was clamped to the spindle trough a self-centering chuck with hard jaws. The specifications of the workpiece are shown in the Table 2.1. Several positions were determined along the workpiece to excite the system (see Table 2.2). The exciter tool was supported (see Figure 2.7) on the workpiece at these positions. Then, the system was excited and the response of the system was measured by means of a PCB356A16 triaxial accelerometer. Finally, system parameters were estimated using model updating method.

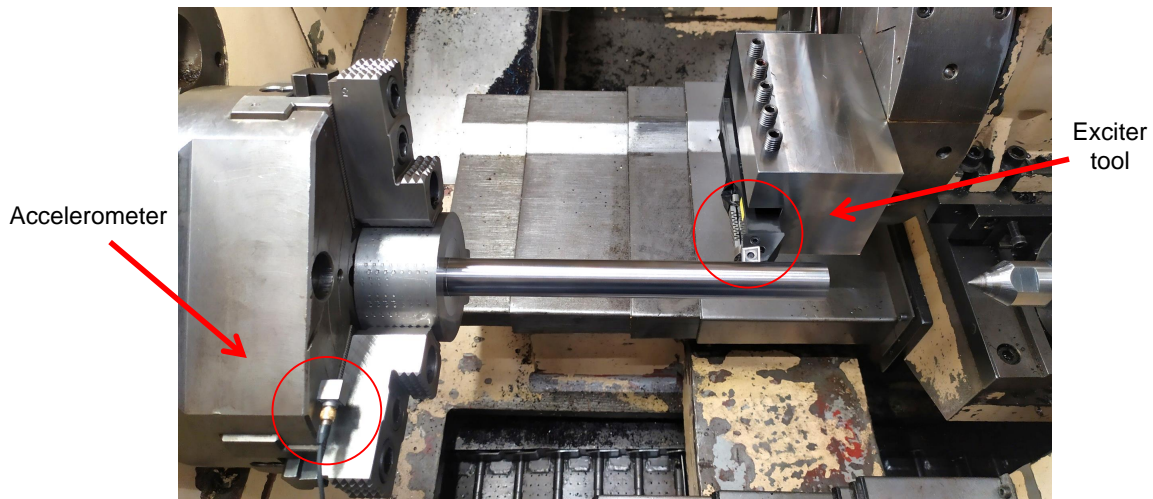


FIGURE 2.7: Experimental test set-up

TABLE 2.1: Workpiece specifications

Parameter	Values
Workpiece material	Steel C45
Material density (ρ)	7800 Kg/m ³
Young's modulus (E)	2×10^{11} Pa
Workpiece length (L)	156 mm
Workpiece diameter (d)	19.5 mm

TABLE 2.2: Experimentally identified modes with different support positions

Tool positions	Values
no support	388.7 Hz
31 mm	399.5 Hz
62 mm	477.4 Hz
93 mm	655.5 Hz
124 mm	858.2 Hz
155 mm	653.1 Hz

Modal testing on the workpiece in the lathe provides measured frequencies required in model updating. Then the model updating problem can therefore be cast as

$$MSE_{min} = \frac{1}{n} \sum_{i=1}^n (\hat{\lambda}_i(x) - \lambda_i)^2 \quad (2.24)$$

where x is the vector containing all unknown parameters, $\hat{\lambda}_i$ is the i th analytical frequency, and λ_i , the i th measured frequency. Based on a nonlinear programming method, one possible optimum is found for unknown parameters: $M = 42$ Kg, $k_s = 4.54 \times 10^9$ N/m, $J = 0.71$ Kg m², $K_s = 1.81 \times 10^6$ N/rad, $k_c = 1 \times 10^{10}$ N/m, $K_c = 4.43 \times 10^5$ N/rad and $k_e = 5.12 \times 10^4$ N/m. The comparison between the frequencies calculated using these updated parameters with those from experiment is shown in the Figure 2.8.

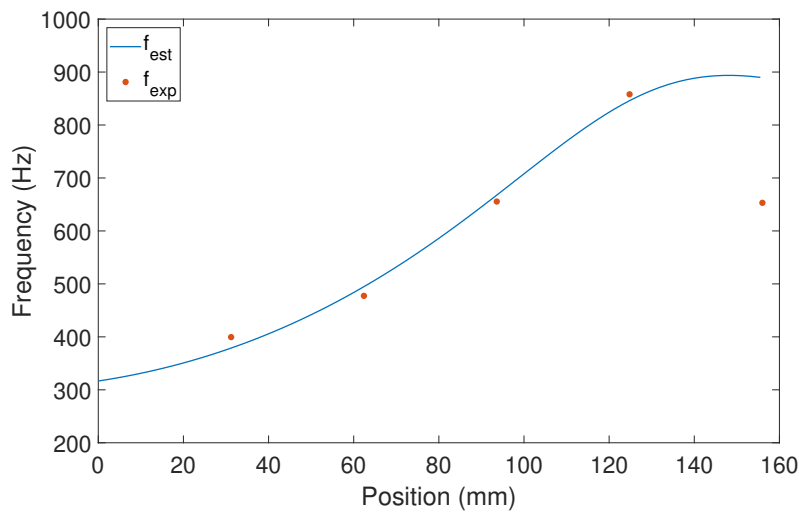


FIGURE 2.8: Experimental modes frequency vs theoretical model modes frequency

The frequency curve obtained using the updated parameters shows good agreement except for the last point. Although the model shows the correct trend, the experimental frequencies decrease strongly at the end of the bar, differing from the theoretical model as it can be observed in the Figure 2.8

Once system parameters were identified, these were replaced in Eq 2.15 and the equations system was solved, obtaining the values of A , B , C and D parameters of the mode shape.

$$W(x) = -0.56926 \cos \lambda x + 0.42228 \sin \lambda x + 0.56927 \cosh \lambda x - 0.41659 \sinh \lambda x \quad (2.25)$$

2.3.2 Turning dynamic model

The turned workpiece is modelled as a circular beam which is subjected to three directional forces moving along z axis and is rotating about its longitudinal axis, z as shown in Figure 2.9. The workpiece has three distinct sections: un-machined, being-machined and machined, where l is the full length of the workpiece, l_1 the length of unmachined section and l_2 the length of unmachined and being- machined sections of the workpiece together. $s(t)$ is the variable distance from the spindle to the location of the moving cutter. During turning, as the cutter travels along the workpiece, the deformations produced in the x and y directions by the moving cutting forces are denoted by v and w . The three directional moving cutting forces are acting on the surface of the beam and they have been translated to the neutral axis of the beam as shown in Figure 2.9.

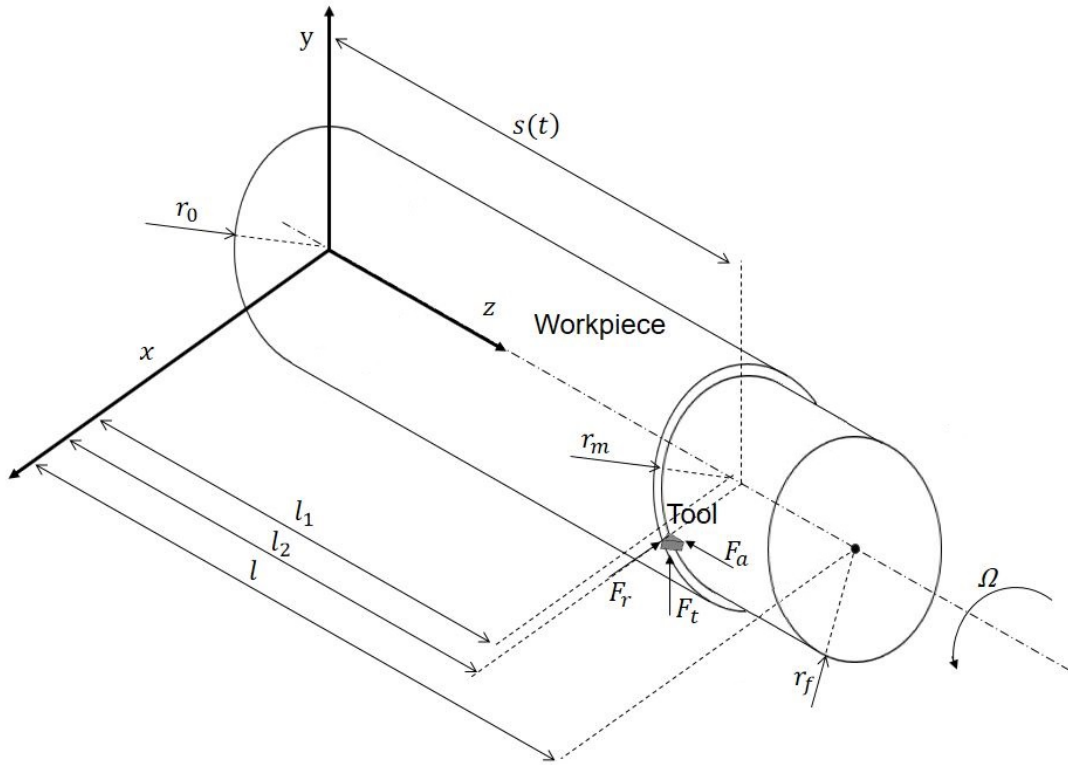


FIGURE 2.9: Workpiece model

The value of v and w will depend not only on time, t but also the position along the workpiece, z . It is assumed that the deflections of the workpiece are,

$$v(z, t) = \sum_{i=1}^n \varphi_i(z) \alpha_i(t) = \boldsymbol{\varphi}^T(z) \boldsymbol{\alpha}(t) \quad (2.26)$$

$$w(z, t) = \sum_{i=1}^n \varphi_i(z) \beta_i(t) = \boldsymbol{\varphi}^T(z) \boldsymbol{\beta}(t) \quad (2.27)$$

where $\boldsymbol{\varphi}^T = \{\varphi_1, \varphi_2 \dots \varphi_n\}$ is a spatial function that satisfies the boundary conditions of the workpiece obtained in the previous section and i th mode is for the stationary beam and $\boldsymbol{\alpha}^T = \{\alpha_1, \alpha_2 \dots \alpha_n\}$ and $\boldsymbol{\beta}^T = \{\beta_1, \beta_2 \dots \beta_n\}$ with $\alpha_i(t)$ and $\beta_i(t)$ is the corresponding modal coordinate. Different boundary conditions mentioned previously are reflected by $\varphi_i(z)$.

In general, the energy of a vibrating system is partly potential and partly kinetic. The kinetic and potential energies of beam are established based on the following assumptions. Beam has homogeneous and isotropic material properties, the elastic

and centroid axes in the cross section of a beam coincide, thus the effects due to eccentricity are not considered. The work performed by the external loads during this displacement is equated to internal work. Based on Rayleigh beam theory, the kinetic energy of the beam can be written as (Han et al., 2012),

$$\begin{aligned}
T_{beam} = & \frac{1}{2} \int_0^{l_1} \rho A_1 \left[\left(\frac{\partial v}{\partial t} \right)^2 + \left(\frac{\partial w}{\partial t} \right)^2 \right] + \rho I_1 \left[\left(\frac{\partial^2 v}{\partial z \partial t} \right)^2 + \left(\frac{\partial^2 w}{\partial z \partial t} \right)^2 \right] \\
& + 2\rho I_1 \Omega \left(\frac{\partial^2 v}{\partial z \partial t} \frac{\partial w}{\partial z} - \frac{\partial^2 w}{\partial z \partial t} \frac{\partial v}{\partial z} \right) + 2\rho I_1 \Omega^2 dz \\
& + \frac{1}{2} \int_{l_1}^{l_2} \rho A_2 \left[\left(\frac{\partial v}{\partial t} \right)^2 + \left(\frac{\partial w}{\partial t} \right)^2 \right] + \rho I_2 \left[\left(\frac{\partial^2 v}{\partial z \partial t} \right)^2 + \left(\frac{\partial^2 w}{\partial z \partial t} \right)^2 \right] \\
& + 2\rho I_2 \Omega \left(\frac{\partial^2 v}{\partial z \partial t} \frac{\partial w}{\partial z} - \frac{\partial^2 w}{\partial z \partial t} \frac{\partial v}{\partial z} \right) + 2\rho I_2 \Omega^2 dz \\
& + \frac{1}{2} \int_{l_2}^l \rho A_3 \left[\left(\frac{\partial v}{\partial t} \right)^2 + \left(\frac{\partial w}{\partial t} \right)^2 \right] + \rho I_3 \left[\left(\frac{\partial^2 v}{\partial z \partial t} \right)^2 + \left(\frac{\partial^2 w}{\partial z \partial t} \right)^2 \right] \\
& + 2\rho I_3 \Omega \left(\frac{\partial^2 v}{\partial z \partial t} \frac{\partial w}{\partial z} - \frac{\partial^2 w}{\partial z \partial t} \frac{\partial v}{\partial z} \right) + 2\rho I_3 \Omega^2 dz
\end{aligned} \tag{2.28}$$

where

$$\frac{\partial v}{\partial t} = \boldsymbol{\varphi}^T(z) \dot{\boldsymbol{\alpha}}(t), \quad \frac{\partial v}{\partial z} = \boldsymbol{\varphi}'^T(z) \boldsymbol{\alpha}(t), \quad \frac{\partial^2 v}{\partial z^2} = \boldsymbol{\varphi}''^T(z) \boldsymbol{\alpha}(t), \quad \frac{\partial^2 v}{\partial z \partial t} = \boldsymbol{\varphi}'^T(z) \dot{\boldsymbol{\alpha}}(t) \tag{2.29}$$

$$\frac{\partial w}{\partial t} = \boldsymbol{\varphi}^T(z) \dot{\boldsymbol{\beta}}(t), \quad \frac{\partial w}{\partial z} = \boldsymbol{\varphi}'^T(z) \boldsymbol{\beta}(t), \quad \frac{\partial^2 w}{\partial z^2} = \boldsymbol{\varphi}''^T(z) \boldsymbol{\beta}(t), \quad \frac{\partial^2 w}{\partial z \partial t} = \boldsymbol{\varphi}'^T(z) \dot{\boldsymbol{\beta}}(t) \tag{2.30}$$

$$A_1 = \pi r_o^2, \quad A_2 = \pi r_m^2, \quad A_3 = \pi r_f^2, \quad I_1 = \frac{\pi r_o^4}{4}, \quad I_2 = \frac{\pi r_m^4}{4}, \quad I_3 = \frac{\pi r_f^4}{4} \tag{2.31}$$

where r_o , r_m and r_f are the workpiece radius of the un-machined, being-machined, and machined sections respectively, ρ is mass density and Ω is the rotational speed of the workpiece.

The Eq. (2.28) can be rewritten as,

$$T_{beam} = \frac{\rho}{2} \dot{\boldsymbol{\alpha}}^T \mathbf{H} \dot{\boldsymbol{\alpha}} + \frac{\rho}{2} \dot{\boldsymbol{\beta}}^T \mathbf{H} \dot{\boldsymbol{\beta}} + \rho \Omega \left[\dot{\boldsymbol{\alpha}}^T \mathbf{H}_2 \boldsymbol{\beta} - \dot{\boldsymbol{\beta}}^T \mathbf{H}_2 \boldsymbol{\alpha} \right] + \rho \mathbf{H}_4 \Omega^2 \tag{2.32}$$

where,

$$\mathbf{H} = \mathbf{H}_1 + \mathbf{H}_2 \quad (2.33)$$

$$\mathbf{H}_1 = A_1 \mathbf{A}1 + A_2 \mathbf{A}2 + A_3 \mathbf{A}3 \quad (2.34)$$

$$A1 = \int_0^{l_1} \boldsymbol{\varphi}(z) \boldsymbol{\varphi}^T(z) dz, \quad A2 = \int_{l_1}^{l_2} \boldsymbol{\varphi}(z) \boldsymbol{\varphi}^T(z) dz, \quad A3 = \int_{l_2}^l \boldsymbol{\varphi}(z) \boldsymbol{\varphi}^T(z) dz \quad (2.35)$$

$$\mathbf{H}_2 = I_1 \mathbf{B}1 + I_2 \mathbf{B}2 + I_3 \mathbf{B}3 \quad (2.36)$$

$$\mathbf{B}1 = \int_0^{l_1} \boldsymbol{\varphi}'(z) \boldsymbol{\varphi}'^T(z) dz, \quad \mathbf{B}2 = \int_{l_1}^{l_2} \boldsymbol{\varphi}'(z) \boldsymbol{\varphi}'^T(z) dz, \quad \mathbf{B}3 = \int_{l_2}^l \boldsymbol{\varphi}'(z) \boldsymbol{\varphi}'^T(z) dz \quad (2.37)$$

$$\mathbf{H}_4 = I_1 \left(s - \frac{t_0}{2} \right) + I_2 (t_0) + I_3 \left(l - s - \frac{t_0}{2} \right) \quad (2.38)$$

On the other hand, the strain energy of the beam, V_{beam} is the same as the work done in deforming the beam. The strain energy of the Rayleigh beam theory can be written as,

$$\begin{aligned} V_{beam} = & \frac{1}{2} \int_0^{l_1} EI_1 \left[\left(\frac{\partial^2 v}{\partial z^2} \right)^2 + \left(\frac{\partial^2 w}{\partial z^2} \right)^2 \right] dz + \frac{1}{2} \int_{l_1}^{l_2} EI_2 \left[\left(\frac{\partial^2 v}{\partial z^2} \right)^2 + \left(\frac{\partial^2 w}{\partial z^2} \right)^2 \right] dz \\ & + \frac{1}{2} \int_{l_2}^l EI_3 \left[\left(\frac{\partial^2 v}{\partial z^2} \right)^2 + \left(\frac{\partial^2 w}{\partial z^2} \right)^2 \right] dz \end{aligned} \quad (2.39)$$

where E is Young's modulus of the beam. The Eq. (2.39) can be rewritten as,

$$V_{beam} = \frac{E}{2} \boldsymbol{\alpha}^T \mathbf{H}_3 \boldsymbol{\alpha} + \frac{E}{2} \boldsymbol{\beta}^T \mathbf{H}_3 \boldsymbol{\beta} \quad (2.40)$$

where,

$$\mathbf{H}_3 = I_1 \mathbf{C}1 + I_2 \mathbf{C}2 + I_3 \mathbf{C}3 \quad (2.41)$$

$$\mathbf{C}1 = \int_0^{l_1} \boldsymbol{\varphi}''(z) \boldsymbol{\varphi}''^T(z) dz, \quad \mathbf{C}2 = \int_{l_1}^{l_2} \boldsymbol{\varphi}''(z) \boldsymbol{\varphi}''^T(z) dz, \quad \mathbf{C}3 = \int_{l_2}^l \boldsymbol{\varphi}''(z) \boldsymbol{\varphi}''^T(z) dz \quad (2.42)$$

$$\mathbf{D}1 = \int_s^l \boldsymbol{\varphi}'(z) \boldsymbol{\varphi}'^T(z) dz, \quad \mathbf{G}1 = \boldsymbol{\varphi}(z) \boldsymbol{\varphi}^T(z) \quad (2.43)$$

The virtual work done by forces F_y , F_z , and moment M_z is,

$$\delta W = -F_r \delta v(s(t), t) - F_t \delta w(s(t), t) + M_t \frac{\partial \delta v}{\partial z} \Big|_{z=s(t)} \quad (2.44)$$

where, the bending moment M_z is resulted from the translation of the axial force F_x as,

$$M_t = -F_a r_m \quad (2.45)$$

The cutting forces are given in the form of,

$$F_r = K_r A_p h, \quad F_t = K_t A_p h, \quad F_a = K_a A_p h \quad (2.46)$$

where K_r , K_t and K_a are the cutting force coefficients, A_p is the depth of cut, h is the chip thickness which can be given as,

$$h = h_m - v(t) + v(t - \tau) \quad (2.47)$$

where h_m is the mean uncut chip thickness. The present workpiece displacement $v(t)$ and the previous revolution displacement $v(t - \tau)$ are detailed:

$$v(t) = \boldsymbol{\varphi}(s)\boldsymbol{\alpha}(t), \quad v(t - \tau) = \boldsymbol{\varphi}(s - h_m\Omega\tau)\boldsymbol{\alpha}(t - \tau) \quad (2.48)$$

The other components in Figure 2.9, the kinetic energy for the spindle and the strain energy for the springs can be expressed as (Lv et al., 2015),

$$T_{spindle} = \frac{1}{2}m_m(\dot{v}_m^2 + \dot{w}_m^2) + \frac{1}{2}J_d(\dot{\theta}_{xm}^2 + \dot{\theta}_{ym}^2) + \frac{1}{2}J_p(\Omega^2 - 2\Omega\dot{\theta}_{ym}\theta_{xm}) \quad (2.49)$$

$$V_{spindle} = \frac{1}{2}k_{cx}(\boldsymbol{\varphi}^T(z)\boldsymbol{\alpha}|_{z=l} - v_m)^2 + \frac{1}{2}k_{cy}(\boldsymbol{\varphi}^T(z)\boldsymbol{\beta}|_{z=l} - w_m)^2 \\ + \frac{1}{2}K_{cx}(\boldsymbol{\varphi}'^T(z)\boldsymbol{\alpha}|_{z=l} - \theta_{xm})^2 + \frac{1}{2}K_{cy}(\boldsymbol{\varphi}'^T(z)\boldsymbol{\beta}|_{z=l} - \theta_{ym})^2 \quad (2.50)$$

where m_m is the mass of the spindle and \dot{v}_m and \dot{w}_m are the velocities of the spindle in the x and y directions, respectively; $\dot{\theta}_{xm}$ and $\dot{\theta}_{ym}$ are the instantaneous angular velocities about the z and x axes which are fixed on the spindle and rotate with it; J_d and J_p are the diametrical moment of inertia about the shaft line and polar moment of inertia about any axis perpendicular to the shaft line.

Lagrange's equations was used for developing equation of motion and it can be obtained as below,

$$L = T - V \quad (2.51)$$

where the Lagrangian function is defined as,

$$\begin{aligned} L = & \frac{\rho}{2} \dot{\boldsymbol{\alpha}}^T \mathbf{H} \dot{\boldsymbol{\alpha}} + \frac{\rho}{2} \dot{\boldsymbol{\beta}}^T \mathbf{H} \dot{\boldsymbol{\beta}} + \rho \Omega \left[\dot{\boldsymbol{\alpha}}^T \mathbf{H}_2 \boldsymbol{\beta} - \dot{\boldsymbol{\beta}}^T \mathbf{H}_2 \boldsymbol{\alpha} \right] + \rho \mathbf{H}_4 \Omega^2 + \frac{1}{2} m_m (\dot{v}_m^2 + \dot{w}_m^2) \\ & + \frac{1}{2} J_d (\dot{\theta}_{xm}^2 + \dot{\theta}_{ym}^2) + \frac{1}{2} J_p (\Omega^2 - 2\Omega \dot{\theta}_{ym} \theta_{xm}) - \frac{E}{2} \boldsymbol{\alpha}^T \mathbf{H}_3 \boldsymbol{\alpha} - \frac{E}{2} \boldsymbol{\beta}^T \mathbf{H}_3 \boldsymbol{\beta} \\ & - \frac{1}{2} k_{cx} (\boldsymbol{\varphi}^T(z) \boldsymbol{\alpha}|_{z=l} - v_m)^2 - \frac{1}{2} k_{cy} (\boldsymbol{\varphi}^T(z) \boldsymbol{\beta}|_{z=l} - w_m)^2 \\ & - \frac{1}{2} K_{cx} (\boldsymbol{\varphi}'^T(z) \boldsymbol{\alpha}|_{z=l} - \theta_{xm})^2 - \frac{1}{2} K_{cy} (\boldsymbol{\varphi}'^T(z) \boldsymbol{\beta}|_{z=l} - \theta_{ym})^2 \end{aligned} \quad (2.52)$$

Applying Lagrange's equations for α ,

$$\frac{d}{dt} \left(\frac{\partial L}{\partial \dot{\boldsymbol{\alpha}}} \right) - \frac{\partial L}{\partial \boldsymbol{\alpha}} = F_{\alpha} \quad (2.53)$$

the following equation is obtained,

$$\begin{aligned} \rho \mathbf{H} \ddot{\boldsymbol{\alpha}} + \rho \dot{\mathbf{H}} \dot{\boldsymbol{\alpha}} + 2\rho \Omega \mathbf{H}_2 \dot{\boldsymbol{\beta}} + \rho \Omega \dot{\mathbf{H}}_2 \boldsymbol{\beta} + E \mathbf{H}_3 \boldsymbol{\alpha} + k_{cx} \boldsymbol{\varphi}(z) \boldsymbol{\varphi}^T(z) \boldsymbol{\alpha}|_{z=l} - k_{cx} v_m \boldsymbol{\varphi}^T(z) \\ + K_{cx} \boldsymbol{\varphi}'(z) \boldsymbol{\varphi}'^T(z) \boldsymbol{\alpha}|_{z=l} - K_{cx} \theta_{xm} \boldsymbol{\varphi}'^T(z) = -F_r \boldsymbol{\varphi}(s) + r_m F_a \boldsymbol{\varphi}'(s) \end{aligned} \quad (2.54)$$

Applying Lagrange's equations for β ,

$$\frac{d}{dt} \left(\frac{\partial L}{\partial \dot{\boldsymbol{\beta}}} \right) - \frac{\partial L}{\partial \boldsymbol{\beta}} = F_{\beta} \quad (2.55)$$

the following equation is obtained,

$$\begin{aligned} \rho \mathbf{H} \ddot{\boldsymbol{\beta}} + \rho \dot{\mathbf{H}} \dot{\boldsymbol{\beta}} - 2\rho \Omega \mathbf{H}_2 \dot{\boldsymbol{\alpha}} - \rho \Omega \dot{\mathbf{H}}_2 \boldsymbol{\alpha} + E \mathbf{H}_3 \boldsymbol{\beta} + k_{cy} \boldsymbol{\varphi}(z) \boldsymbol{\varphi}^T(z) \boldsymbol{\beta}|_{z=l} - k_{cy} w_m \boldsymbol{\varphi}^T(z) \\ + K_{cy} \boldsymbol{\varphi}'(z) \boldsymbol{\varphi}'^T(z) \boldsymbol{\beta}|_{z=l} - K_{cy} \theta_{ym} \boldsymbol{\varphi}'^T(z) = -F_t \boldsymbol{\varphi}(s) \end{aligned} \quad (2.56)$$

Applying Lagrange's equations for v_m , w_m , θ_{xm} and θ_{ym} ,

$$\frac{d}{dt} \left(\frac{\partial L}{\partial \dot{v}_m} \right) - \frac{\partial L}{\partial v_m} = 0 \quad (2.57)$$

$$\frac{d}{dt} \left(\frac{\partial L}{\partial \dot{w}_m} \right) - \frac{\partial L}{\partial w_m} = 0 \quad (2.58)$$

$$\frac{d}{dt} \left(\frac{\partial L}{\partial \dot{\theta}_{xm}} \right) - \frac{\partial L}{\partial \theta_{xm}} = 0 \quad (2.59)$$

$$\frac{d}{dt} \left(\frac{\partial L}{\partial \dot{\theta}_{ym}} \right) - \frac{\partial L}{\partial \theta_{ym}} = 0 \quad (2.60)$$

the following equations are obtained respectively,

$$m_m \ddot{v}_m + k_{cx} v_m - k_{cx} \boldsymbol{\varphi}^T(z) \boldsymbol{\alpha}|_{z=l} = 0 \quad (2.61)$$

$$m_m \ddot{w}_m + k_{cy} w_m - k_{cy} \boldsymbol{\varphi}^T(z) \boldsymbol{\beta}|_{z=l} = 0 \quad (2.62)$$

$$J_d \ddot{\theta}_{xm} + J_p \Omega \dot{\theta}_{ym} + K_{cx} \theta_{xm} - K_{cx} \boldsymbol{\varphi}^T(z) \boldsymbol{\alpha}|_{z=l} = 0 \quad (2.63)$$

$$J_d \ddot{\theta}_{ym} - J_p \Omega \dot{\theta}_{xm} + K_{cy} \theta_{ym} - K_{cy} \boldsymbol{\varphi}^T(z) \boldsymbol{\beta}|_{z=l} = 0 \quad (2.64)$$

by joining Eq. (2.54), Eq. (2.56), Eq. (2.61), Eq. (2.62), Eq. (2.63) and Eq. (2.64), system dynamics are described,

$$\begin{aligned} & \rho \mathbf{H} \ddot{\boldsymbol{\alpha}} + \rho \dot{\mathbf{H}} \dot{\boldsymbol{\alpha}} + 2\rho \Omega \mathbf{H}_2 \dot{\boldsymbol{\beta}} + \rho \Omega \dot{\mathbf{H}}_2 \boldsymbol{\beta} + E \mathbf{H}_3 \boldsymbol{\alpha} + k_{cx} \boldsymbol{\varphi}(z) \boldsymbol{\varphi}^T(z) \boldsymbol{\alpha}|_{z=l} - k_{cx} v_m \boldsymbol{\varphi}^T(z) \\ & \quad + K_{cx} \boldsymbol{\varphi}'(z) \boldsymbol{\varphi}'^T(z) \boldsymbol{\alpha}|_{z=l} - K_{cx} \theta_{xm} \boldsymbol{\varphi}'^T(z) = -F_r \boldsymbol{\varphi}(s) + r_m F_a \boldsymbol{\varphi}'(s) \\ & \rho \mathbf{H} \ddot{\boldsymbol{\beta}} + \rho \dot{\mathbf{H}} \dot{\boldsymbol{\beta}} - 2\rho \Omega \mathbf{H}_2 \dot{\boldsymbol{\alpha}} - \rho \Omega \dot{\mathbf{H}}_2 \boldsymbol{\alpha} + E \mathbf{H}_3 \boldsymbol{\beta} + k_{cy} \boldsymbol{\varphi}(z) \boldsymbol{\varphi}^T(z) \boldsymbol{\beta}|_{z=l} - k_{cy} w_m \boldsymbol{\varphi}^T(z) \\ & \quad + K_{cy} \boldsymbol{\varphi}'(z) \boldsymbol{\varphi}'^T(z) \boldsymbol{\beta}|_{z=l} - K_{cy} \theta_{ym} \boldsymbol{\varphi}'^T(z) = -F_t \boldsymbol{\varphi}(s) \\ & m_m \ddot{v}_m + k_{cx} v_m - k_{cx} \boldsymbol{\varphi}^T(z) \boldsymbol{\alpha}|_{z=l} = 0 \\ & m_m \ddot{w}_m + k_{cy} w_m - k_{cy} \boldsymbol{\varphi}^T(z) \boldsymbol{\beta}|_{z=l} = 0 \\ & J_d \ddot{\theta}_{xm} + J_p \Omega \dot{\theta}_{ym} + K_{cx} \theta_{xm} - K_{cx} \boldsymbol{\varphi}^T(z) \boldsymbol{\alpha}|_{z=l} = 0 \\ & J_d \ddot{\theta}_{ym} - J_p \Omega \dot{\theta}_{xm} + K_{cy} \theta_{ym} - K_{cy} \boldsymbol{\varphi}^T(z) \boldsymbol{\beta}|_{z=l} = 0 \end{aligned} \quad (2.65)$$

the Eqs. (2.65) of motion can then be expressed in a matrix form as

$$\dot{\mathbf{q}}(t) = \mathbf{R}\mathbf{q}(t) + \mathbf{S}\mathbf{q}(t - \tau) + \mathbf{T} \quad (2.66)$$

where

$$\mathbf{q} = \left[\alpha \quad \dot{\alpha} \quad \beta \quad \dot{\beta} \quad v_m \quad \dot{v}_m \quad w_m \quad \dot{w}_m \quad \theta_{xm} \quad \dot{\theta}_{xm} \quad \theta_{ym} \quad \dot{\theta}_{ym} \right]^T \quad (2.67)$$

and

$$\mathbf{R} = \begin{bmatrix} 0 & I & 0 & 0 & 0 & 0 & 0 & 0 & 0 & 0 & 0 & 0 \\ \frac{K1}{M1} & \frac{G1}{M1} & \frac{K2}{M1} & \frac{G2}{M1} & \frac{K3}{M1} & 0 & 0 & 0 & \frac{K4}{M1} & 0 & 0 & 0 \\ 0 & 0 & 0 & I & 0 & 0 & 0 & 0 & 0 & 0 & 0 & 0 \\ \frac{K5}{M1} & -\frac{G2}{M1} & \frac{K6}{M1} & \frac{G1}{M1} & 0 & 0 & \frac{K7}{M1} & 0 & 0 & 0 & \frac{K8}{M1} & 0 \\ 0 & 0 & 0 & 0 & 0 & I & 0 & 0 & 0 & 0 & 0 & 0 \\ \frac{K9}{M2} & 0 & 0 & 0 & \frac{K10}{M2} & 0 & 0 & 0 & 0 & 0 & 0 & 0 \\ 0 & 0 & 0 & 0 & 0 & 0 & 0 & I & 0 & 0 & 0 & 0 \\ 0 & 0 & \frac{K11}{M2} & 0 & 0 & 0 & \frac{K12}{M2} & 0 & 0 & 0 & 0 & 0 \\ 0 & 0 & 0 & 0 & 0 & 0 & 0 & 0 & I & 0 & 0 & 0 \\ \frac{K13}{M3} & 0 & 0 & 0 & 0 & 0 & 0 & \frac{K14}{M3} & 0 & 0 & 0 & -\frac{G3}{M3} \\ 0 & 0 & 0 & 0 & 0 & 0 & 0 & 0 & 0 & 0 & 0 & I \\ 0 & 0 & \frac{K15}{M3} & 0 & 0 & 0 & 0 & 0 & 0 & \frac{G3}{M3} & \frac{K16}{M3} & 0 \end{bmatrix} \quad (2.68)$$

$$\mathbf{S} = \begin{bmatrix} 0 & 0 & 0 & 0 & 0 & 0 & 0 & 0 & 0 & 0 & 0 & 0 \\ \frac{S1}{M1} & 0 & 0 & 0 & 0 & 0 & 0 & 0 & 0 & 0 & 0 & 0 \\ 0 & 0 & 0 & 0 & 0 & 0 & 0 & 0 & 0 & 0 & 0 & 0 \\ \frac{S2}{M1} & 0 & 0 & 0 & 0 & 0 & 0 & 0 & 0 & 0 & 0 & 0 \\ 0 & 0 & 0 & 0 & 0 & 0 & 0 & 0 & 0 & 0 & 0 & 0 \\ 0 & 0 & 0 & 0 & 0 & 0 & 0 & 0 & 0 & 0 & 0 & 0 \\ 0 & 0 & 0 & 0 & 0 & 0 & 0 & 0 & 0 & 0 & 0 & 0 \\ 0 & 0 & 0 & 0 & 0 & 0 & 0 & 0 & 0 & 0 & 0 & 0 \\ 0 & 0 & 0 & 0 & 0 & 0 & 0 & 0 & 0 & 0 & 0 & 0 \\ 0 & 0 & 0 & 0 & 0 & 0 & 0 & 0 & 0 & 0 & 0 & 0 \\ 0 & 0 & 0 & 0 & 0 & 0 & 0 & 0 & 0 & 0 & 0 & 0 \\ 0 & 0 & 0 & 0 & 0 & 0 & 0 & 0 & 0 & 0 & 0 & 0 \\ 0 & 0 & 0 & 0 & 0 & 0 & 0 & 0 & 0 & 0 & 0 & 0 \\ 0 & 0 & 0 & 0 & 0 & 0 & 0 & 0 & 0 & 0 & 0 & 0 \\ 0 & 0 & 0 & 0 & 0 & 0 & 0 & 0 & 0 & 0 & 0 & 0 \end{bmatrix}, \quad \mathbf{T} = \begin{bmatrix} 0 \\ \frac{T1}{M1} \\ 0 \\ \frac{T2}{M1} \\ 0 \\ 0 \\ 0 \\ 0 \\ 0 \\ 0 \\ 0 \\ 0 \\ 0 \\ 0 \\ 0 \\ 0 \end{bmatrix} \quad (2.69)$$

where

$$M1 = \rho H$$

$$M2 = m_m$$

$$M3 = J_d$$

$$K1 = A_p K_r \boldsymbol{\varphi}(s) \boldsymbol{\varphi}^T(s) - r K_a \boldsymbol{\varphi}(s) \boldsymbol{\varphi}'^T(s) - E H_3 - k_{cx} \boldsymbol{\varphi}(z) \boldsymbol{\varphi}^T(z)|_{z=l} - K_{cx} \boldsymbol{\varphi}'(z) \boldsymbol{\varphi}'^T(z)|_{z=l}$$

$$K2 = -\rho \Omega \dot{H}_2$$

$$K3 = k_{cx} \boldsymbol{\varphi}^T(z)|_{z=l}$$

$$K4 = K_{cx} \boldsymbol{\varphi}'^T(z)|_{z=l}$$

$$K5 = \rho \Omega \dot{H}_2 + A_p K_i \boldsymbol{\varphi}(s) \boldsymbol{\varphi}^T(s)$$

$$K6 = -E H_3 - k_{cy} \boldsymbol{\varphi}(z) \boldsymbol{\varphi}^T(z)|_{z=l} - K_{cy} \boldsymbol{\varphi}'(z) \boldsymbol{\varphi}'^T(z)|_{z=l}$$

$$K7 = k_{cy} \boldsymbol{\varphi}^T(z)|_{z=l}$$

$$K8 = K_{cy} \boldsymbol{\varphi}'^T(z)|_{z=l}$$

$$K9 = -k_{cx}$$

$$K10 = -k_{cy}$$

$$K11 = -K_{cx}$$

$$K12 = -K_{cy}$$

(2.70)

$$\begin{aligned}
G1 &= -\rho H_1 \\
G2 &= -2\rho\Omega H_2 \\
G3 &= -J_p\Omega \\
S1 &= -A_p K_r \boldsymbol{\varphi}(s - h_m\Omega\tau) \boldsymbol{\varphi}(s) + r A_p K_a \boldsymbol{\varphi}(s - h_m\Omega\tau) \boldsymbol{\varphi}'(s) \\
S2 &= -A_p K_t \boldsymbol{\varphi}(s - h_m\Omega\tau) \boldsymbol{\varphi}(s) \\
T1 &= -A_p h_m K_r \boldsymbol{\varphi}(s) + r A_p h_m K_a \boldsymbol{\varphi}'(s) \\
T2 &= -A_p h_m K_t \boldsymbol{\varphi}(s)
\end{aligned} \tag{2.71}$$

2.3.3 Numerical simulation

The model presented in Section 2.3.2 was simulated, considering parameters identified in Section 2.3.1. The cutting conditions and simulation parameters are presented in Table 2.3 and Table 2.4. Since the regenerative effect is considered, it is a system of DDEs, where the derivative also depends on the solution at earlier times. Matlab's DDE23 solver was used to run the simulation.

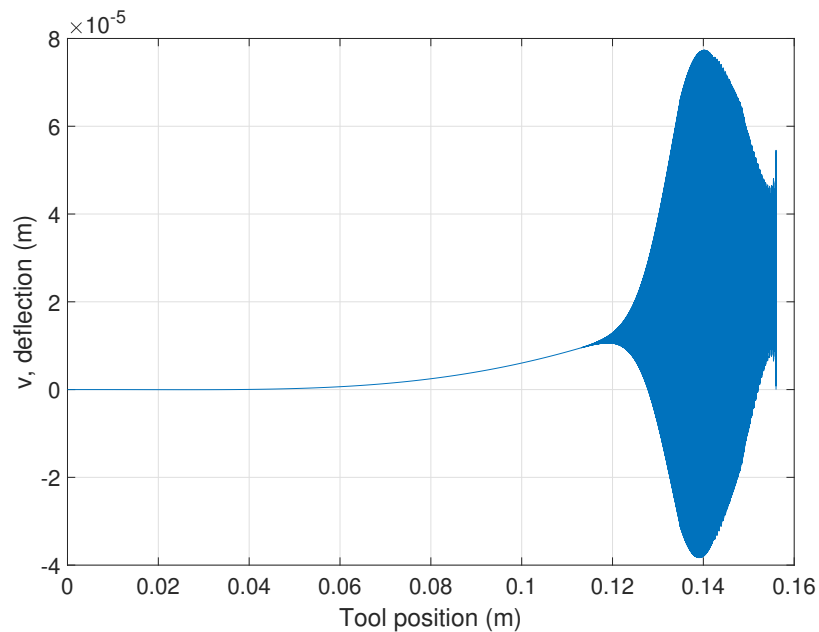
TABLE 2.3: Simulation parameters

Workpiece parameters	Values
Material density (ρ)	7800 Kg/m ³
Young's modulus (E)	2×10^{11} Pa
Workpiece length (l)	156 mm
Workpiece diameter (d)	19.5 mm
Identified parameters	Values
Spindle-beam spring (k_c)	1×10^{10} N/m
Spindle-beam rotational spring (K_c)	4.43×10^5 N/rad
Mass of the spindle (m_m)	42 Kg
Spindle inertia (J_d)	0.7 Kg m ²
Spindle polar inertia (J_p)	0.35 Kg m ²
Spindle spring (k_s)	4.54×10^9 N/m
Spindle rotational spring (K_s)	1.81×10^6 N/rad

TABLE 2.4: Simulation parameters

Cutting parameters	Values
Depth of cut (A_p)	1 mm
Feed (h_m)	0.3 mm/rev
Workpiece rotation speed (n)	1200 RPM
Tangential cutting constant (K_t)	2.61×10^9 N/m ²
Radial cutting constant (K_r)	1.15×10^9 N/m ²
Axial cutting constant (K_a)	1.22×10^9 N/m ²

Figure 2.10 and 2.11 show the workpiece deflection in v and w direction respectively during the turning operation. The tool position indicates the distance at which the tool is from the spindle, where zero is the clamping location. As the piece is not supported by a tailstock, it is more flexible at the end of the bar. Strong deflection are observed at the end of the workpiece in both directions. As the machining progresses, it can be seen that the amplitude of decreases.

FIGURE 2.10: Workpiece deflection in v direction in a turning operation

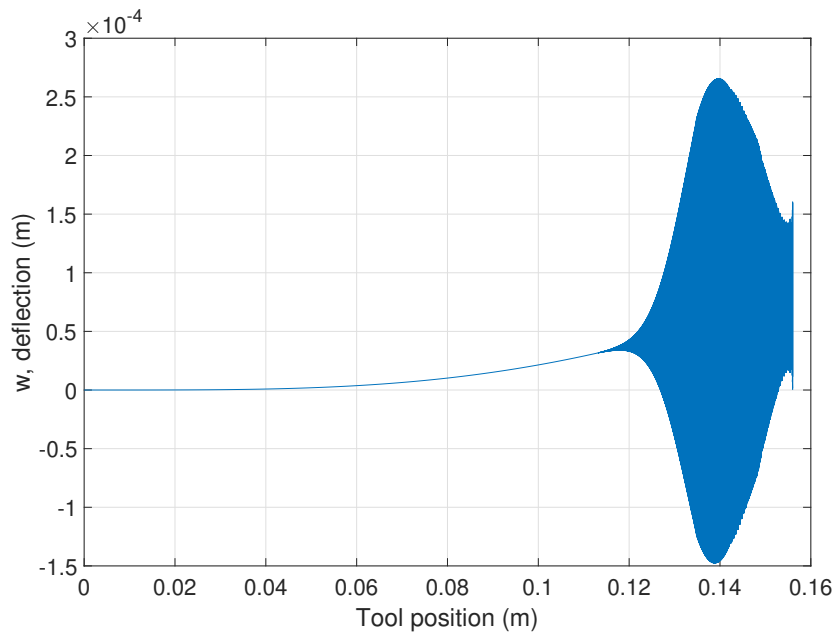


FIGURE 2.11: Workpiece deflection in w direction in a turning operation

This phenomena is because the effective stiffness varies throughout the workpiece, decreasing exponentially as the tool moves away from the spindle, as shown in the Figure 2.12. The effective stiffness at the end of the workpiece is 4.8×10^6 N/m. These results suggest that the most critical area in the machining of slender parts is the end zone of the bar.

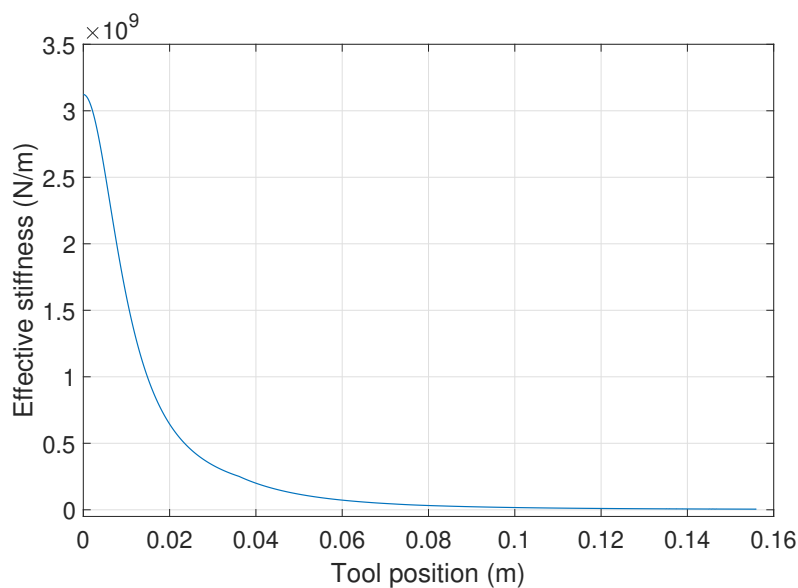


FIGURE 2.12: Effective stiffness along the workpiece

Chapter 3

Slender workpiece cutting process stability analysis

3.1 Introduction

This chapter is focused on analysing the stability at the end of the workpiece. A facing operation has been modelled in the state space and an eigenvalue analysis is carried out. The evolution of natural frequencies is analysed and the stability of the process is determined. Finally, the theoretical results are validated by experimental tests.

3.2 State-Space Model

A flexible workpiece with 2 DoF under orthogonal metal cutting forces is considered. The following assumptions are also considered:

- Nonlinear force model with variable cutting coefficients; the cutting constants vary with the cutting speed.
- A flexible workpiece and the rigid tool are always in contact: a 2 DoF model is used to study the case of flexible workpiece that has two planes of symmetry, which are about 90 degrees because the workpiece is cylindrical.
- The gyroscopic effect due to the rotation of the workpiece is neglected.

- The natural frequencies (ω) are far higher than the workpiece rotation frequency (f_r), so the system is slowly varying Linear Periodic Time Variant (LPTV).

Figure 3.1 describes a flexible workpiece with 2 DoF (x_1 and x_2) under orthogonal metal cutting force and a tool moving around with a constant cutting speed (V_c). For each DoF of the workpiece, is associated a stiffness, k_i , a viscous damping c_i and an effective mass m_i . F_r and F_t are radial and tangential forces respectively. The tool angular position relative to the workpiece is represented by α .

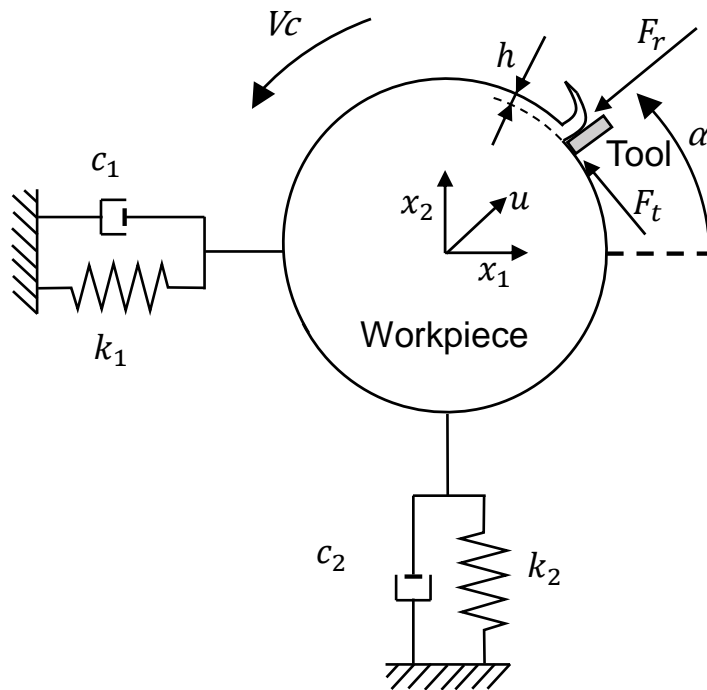


FIGURE 3.1: 2 DoF model in orthogonal metal cutting

Based on orthogonal model of cutting, the cutting force magnitude is proportional to the uncut chip section as:

$$\begin{aligned}
 F(t) &= K_s A_p h(t) = K_s A_p (h_m - u(t)) \\
 &= K_s A_p (h_m - (x_1(t) \cos \alpha + x_2(t) \sin \alpha))
 \end{aligned}
 \tag{3.1}$$

where K_s is the cutting constant, A_p is the depth of cut, h_m is the mean uncut chip thickness and $u(t)$ is the workpiece displacement. Cutting constant vary with the

cutting speed. The mathematical relation between them is given by a power function and it is taken into account by the model with following expression:

$$K_s = K_i V_c \rightarrow K_i = ((a_i V_c^{b_i}) / (V_c)) = a_i V_c^{b_i - 1} \quad (3.2)$$

where a_i and b_i are constants which stand for the rest of cutting parameters for each direction. The constants values are experimentally obtained, and the methodology used to determine them is described in section 3.4.2.

The forces are given by the following expressions:

$$F_r(t) = K_r V_c A_p (x_1(t) \cos \alpha + x_2(t) \sin \alpha) \quad (3.3)$$

$$F_t(t) = K_t V_c A_p (x_1(t) \sin \alpha + x_2(t) \cos \alpha) \quad (3.4)$$

The dynamic equations for 2 DoF are:

$$m_1 \ddot{x}_1 + c_1 \dot{x}_1 + k_1 x_1 = -F_r \cos \alpha - F_t \sin \alpha \quad (3.5)$$

$$m_2 \ddot{x}_2 + c_2 \dot{x}_2 + k_2 x_2 = -F_r \sin \alpha + F_t \cos \alpha \quad (3.6)$$

which can be rearranged in a state-space matrix form as:

$$\begin{bmatrix} \dot{\mathbf{x}} \\ \ddot{\mathbf{x}} \end{bmatrix} = \begin{bmatrix} \mathbf{O} & \mathbf{I} \\ \mathbf{M}^{-1} \mathbf{K} & -\mathbf{M}^{-1} \mathbf{C} \end{bmatrix} \begin{bmatrix} \mathbf{x} \\ \dot{\mathbf{x}} \end{bmatrix} \quad (3.7)$$

where \mathbf{O} is the null matrix, \mathbf{I} is the identity matrix and the rest of the matrices are detailed as:

$$\begin{aligned} \mathbf{x} &= \begin{bmatrix} x_1 \\ x_2 \end{bmatrix}; \mathbf{K} = \begin{bmatrix} K_{11} & K_{12} \\ K_{21} & K_{22} \end{bmatrix}; \\ \mathbf{C} &= \begin{bmatrix} c_1 & 0 \\ 0 & c_2 \end{bmatrix}; \mathbf{M} = \begin{bmatrix} m_1 & 0 \\ 0 & m_2 \end{bmatrix} \end{aligned} \quad (3.8)$$

where

$$\begin{aligned}
 K_{11} &= V_c A_p (K_r \cos^2 \alpha + K_t \cos \alpha \sin \alpha) - \omega_1^2 \\
 K_{12} &= V_c A_p \sin \alpha (K_r \cos \alpha + K_t \sin \alpha) \\
 K_{21} &= V_c A_p \cos \alpha (K_r \sin \alpha - K_t \cos \alpha) \\
 K_{22} &= V_c A_p (K_r \sin^2 \alpha - K_t \cos \alpha \sin \alpha) - \omega_2^2
 \end{aligned} \tag{3.9}$$

From Eq. 3.7, matrix form equations for a lightly dampened structure are the following:

$$\{\ddot{\mathbf{x}}\} = \mathbf{H}\{\mathbf{x}\} \quad ; \quad \mathbf{H} = \mathbf{M}^{-1}\mathbf{K} = [\Sigma_m + \Sigma_p] \tag{3.10}$$

where

$$\Sigma_m = \begin{bmatrix} -\omega_1^2 & 0 \\ 0 & -\omega_2^2 \end{bmatrix} \tag{3.11}$$

and

$$\Sigma_p = V_c A_p \begin{bmatrix} P_{11} & P_{12} \\ P_{21} & P_{22} \end{bmatrix} \tag{3.12}$$

where

$$P_{11} = \frac{K_r \cos^2 \alpha + K_t \cos \alpha \sin \alpha}{m_1} \tag{3.13}$$

$$P_{12} = \frac{\sin \alpha (K_r \cos \alpha + K_t \sin \alpha)}{m_1} \tag{3.14}$$

$$P_{21} = \frac{\cos \alpha (K_r \sin \alpha - K_t \cos \alpha)}{m_2} \tag{3.15}$$

$$P_{22} = \frac{K_r \sin^2 \alpha - K_t \cos \alpha \sin \alpha}{m_2} \tag{3.16}$$

The matrices Σ_m and Σ_p respectively consider the workpiece and the cutting process.

3.3 Stability analysis of the system

When the dynamics of a system are slowly varying, the concept of a frozen system makes sense. The frozen system is obtained by freezing the physical parameters of the time varying system at a time instant. The FTF is then defined as the transfer function of the frozen system (Zadeh, 1951; Louarroudi et al., 2012). From Eq. 3.10, the following assumptions were considered to simplify the system stability analysis.

- The system is lightly dampened ($c_1 = c_2 = 0$). In machining, damping values of workpiece are usually small (Urbikain et al., 2015).
- The effective masses are similar for both modes ($m_1 \approx m_2 \approx m$) because the workpiece is a symmetrical cylinder.

The characteristic equation is obtained solving $\det(H - \lambda I) = 0$. The following closed form expression for the squared eigenvalues of matrix H is obtained:

$$\lambda^2 = \frac{1}{2} \left[\frac{V_c A_p K_r}{m} - \omega_1^2 - \omega_2^2 \pm \frac{A_p K_r}{m} \sqrt{V_c^2 + ABV_c + D} \right] \quad (3.17)$$

where

$$A = \frac{2m \sqrt{K_r^2 + K_t^2} (\omega_2^2 - \omega_1^2)}{A_p K_r^2} \quad (3.18)$$

$$B = \cos \left[2\alpha + \arctan \left(\frac{K_t}{K_r} \right) \right] \quad (3.19)$$

$$D = \left[\frac{m (\omega_2^2 - \omega_1^2)}{A_p K_r} \right]^2 \quad (3.20)$$

From Eq. 3.17, two couples of complex conjugated eigenvalues are obtained ($\lambda_i = \sigma_i \pm j\omega_i$), which both depend on the workpiece parameters (m , ω_1 and ω_2) and the cutting conditions (V_c , K_r , K_t and A_p). When at least one of the eigenvalues has a positive real part, the system is unstable. For $K_r = K_t = 0$ system eigenvalues are a couple of conjugated imaginary numbers, $\pm j\omega_1$ and $\pm j\omega_2$, which are the eigenvalues of the workpiece without considering the influence of the cutting process.

3.3.1 Analysis of system stability, as a function of cutting speed and tool relative angular position

According to Eq. 3.17, the stability of the system depends on the discriminant, $g(V_c, \alpha)$ (see Eq. 3.21). When $g(V_c, \alpha) < 0$, the real part of one of eigenvalues is positive, so the system becomes unstable. Therefore, the system stability depends on the sign of $g(V_c, \alpha)$. In figure 3.2 the surface of function $g(V_c, \alpha)$ is presented:

$$g(V_c, \alpha) = V_c^2 + ABV_c + D \quad (3.21)$$

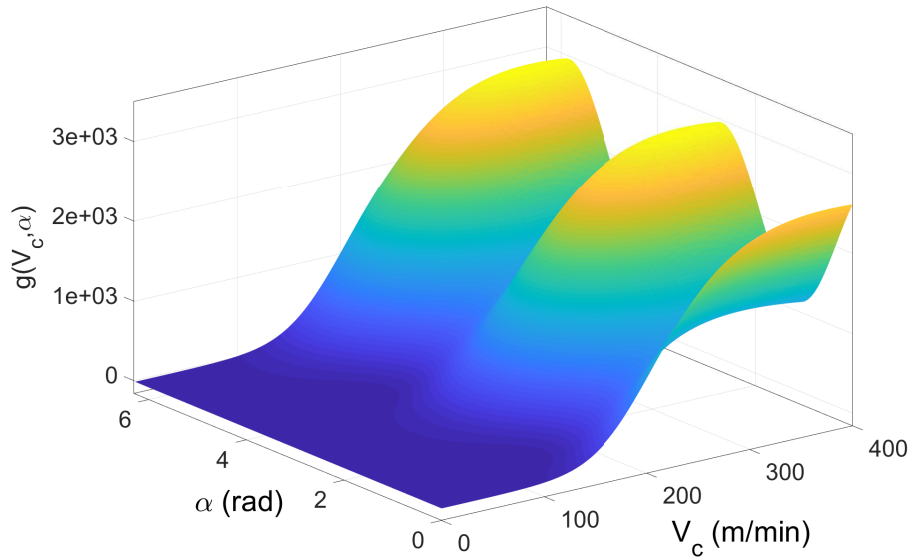


FIGURE 3.2: Surface of function $g(V_c, \alpha)$

Taking into account that $D > 0$ and that V_c , K_r and K_t are real positive numbers, there are only two cases (C_1 and C_2) that depend on the tool relative angular position (α) and the cutting speed (V_c) (see table 3.1). Depending on the tool relative angular position, B can take values between $[-1, 1]$. The minimum amplitude for $g(V_c, \alpha)$ occurs when $B = -1$ and the resulting equation is:

$$g(V_c)_{\min} = V_c^2 - AV_c + D \quad (3.22)$$

Figure 3.3a shows C_1 and C_2 cases of $g(V_c, \alpha)$ depending on the value of V_c . For case C_1 , $g(V_c, \alpha)$ takes always positive values, and it is given by:

$$V_c^2 + D > |-AV_c| \quad (3.23)$$

On the other hand, case C_2 considers the case where $g(V_c)_{\min} < 0$, which is fulfilled in the range $[V_{c1}, V_{c2}]$ (see figure 3.3b).

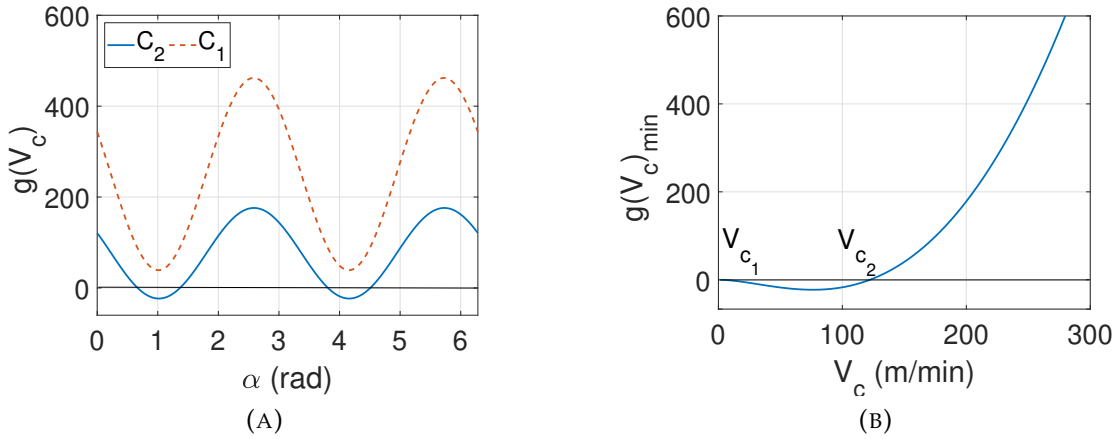


FIGURE 3.3: **A** C_1 and C_2 curves, **B** $g(V_c)_{\min}$ for C_2 curve

TABLE 3.1: Stability cases

Cases	Condition	Stability
-	$g(V_c)_{\max} < 0$	unstable
C_1	$g(V_c)_{\min} > 0$	conditional stability
C_2	$g(V_c)_{\min} < 0, V_{c1} < V_c < V_{c2}$	stable-unstable

Case C_1 . Conditional stability as a function of V_c

From the square root of function $g(V_c, \alpha)$, two real values ($\pm d$) are obtained as solutions due to $g(V_c)_{\min} > 0$. From the negative solution ($-d$), a couple of conjugated imaginary eigenvalues ($\lambda = \pm j\omega$) are obtained from Eq. 3.17 if

$$V_c < \frac{m(\omega_1^2 + \omega_2^2)}{A_p K_r} \quad (3.24)$$

On the other hand, the eigenvalues obtained from the positive solution(+ d) are also a couple of conjugated imaginary numbers ($\lambda = \pm j\omega$) only if

$$\left| \frac{V_c A_p K_r}{m} - \omega_1^2 - \omega_2^2 \right| > \left| \frac{A_p K_r}{m} \sqrt{V_c^2 - AV_c + D} \right| \quad (3.25)$$

Correspondingly, the system is stable in a Bounded Input Bounded Output (BIBO) sense.

Case C_2 . Stable-unstable case

In this case, $g(V_c)_{min}$ function takes negative values when V_c is in the range $[V_{c1}, V_{c2}]$. As it is shown in figure 3.3a, case C_2 , the system becomes unstable depending on the tool relative angular position, so that the system has stable and unstable intervals in each round. In the range $[V_{c1}, V_{c2}]$ natural frequencies converge to ω_c frequency (see figure 3.4b) while the interval is unstable and it is defined by:

$$\omega_c = \text{Imag} \left\{ \sqrt{\frac{1}{2} \left(\frac{V_c A_p K_r}{m} - \omega_1^2 - \omega_2^2 \right)} \right\} \quad (3.26)$$

Figures 3.4a and 3.4b show the natural frequencies for B equal to 1 and -1 respectively. The eigenvalues obtained for unstable interval from Eq. 3.17 are two complex numbers which give place to the following four eigenvalues, $\lambda = \pm \sqrt{a \pm j\omega}$ with $a, \omega \in \mathbb{R}$. Eigenvalues are couples of conjugated complex numbers. As the real part of one of the couples is positive, the system is unstable.

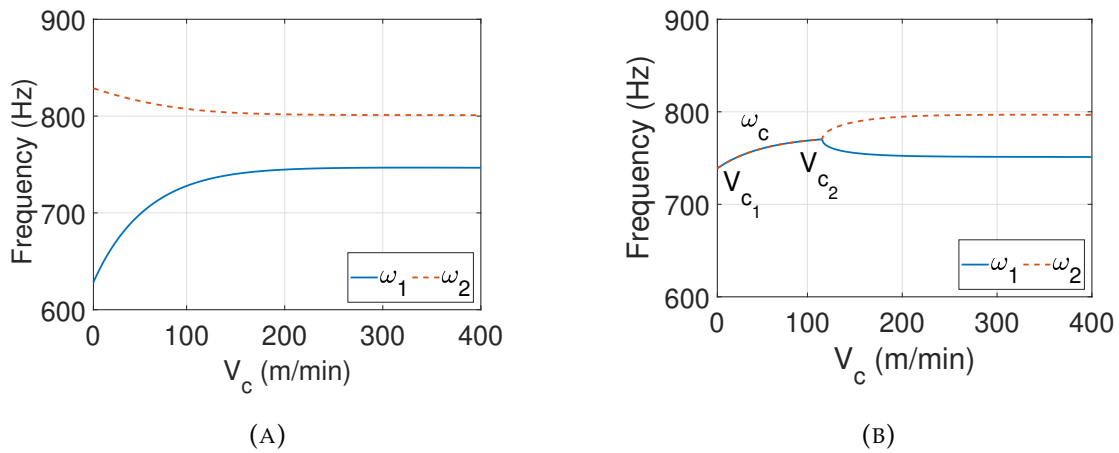


FIGURE 3.4: **A** Natural frequencies evolution as a function of V_c for the stable interval, **B** Natural frequencies evolution as a function of V_c for the unstable interval

3.4 Experimental results

The validation procedure for the developed model was divided into three main part: (I) system parameter identification, (II) model simulation with identified parameters and (III) experimental test in a CNC lathe.

First, the dimensions and the material of a slender workpiece were defined and it was clamped to the spindle trough a self-centering chuck with hard jaws. Then, a modal analysis were carried out to obtain the modal parameters of the system. Moreover, machining tests were carried out to obtain the cutting constants of the workpiece material. After that, numerical simulations with the identified parameters were carried out to obtain the stability predictions by the developed model. Finally, machining tests were carried out on the lathe to validate the results obtained by numerical simulations of the model.

3.4.1 System parameters identification

The experimental work was carried out in a Danobat Danumerik CNC lathe which is shown in Figure 3.5. A slender C45 steel workpiece, which dimensions are specified in table 3.2, was clamped to the spindle trough a self-centering chuck with hard jaws.



FIGURE 3.5: Danobat Danumerik CNC lathe

TABLE 3.2: Workpiece parameters

Parameter	Values
Workpiece material	Steel C45
Material density (ρ)	7800 Kg/m ³
Workpiece length (l)	121.7 mm
Workpiece diameter (d)	38.2 mm

The lower two structural modes were identified by a hammer impact test using a Bruel & Kjaer 8206-003 impact hammer and PCB356A16 triaxial accelerometer. Several tests were carried out in different angular positions of the workpiece. Figure 3.6 shows the FRFs of the workpiece fixed in the lathe at 70, 110 and 150 degrees. According to Blevins (2015), the theoretical natural frequency of the clamped beam

described in table 3.2 would be 1827 Hz. However, since the clamping with with hard jaws is not totally stiff, the frequencies are lower than theoretical, as explained in chapter 2. Two nearby main modes of 784.8 Hz and 805.5 Hz were identified and the maximum magnitude of these modes were in 70 and 150 degrees position respectively. Figure 3.7 shows workpiece mode directions. The workpiece parameters are shown in the Table 3.3.

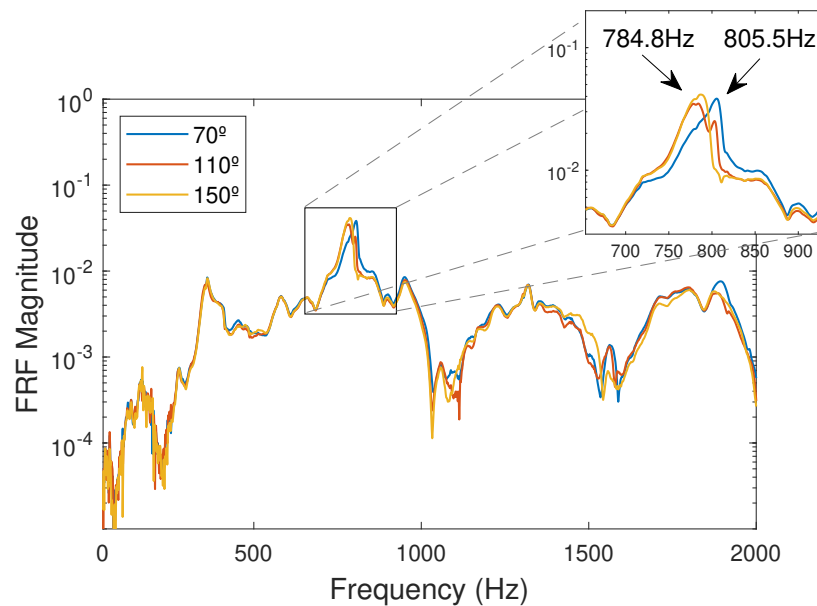


FIGURE 3.6: Frequency response function of the workpiece in different angular positions obtained by a hammer impact test

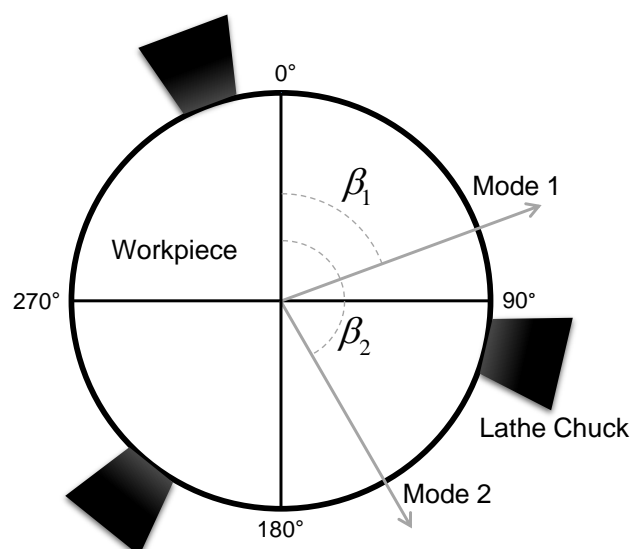


FIGURE 3.7: Workpiece mode directions

TABLE 3.3: Workpiece modal parameters

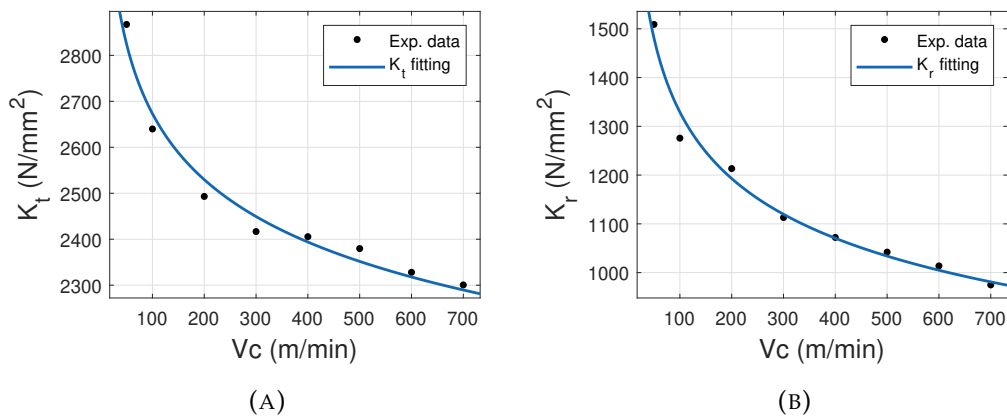
Parameter	Values
Mode 1	
Natural frequency (ω_1)	784.8 Hz
Direction angle (β_1)	70°
Modal mass (m_1)	4.18 Kg
Damping ratio (ζ_1)	0.71 %
Mode 2	
Natural frequency (ω_2)	805.5 Hz
Direction angle (β_2)	150°
Modal mass (m_2)	4.16 Kg
Damping ratio (ζ_2)	0.74 %

The cutting constants were experimentally obtained. The material employed was carbon steel C45. The bars were processed by isothermal annealing, in which the austenization temperature was set to 860°. The ferrite-pearlite ratio (%ferrite / %pearlite) of the material was 25/75, and the average grain size of ferrite/perlite was 17/25 microns. With regards to the mechanical properties, mechanical tests gave 339 MPa yield stress and 863 MPa ultimate tensile strength at 0.5 s⁻¹ strain rate and ambient temperature. Several machining tests were carried out using the cutting conditions presented in Table 3.4. Cutting constants were calculated from $K_s = F/A_p h_m$. Figure 3.8a and 3.8b shows the evolution of the radial and tangential cutting constants with the cutting speed for $h_m = 0.2$ mm/rev. These were obtained in the Matlab Curve Fitting tool using a Power function defined as:

$$K_i = a_i V_c^{b_i - 1} \quad (3.27)$$

TABLE 3.4: Parameters and measuring instruments

Parameters	Cutting Conditions
Cutting speed (V_c)	50-700 <i>m/min</i>
Depth of cut (A_p)	1 <i>mm</i>
Feed (h_m)	0.1-0.4 <i>mm/rev</i>

FIGURE 3.8: Evolution of cutting constants with V_c

3.4.2 Model Simulation

The model presented in Section 3.2 was simulated, considering parameters from the experimental set-up. The cutting conditions and the simulation parameters are presented in table 3.5. The workpiece rotation speed was fixed in order to analyse the cutting speed influence on the stability. Therefore, the cutting speed decreases as the workpiece is machined.

TABLE 3.5: Simulation parameters

Parameter	Values
Solver	Runge-Kutta 4
Step time	1×10^{-4} s
Simulation time	7 s
Workpiece initial diameter	38.2 mm
Workpiece rotation speed (n)	1200 RPM
Workpiece rotation frequency (f_r)	20 Hz
Cutting speed (V_c)	144 to 50 m/min
Depth of cut (A_p)	1 mm
Feed (h_m)	0.2 mm/rev

The model presented in section 3.2 assuming $c_1 = c_2 = 0$ was simulated (Eq. 3.7). Figure 3.9 shows the system natural frequencies as a function of the cutting speed, V_c . Continuous lines represents the natural frequencies obtained from model simulation. Dashed lines and dotted lines correspond to the natural frequencies calculated from Eq. 3.17 when B takes the value -1 and 1 , $g(V_c)_{min}$ and $g(V_c)_{max}$ respectively. The frequencies (ω_1, ω_2) oscillate between minimum and maximum lines with workpiece rotation frequency. It can be observed that frequencies (ω_1, ω_2) converge at unstable intervals to the same value, $\omega_c = 792.8$ Hz, from $V_c = 120$ m/min.

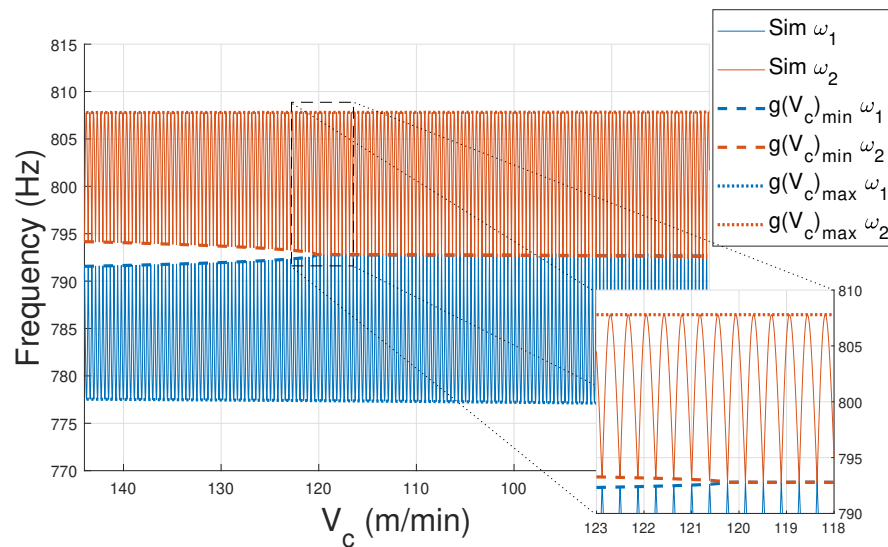


FIGURE 3.9: Natural frequencies as a function of V_c without damping

The real system stability was also analysed taking into account damping values obtained from the hammer impact test in section 3.4.1. In figure 3.10 can be observed that the system turns unstable at $V_c = 105$ m/min. Dashed lines correspond to the natural frequencies calculated from Eq. 3.17 (without damping) in order to show the damping influence. The simulation shows a similar system behaviour. Results suggest that the assumptions made in section 3.2 were valid. Nevertheless, taking into account the damping, the system is still stable at lower cutting speeds as expected.

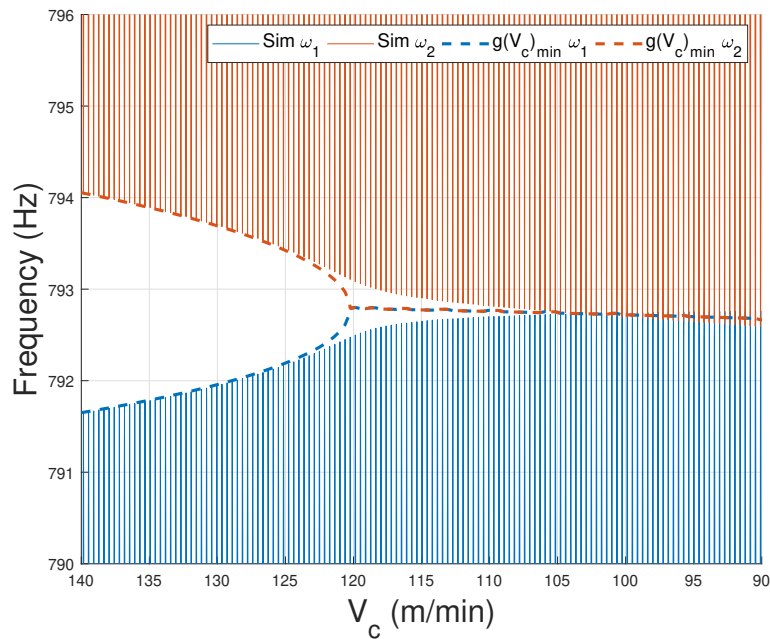


FIGURE 3.10: Natural frequencies as a function of V_c with damping

It must be emphasized that the system only gets unstable for intervals in each turn, so the system is stable for most of the cycle. However, the system tends to be unstable due to wave regeneration. In unstable intervals, waves are generated on the surface due to the vibration of the workpiece. In the next revolution, the previous revolution surface ($u(t - \tau)$), affects on the dynamic chip thickness, resulting in $h(t) = h_m - u(t) + u(t - \tau)$. This phenomena is known as regenerative effect. Figure 3.11 shows time domain simulation considering the regenerative effect where it can be observed that the system turns unstable from $V_c = 105$ m/min. The dashed line shows when the tool loose contact with the workpiece due to the displacement in radial direction is higher than the cutting feed.

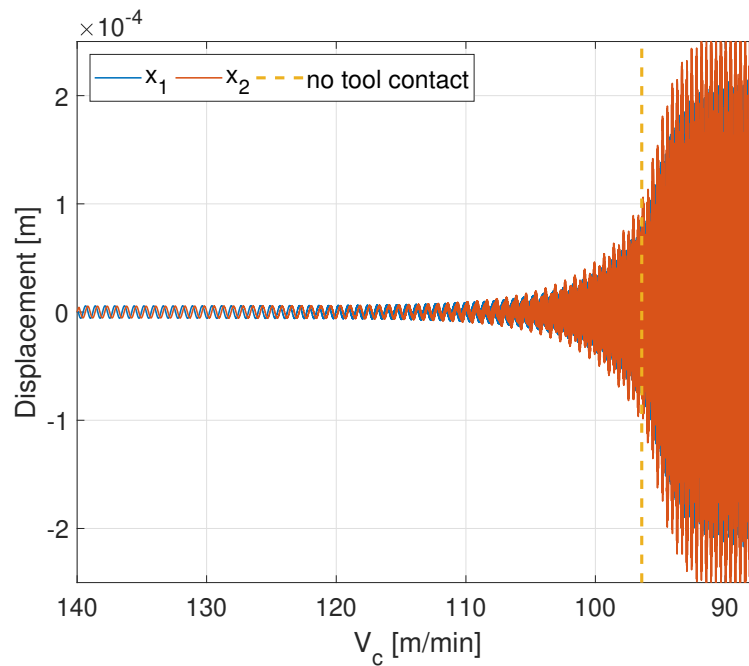


FIGURE 3.11: Time domain simulation considering the regenerative effect

3.4.3 Machining tests

Experimental tests were conducted in a Danobat Danumerik CNC lathe to verify the simulated results. A slender bar was machined by a facing operation with constant feed (h_m) and rotation speed (n). The diameter of the piece decreases as the workpiece is machined, causing a reduction in cutting speed (V_c). Cutting forces, workpiece vibrations and machine tool vibrations were measured (see Figure 3.12 and 3.12). Experimental test parameters, cutting conditions and measuring instruments are presented in Table 3.6.

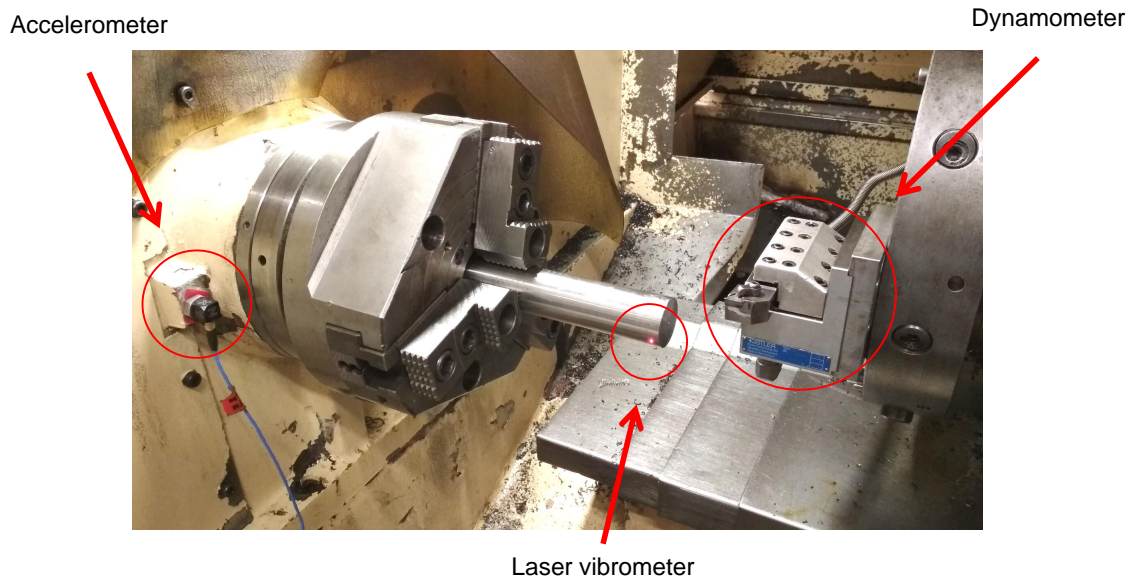


FIGURE 3.12: CNC experimental set-up

TABLE 3.6: Test parameters, cutting conditions and measuring instruments

Parameters	
Machine Tool	Danobat horizontal lathe
Tool	TPUN160308 TTM
Workpiece material	Steel C45
Workpiece cantilever length	121.7 mm
Workpiece diameter	38.2 mm
Cutting conditions	
Spindle speed (n)	1200 RPM
Cutting speed (V_c)	145 to 75 m/min
Depth of cut (A_p)	1 mm
Feed (h_m)	0.2 mm/rev
Measuring Instruments	
Cutting forces	Kistler 9121 dynamometer
Workpiece vibrations	Polytec OFV 5000 laser vibrometer
Machine vibrations	PCB356A16 triaxial accelerometer
Acquisition equipment	NI cDAQ7178 with NI9239 & NI9234 at 10240S/s

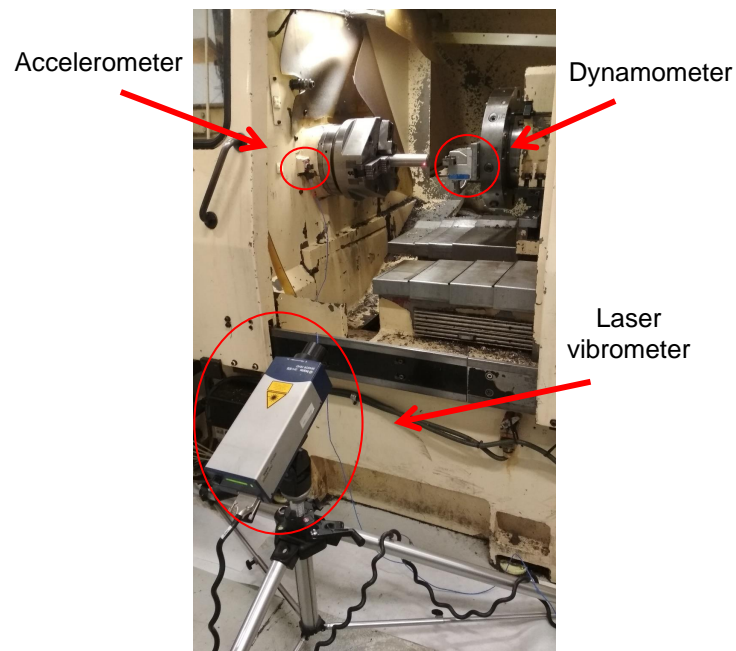


FIGURE 3.13: CNC experimental set-up

Figure 3.14 shows the measured cutting forces. The test began cutting at 145 m/min. The cutting process remained stable up to $V_c = 105$ m/min, as predicted by the theoretical model. At this point, the system became unstable and a strong cutting force variation can be observed. It is worth highlighting that the mean value of the cutting forces tends to increase as cutting speed decreases. Figures 3.15a and 3.15b show tangential cutting forces and machine tool vibrations respectively in the frequency domain for stable and unstable periods. Importantly, a strong frequency component is observed at 792.5 Hz for the unstable period in both measurements.

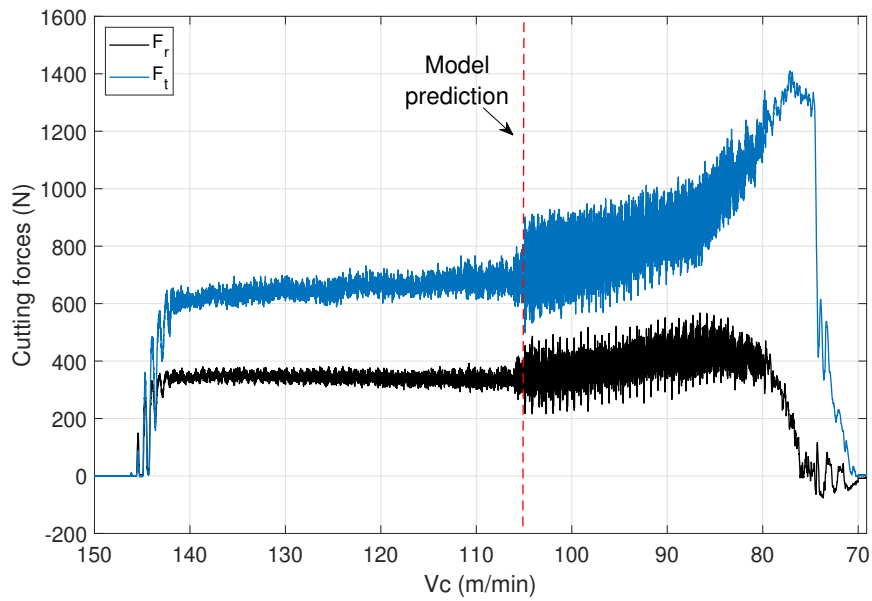


FIGURE 3.14: Radial and tangential cutting forces

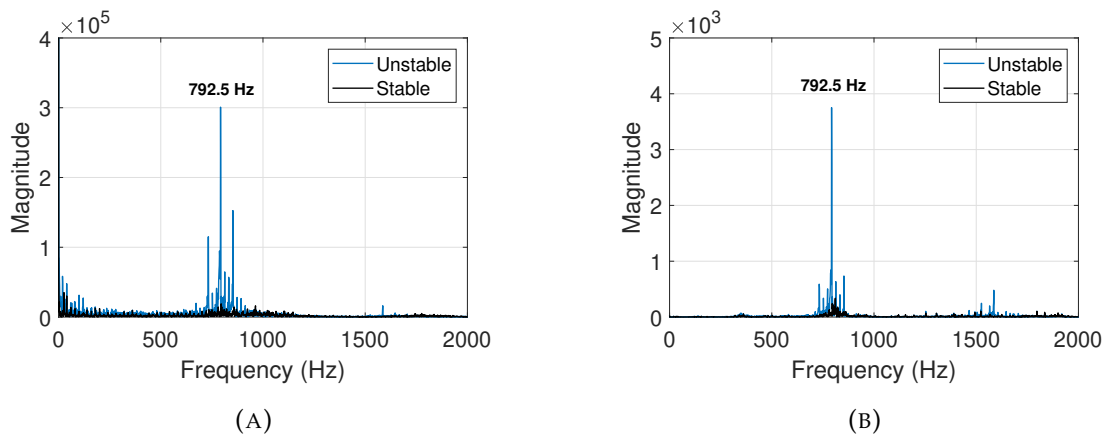
FIGURE 3.15: **A** Tangential cutting forces and **B** machine-tool accelerations in the frequency domain during unstable/stable machining

Figure 3.16 shows the workpiece vibration velocity measured by the laser vibrometer. At $V_c = 105$ m/min, the amplitude of the vibration started to increase significantly. The system became unstable, in agreement with the theoretical model.

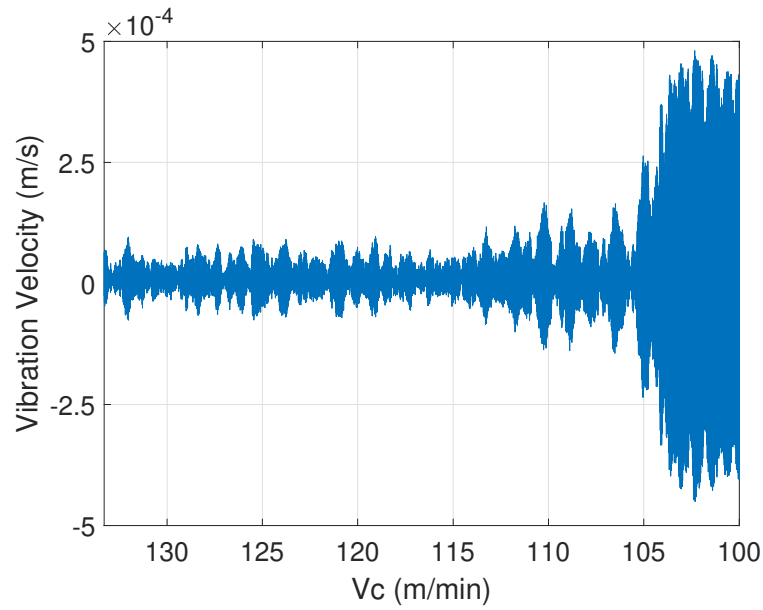


FIGURE 3.16: Workpiece vibration velocity in the time domain

Figure 3.17 shows the workpiece vibration velocity's spectrogram versus simulation $g(V_c)_{min}$ and $g(V_c)_{max}$ frequencies. It can be observed the two mode frequencies converging to 792.5Hz due to the mode coupling, in agreement with the theoretical model.

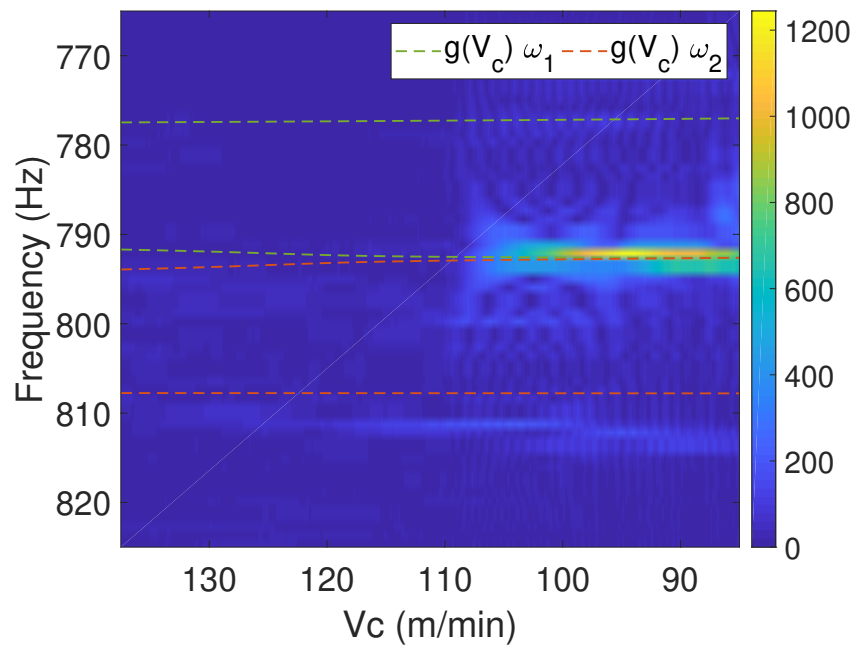


FIGURE 3.17: Workpiece vibration velocity spectrogram

According to the proposed method, its time the workpiece is clamped to the machine or the workpiece is machined, a new modal test should be carried out. The industrial application of this methodology becomes costly. In order to simplify the procedure, the following assumptions has been evaluated experimentally:

- The two modes angle are defined as $\beta_1 - \beta_2 = \pi/2$.
- The damping ratio is obtained once for each workpiece, clamping and machine tool.

With these assumptions, just detecting the natural frequencies, estimation of the stability of the cutting process can be approximated. Two additional case studies have been carried out considering these assumptions: (I) a case study with other geometry where the process is unstabilized during the machining and (II) a case study with another geometry where the process is stable during the machining test.

In the first case, the workpiece cantilever has been increased by 3 mm. The other cutting conditions of the test were not changed. The natural frequencies identified were $\omega_1 = 763.2$ Hz and $\omega_2 = 785.7$ Hz. Considering the assumptions listed above, according to the model the system turns unstable at $V_c = 115$ m/min. In Figure 3.18, it can be observed that the system is unstabilized at $V_c = 112$ m/min in the experimental test.

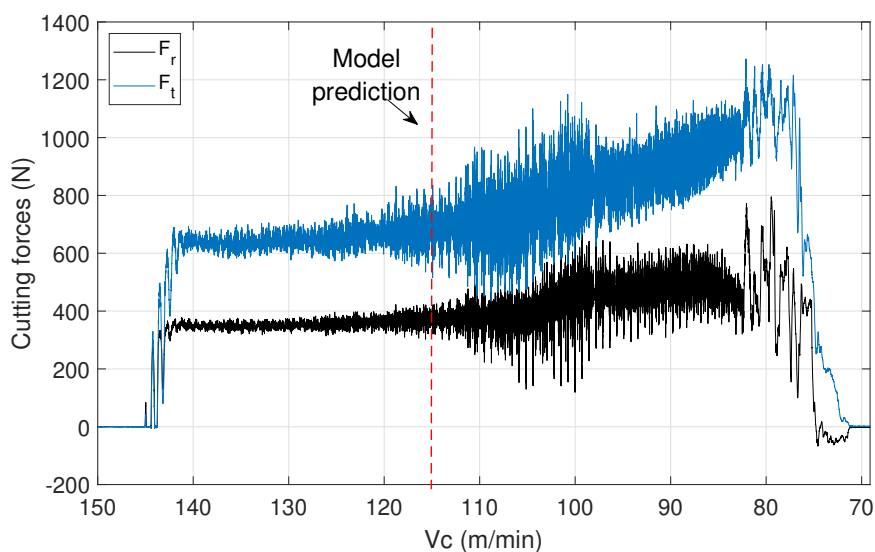


FIGURE 3.18: Radial and tangential cutting forces of case study 1

In the second case, the workpiece cantilever has been decreased to 100 mm ensuring the stability of the process according to the model. The other cutting conditions of the test were not changed. The natural frequencies identified were $\omega_1 = 901.3$ Hz and $\omega_2 = 920.1$ Hz. Considering the assumptions listed above, according to the model the system is always stable between experimental test cutting conditions. Figure 3.19 shows the cutting forces during the machining test with 100 mm cantilever. It can be observed that the machining is stable throughout the test.

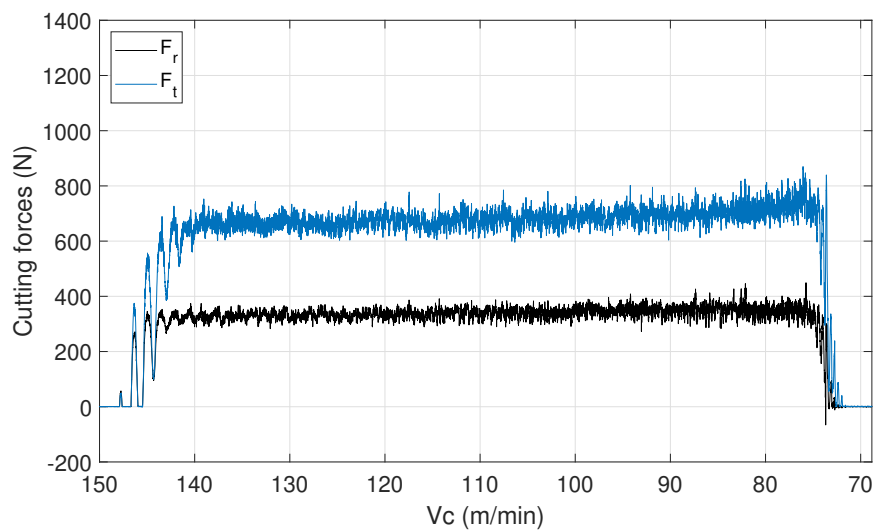


FIGURE 3.19: Radial and tangential cutting forces of case study 2

It can be said that the stability prediction obtained from the simulations shows good agreement with the experimental results and the considered assumptions are valid to obtain an approximate estimation of the stability of the cutting process.

Chapter 4

Stability prediction by LTP model

4.1 Introduction

The optimal selection of cutting conditions in machining is crucial. Both process productivity and stability depend on them. The selection of severe cutting conditions will improve the MRR of the process, increasing productivity. However, this can lead to stability problems in the cutting process and negatively affect the finishing of the part.

In this chapter, the system is modelled as an LTP system and the SLDs are obtained to determine the chatter-free cutting conditions. The model takes into account both modal coupling and regenerative effect. Finally, the theoretical results are validated against the experimental results.

4.2 State-Space LTP Model

A flexible workpiece with 2 DoF under orthogonal metal cutting forces was modelled as a LTP system. The model was based on the following assumptions:

- A nonlinear force model with variable cutting coefficients: the cutting constants varies with the cutting speed.
- A flexible workpiece and a rigid tool are always in contact: a 2 DoF model is used to study the case of flexible workpiece.

- The gyroscopic effect due to the rotation of the workpiece is neglected.

Figure 4.1 describes a flexible workpiece with 2 DoF (x_1 and x_2) under orthogonal metal cutting forces with a tool moving around the workpiece with a constant cutting speed (V_c). For each DoF, the workpiece has associated stiffness, k_i , viscous damping c_i and effective mass m_i . F_r and F_t are radial and tangential forces respectively. The angular position of the tool relative to the workpiece is represented by $\omega_r t$, where ω_r is the workpiece angular velocity.

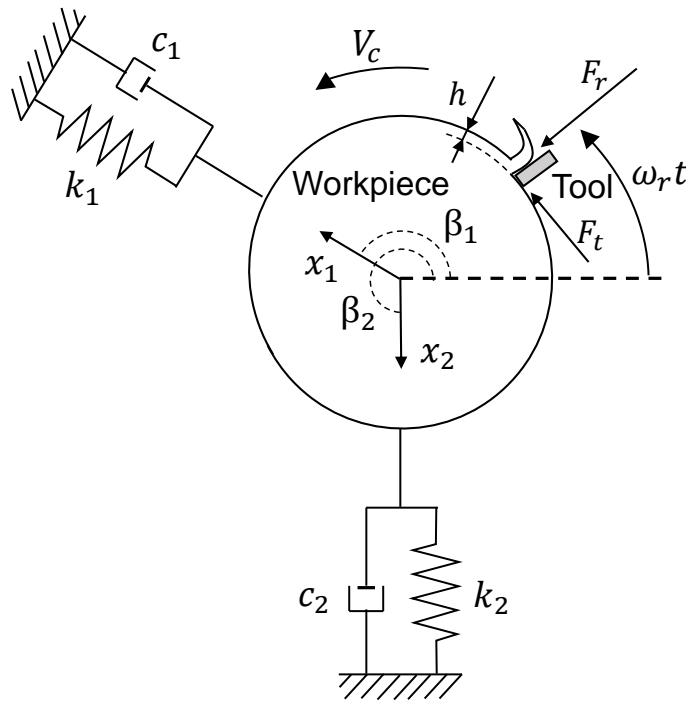


FIGURE 4.1: 2 DoF model in orthogonal metal cutting

Based on the orthogonal model of cutting, the cutting force magnitude is proportional to the uncut chip section as:

$$F(t) = K_s A_p h(t) = K_s A_p (h_m - u(t) + u(t - \tau)) \quad (4.1)$$

where h_m is the mean uncut chip thickness, A_p is the depth of cut, K_s is the cutting constant.

The present workpiece displacement $u(t)$ and the previous revolution displacement $u(t - \tau)$ are detailed:

$$u(t) = x_1(t)\cos(\omega_r t - \beta_1) + x_2(t)\cos(\omega_r t - \beta_2) \quad (4.2)$$

$$u(t - \tau) = x_1(t - \tau)\cos(\omega_r t - \beta_1) + x_2(t - \tau)\cos(\omega_r t - \beta_2) \quad (4.3)$$

The variation of cutting coefficients with the cutting speed is taken into account by the model as described in previous chapter. So, the cutting forces are given by the following expressions:

$$F_r(t) = K_r V_c A_p (u(t - \tau) - u(t)) \quad (4.4)$$

$$F_t(t) = K_t V_c A_p (u(t - \tau) - u(t)) \quad (4.5)$$

The dynamic equations for 2 DoF are:

$$m_1 \ddot{x}_1(t) + c_1 \dot{x}_1(t) + k_1 x_1(t) = -F_r \cos(\omega_r t - \beta_1) - F_t \sin(\omega_r t - \beta_1) \quad (4.6)$$

$$m_2 \ddot{x}_2(t) + c_2 \dot{x}_2(t) + k_2 x_2(t) = -F_r \cos(\omega_r t - \beta_2) - F_t \sin(\omega_r t - \beta_2) \quad (4.7)$$

which can be rearranged in a state-space matrix form:

$$\begin{bmatrix} \dot{\mathbf{x}}(t) \\ \ddot{\mathbf{x}}(t) \end{bmatrix} = \begin{bmatrix} \mathbf{O} & \mathbf{I} \\ \mathbf{M}^{-1}\mathbf{K}(t) & -\mathbf{M}^{-1}\mathbf{C} \end{bmatrix} \begin{bmatrix} \mathbf{x}(t) \\ \dot{\mathbf{x}}(t) \end{bmatrix} + \begin{bmatrix} \mathbf{O} \\ \mathbf{M}^{-1}\mathbf{B}(t) \end{bmatrix} \mathbf{x}(t - \tau) \quad (4.8)$$

where \mathbf{O} is the null matrix, \mathbf{I} is the identity matrix and the rest of the matrices are detailed as:

$$\begin{aligned} \mathbf{x}(t) &= \begin{bmatrix} x_1(t) \\ x_2(t) \end{bmatrix}; \mathbf{K}(t) = \begin{bmatrix} K_{11} & K_{12} \\ K_{21} & K_{22} \end{bmatrix}; \mathbf{C} = \begin{bmatrix} c_1 & 0 \\ 0 & c_2 \end{bmatrix}; \\ \mathbf{M} &= \begin{bmatrix} m_1 & 0 \\ 0 & m_2 \end{bmatrix}; \mathbf{B}(t) = \begin{bmatrix} B_{11} & B_{12} \\ B_{21} & B_{22} \end{bmatrix}; \mathbf{x}(t - \tau) = \begin{bmatrix} x_1(t - \tau) \\ x_2(t - \tau) \end{bmatrix} \end{aligned} \quad (4.9)$$

where

$$\begin{aligned}
K_{11} &= V_c A_p (K_r \cos^2(\omega_r t - \beta_1) + K_t \cos(\omega_r t - \beta_1) \sin(\omega_r t - \beta_1)) - \omega_1^2 \\
K_{12} &= V_c A_p \sin(\omega_r t - \beta_2) (K_r \cos(\omega_r t - \beta_1) + K_t \sin(\omega_r t - \beta_1)) \\
K_{21} &= V_c A_p \cos(\omega_r t - \beta_1) (K_r \cos(\omega_r t - \beta_2) + K_t \sin(\omega_r t - \beta_2)) \\
K_{22} &= V_c A_p (K_r \cos^2(\omega_r t - \beta_2) + K_t \cos(\omega_r t - \beta_2) \sin(\omega_r t - \beta_2)) - \omega_2^2
\end{aligned} \tag{4.10}$$

and

$$\begin{aligned}
B_{11} &= V_c A_p \cos(\omega_r t - \beta_1) (K_r \cos(\omega_r t - \beta_1) - K_t \sin(\omega_r t - \beta_1)) \\
B_{12} &= V_c A_p \cos(\omega_r t - \beta_2) (K_r \cos(\omega_r t - \beta_1) - K_t \sin(\omega_r t - \beta_1)) \\
B_{21} &= V_c A_p \cos(\omega_r t - \beta_1) (K_r \cos(\omega_r t - \beta_2) - K_t \sin(\omega_r t - \beta_2)) \\
B_{22} &= V_c A_p \cos(\omega_r t - \beta_2) (K_r \cos(\omega_r t - \beta_2) - K_t \sin(\omega_r t - \beta_2))
\end{aligned} \tag{4.11}$$

4.3 Stability of a LTP system

The state space model presented in Section 4.2 has the following form:

$$\dot{x}(t) = A(t)x(t) + B(t)x(t - \tau) \tag{4.12}$$

where $A(t)$ and $B(t)$ matrices vary periodically over time.

The most commonly used case of linear system theory is the LTI system where the coefficient matrices are constant. The response is independent from the time the input is applied. When matrices vary periodically over time, the system is called LTP. The dynamics of an LTP system can be analysed using Floquet Theory (Floquet, 1883), which essentially converts a periodic matrix to a time invariant matrix via coordinate transformation. Thus the new state space model has the mathematical form of an LTI system, and can be studied using the well-established LTI techniques. The periodic response can be obtained by converting the solution of the new LTI model to the original coordinates (Insperger and Stepen, 2011).

$$\dot{x}(t) = \mathbf{A}(t), \quad \mathbf{A}(t) = \mathbf{A}(t + T) \tag{4.13}$$

Matrix $\mathbf{A}(t)$ is time-periodic at period T , called the principal period in contrast to the constant-coefficient matrix of LTI systems. For periodic ODEs, a stability condition is provided by the Floquet theory. The solution of Eq. (4.13) with the initial condition $\mathbf{x}(0)$ is given by $\mathbf{x}(t) = \mathbf{\Phi}(t)\mathbf{x}(0)$, where $\mathbf{\Phi}(t)$ is a fundamental matrix of Eq. (4.13). According to the Floquet theory, the fundamental matrix can be written in the form $\mathbf{\Phi}(t) = \mathbf{P}(t)e^{\mathbf{C}t}$, where $\mathbf{P}(t) = \mathbf{P}(t + T)$ is a periodic matrix with initial value $\mathbf{P}(0) = \mathbf{I}$, and \mathbf{C} is a constant matrix. The matrix $\mathbf{\Phi}(T) = e^{\mathbf{C}T}$ is called the monodromy matrix or Floquet transition matrix of Eq. (4.13). This matrix gives the connection between the initial state and the state one principal period later, $\mathbf{x}(T) = \mathbf{\Phi}(T)\mathbf{x}(0)$. The eigenvalues of $\mathbf{\Phi}(T)$ are the characteristic multipliers ($\mu_j, j = 1, 2, \dots, n$) also called Floquet multipliers calculated from

$$\det(\mu\mathbf{I} - \mathbf{\Phi}(T)) = 0 \quad (4.14)$$

The eigenvalues of matrix \mathbf{C} are the characteristic exponents ($\lambda_j, j = 1, 2, \dots, n$) given by

$$\det(\lambda\mathbf{I} - \mathbf{C}) = 0 \quad (4.15)$$

If μ is a characteristic multiplier, then there are characteristic exponents λ such that $\mu = e^{\lambda T}$, and vice versa. Due to the periodicity of the complex exponential function, each characteristic multiplier is associated with infinitely many characteristic exponents of the form $\lambda_k = \gamma + i(\omega + k2\pi/T)$, where $\lambda, \omega \in \mathbb{R}$, $k \in \mathbb{Z}$, and $T\omega \in [-\pi, \pi]$

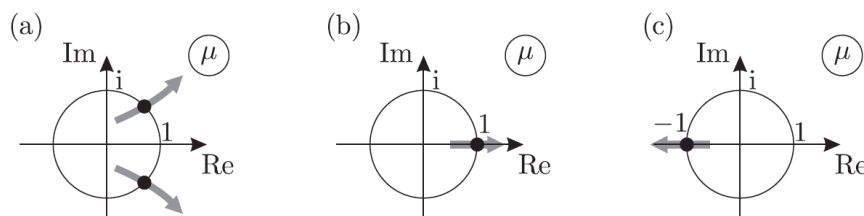


FIGURE 4.2: Critical characteristic multipliers for periodic systems: (a) secondary Hopf bifurcation, (b) cyclic-fold bifurcation, and (c) period-doubling bifurcation. (Insperger and Stepan, 2011)

The trivial solution $x(t) \equiv 0$ of Eq. (4.13) is asymptotically stable if and only if all the characteristic multipliers have modulus less than one, that is, all the characteristic exponents have negative real parts. Similarly to autonomous systems, the basic types of loss of stability can be classified according to the location of the critical characteristic multipliers (Guckenheimer and Holmes, 1983). For periodic systems, there are three typical cases:

1. The critical characteristic multipliers form a complex conjugate pair crossing the unit circle, i.e., $|\mu| = 1$ and $|\bar{\mu}| = 1$, as shown by case (a) in Figure 4.2. This case is topologically equivalent to the Hopf bifurcation of autonomous systems and is called secondary Hopf (or Neimark–Sacker) bifurcation.
2. The critical characteristic multiplier is real and crosses the unit circle at $+1$, as shown by case (b) in Figure 4.2. The bifurcation that arises is topologically equivalent to the saddle-node bifurcation of autonomous systems and is called cyclic-fold (or period-one) bifurcation.
3. The critical characteristic multiplier is real and crosses the unit circle at -1 , as shown by case (c) in Figure 4.2. There is no topologically equivalent type of bifurcation for autonomous systems. This case is called period-doubling (or period-two or flip) bifurcation.

Generally, the monodromy matrix cannot be determined in closed form, but there exist several numerical and semi-analytical techniques to approximate it. Using zeroth-order semi-discretization (Insperger and Stepan, 2011) results in:

$$\dot{\mathbf{y}}(t) = \mathbf{A}_i \mathbf{y}(t) + \mathbf{B}_i \mathbf{y}(t_{i-r}), \quad t \in [t_i, t_{i+1}] \quad (4.16)$$

where $t_i = ih$ is the discrete time scale, $h = T/p$ is the discretization step, p is the period resolution, $r = \text{int}(\tau/h)$ is the delay resolution, and

$$\mathbf{A}_i = \frac{1}{h} \int_{t_i}^{t_{i+1}} \mathbf{A}(t) dt, \quad \mathbf{B}_i = \frac{1}{h} \int_{t_i}^{t_{i+1}} \mathbf{B}(t) dt \quad (4.17)$$

Solving over the interval $[t_i, t_{i+1}]$ gives

$$\mathbf{y}_{i+1} = \mathbf{P}_i \mathbf{y}_i + \mathbf{R}_{i,0} \mathbf{y}_{i-r} \quad (4.18)$$

where

$$\mathbf{P}_i = e^{\mathbf{A}_i h} \quad (4.19)$$

$$\mathbf{R}_{i,0} = \int_0^h e^{\mathbf{A}_i(h-s)} ds \mathbf{B}_i \quad (4.20)$$

The monodromy matrix (Φ) is obtained by p repeated applications of the discrete map $\mathbf{z}_{i+1} = \mathbf{G}_i \mathbf{z}_i$ with initial state \mathbf{z}_0 ,

$$\Phi = \mathbf{G}_{p-1} \mathbf{G}_{p-2} \cdots \mathbf{G}_0 \quad (4.21)$$

where

$$\mathbf{z}_i = \begin{pmatrix} \mathbf{y}_i & \mathbf{y}_{i-1} & \mathbf{y}_{i-2} & \cdots & \mathbf{y}_{i-r} \end{pmatrix}^T = \begin{pmatrix} x_i & \dot{x}_i & x_{i-1} & x_{i-2} & \cdots & x_{i-r} \end{pmatrix}^T \quad (4.22)$$

and

$$\mathbf{G}_i = \begin{bmatrix} \mathbf{P}_i & 0 & \cdots & 0 & \mathbf{R}_{i,0} \\ \mathbf{D} & 0 & \cdots & 0 & 0 \\ 0 & \mathbf{I} & \cdots & 0 & 0 \\ \vdots & & \ddots & & \vdots \\ 0 & 0 & \cdots & \mathbf{I} & 0 \end{bmatrix} \quad (4.23)$$

4.4 Stability limits prediction

The stability limits of the model presented in Section 4.2 was analysed considering the parameters obtained in Section 3.4.1. The parameters of the workpiece are shown in table 4.1.

TABLE 4.1: Workpiece parameters

Parameter	Values
Workpiece material	Steel C45
Material density (ρ)	7800 Kg/m ³
Workpiece length (l)	121.7 mm
Workpiece diameter (d)	38.2 mm
Mode 1	
Natural frequency (ω_1)	784.8 Hz
Direction angle (β_1)	70°
Effective mass (m_1)	4.18 Kg
Damping ratio (ζ_1)	0.71 %
Mode 2	
Natural frequency (ω_2)	805.5 Hz
Direction angle (β_2)	150°
Effective mass (m_2)	4.16 Kg
Damping ratio (ζ_2)	0.74 %

The SLD obtained by means of the LTP model presented in section 4.2 and Altintas well known LTI model from the literature (Altintas, 2012) were compared. In the comparison, the cutting speed influence was not taken into account. Figure 4.3 shows the SLDs obtained from the presented LTP model analysed by Floquet theory and the LTI model from the literature using Table 4.1 parameters and $h_m = 0.2$ mm/rev. It is apparent from this figure that the LTI model is more stable than the LTP model. It can be observed that the minimum and maximum critical depth of cut (b_{lim}) for the LTP model are lower. The minimum b_{lim} for the LTI model is 1.1

mm. Interestingly, for the LTP model the minimum b_{lim} decreases slightly to 0.9 mm as the workpiece rotation speed (n) increases.

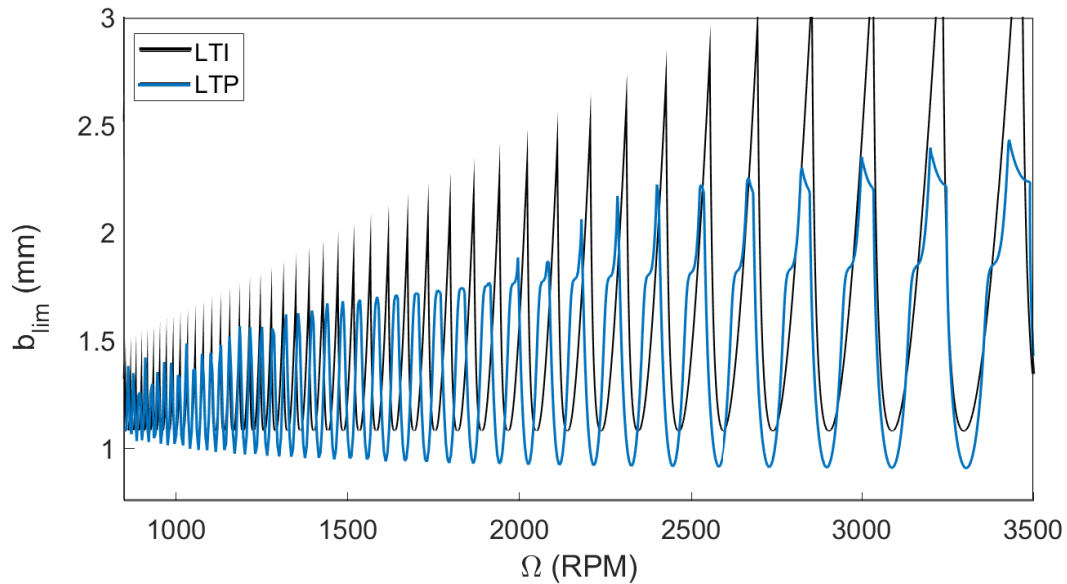


FIGURE 4.3: Comparison of SLD obtained from the LTI model and the LTP model

On the other hand, taking into account the cutting speed influence, more accurate stability limits were obtained. Figure 4.4 shows the critical depth of cut for the workpiece rotation speed of 1200 Revolutions per minute (RPM). It can be observed that the critical depth of cut of the system increases with the cutting speed. Under these conditions, the cutting process with 1mm of depth of cut is stable up to $V_c = 105$ m/min. Although the most important parameter is the rotation speed, it is worth highlighting that the cutting speed has a significant influence on the b_{lim} .

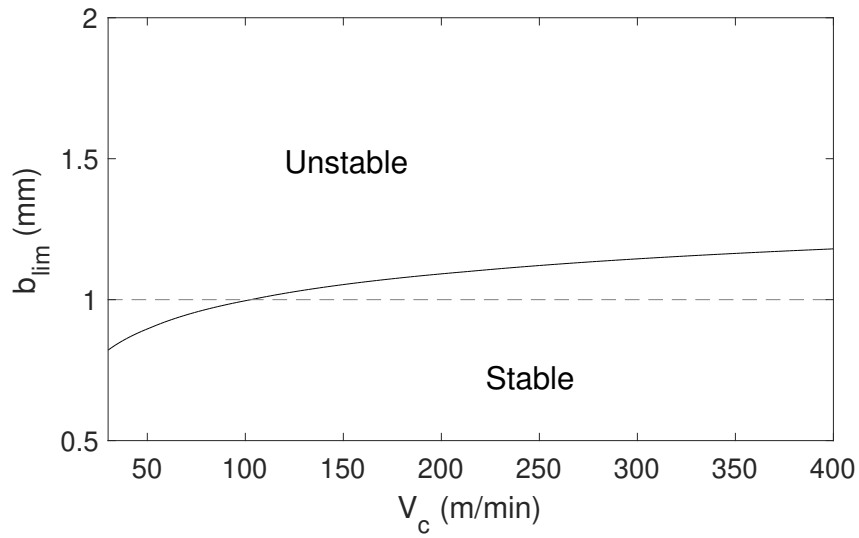


FIGURE 4.4: Stability lobe obtained from LTP model considering the cutting speed influence

Combining both variables, cutting speed and rotation speed, a 3D SLD is obtained. The critical depth of cut (b_{lim}) for each condition is shown in the Figure 4.5.

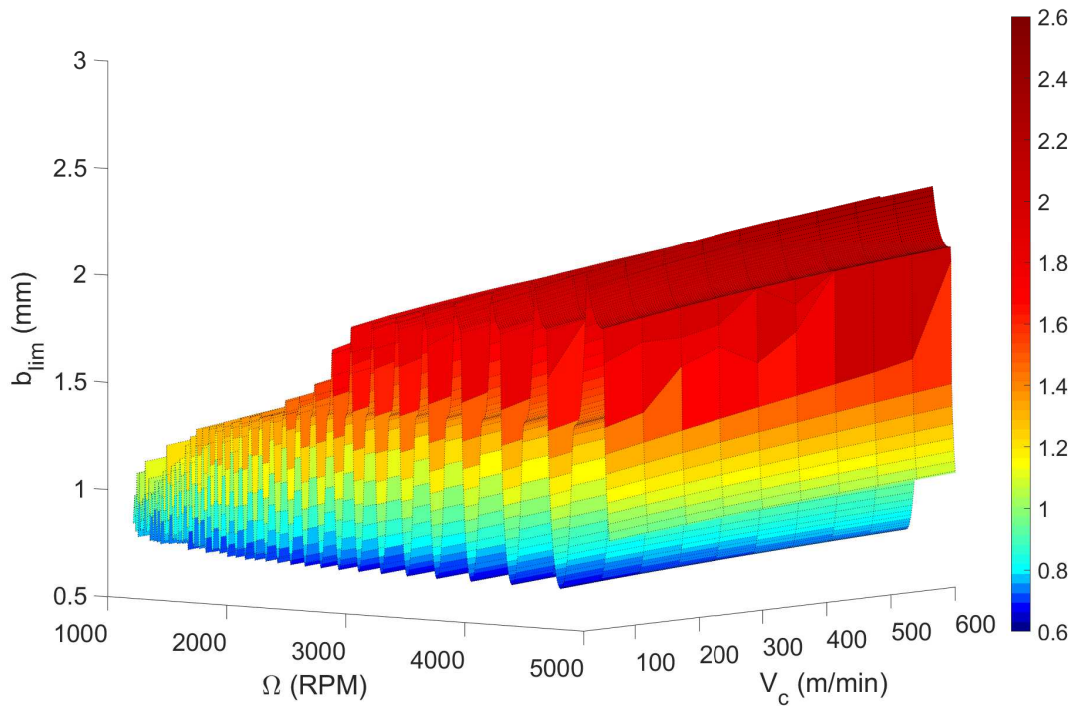


FIGURE 4.5: SLD obtained from LTP model considering both cutting speed and rotation speed

The optimum cutting conditions for the described workpiece can be determined based on the 3D SLD obtained from the LTP model. It is worth highlighting that these calculations require a high computational cost.

On the other hand, the time domain simulation of the LTP model was carried out using the cutting conditions and simulation parameters presented in table 4.2. The diameter of the piece decreases as the workpiece is machined and therefore the cutting speed also reduces.

TABLE 4.2: Simulation parameters

Parameter	Values
Step time	1×10^{-4} s
Workpiece initial diameter	38.2 mm
Workpiece rotation speed (n)	1200 RPM
Workpiece rotation frequency (f_r)	20 Hz
Cutting speed (V_c)	145 to 50 m/min
Depth of cut (A_p)	1 mm
Feed (h_m)	0.2 mm/rev

Figure 4.6 shows the time domain simulation of the LTP model where it can be observed that the system became unstable at about $V_c = 105$ m/min. The dashed line shows the instant when the tool lost contact with the workpiece due to the fact that the radial displacement was greater than the cutting feed.

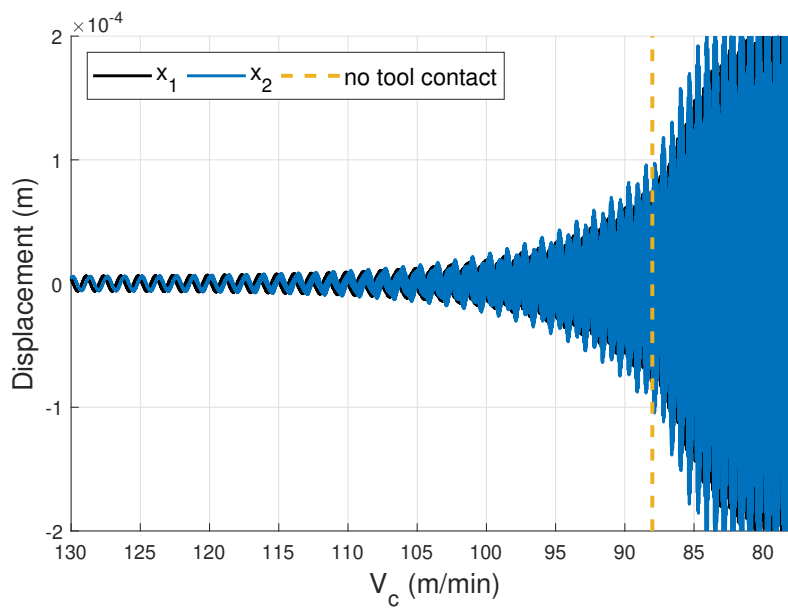


FIGURE 4.6: Time domain simulation of LTP model

4.5 Experimental results

The stability prediction obtained from the SLD and time simulations of the LTP model show good agreement with the experimental results presented in Section 3.4 (see Figures 3.14, 3.15a, 3.15b, 3.16 and 3.17). Figure 4.7 shows the cutting forces. The system became unstable as the cutting speed decreased, as predicted by the model at $V_c = 105$ m/min (see Figure 4.4).

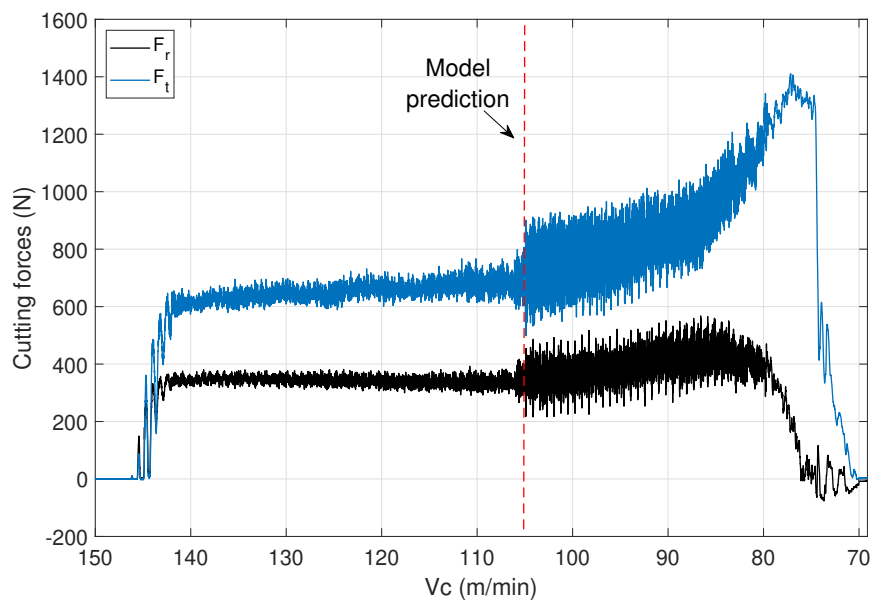


FIGURE 4.7: Radial and tangential cutting forces

These results suggest that the proposed LTP model accurately describes machining dynamics of slender workpieces. The model allows to define chatter-free cutting conditions and improve productivity by maximizing the MRR.

Chapter 5

Internal signals based chatter monitoring

5.1 Introduction

Integration of sensors for process monitoring and control is expected to have a major impact on manufacturing in the coming years. There are two measurement methods to monitoring the machining process: direct and indirect methods.

Direct methods provide a direct measurement of the desired physical quantity with high accuracy. However, these methods remain expensive and difficult to apply in industrial environments because (I) the machining zone is hostile, (II) they modify the stiffness of the system and (III) the available space limits the size of the sensor to be employed. In contrast, indirect methods are more suitable for monitoring machining processes and are based on sensors that do not infer in the machining process as internal signals (currents, voltages, encoders). The major drawback is the capability of the captured signal to reflect the phenomena to be monitored.

In this chapter, process monitoring based on different signals is compared. Chatter detection is performed using available internal signals from the regulator. The accuracy and feasibility of internal signals for chatter monitoring is evaluated by direct measurements. Then, a monitoring system is developed on a fast prototyping generic hardware. Finally, the monitoring system is experimentally validated on a CNC lathe.

5.2 Feasibility of internal signals

According to the literature it can be said that cutting forces provide valuable information about the cutting process and the process stability. As it has been shown in chapter 3, when chatter occurs, vibrations are reflected in the cutting forces, where strong variations can be observed on force magnitudes at chatter frequency.

The cutting forces are related to the forces exerted by the motors of the axis and the spindle of the machine tool. Tangential cutting forces are related to the forces exerted by the spindle and are therefore related to the power consumption of the motor that drives the spindle. On the other hand, the axial and radial forces are related to the power consumption of the motors of the machine tool axis. This leads to the conclusion that by analysing the signals of currents and voltages of the motors, it could be possible to detect chatter.

On the other hand, accelerometers are also sensors widely used to detect chatter. These devices measure the vibrations produced in the machining process and provide direct measurements of magnitude and frequency of the vibration. Position encoders are used to measure, for example, the angular position of the spindle and the axis. These encoders are usually sensors with high precision, which could measure the position variations generated by chatter vibrations. The most common encoders used in machining are Transistor-Transistor Logic (TTL) or Sin-Cos type.

TTL encoders are digital sensors that generate pulses at the output when motion is detected. The resolution is determined by the number of pulses that the encoder transfers to the controller in a revolution. Sin-Cos encoders are analog sensors that generate sinusoidal outputs (see Figure 5.1). Analog waveform can provide infinite position resolution, so the measurement resolution is given by the resolution of the Analog-to-Digital Converter (ADC). Depending on the type of encoder, TTL or Sin-Cos type, a specific signal processing is required to obtain the position or displacement.

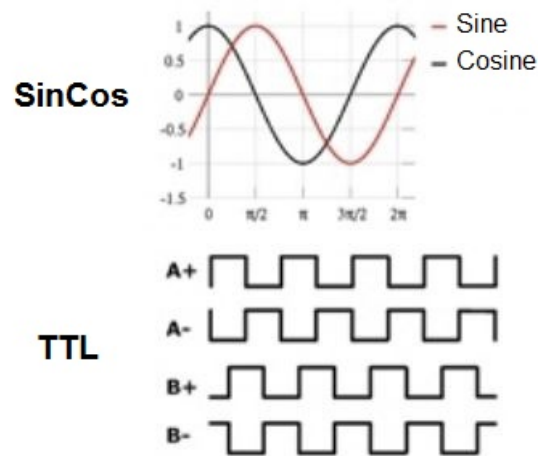


FIGURE 5.1: Sin-Cos and TTL encoders

To analyse the feasibility of internal signals to detect chatter, using the experimental set-up shown in chapter 3, the following methodology was carried out:

1. Perform preliminary machining tests with a slender workpiece in which the process becomes unstable and chatter is produced.
2. Measure the signals to be evaluated during machining tests: cutting forces, vibrations, currents, voltages and encoder signals.
3. Process and analyse the measured signals to identify chatter indicators.
4. Selection of the most suitable signals for chatter monitoring.

5.3 Experimental signal acquisition and comparison

Preliminary tests were carried out with chatter conditions. A turning operation of a slender bar with a diameter of 25 mm and length of 200 mm was carried out in the Danumerik lathe. In the experimental tests, in order to analyse the suitability for chatter detection, the following signals were measured with the listed equipment:

- Cutting forces by a Kistler 9121 dynamometer with a NI9239 module at 50 kS/s.

- Accelerations by PCB356A16 triaxial accelerometer with a NI9234 module at 50 kS/s.
- Spindle/ Axis currents by NI 9227 module at 50 kS/s.
- Spindle/ Axis voltages by NI9225 and NI9244 modules at 50 kS/s.
- Position from encoders by NI9223 module at 50 kS/s.

The voltage, current and encoder signals of the spindle and the two axis were obtained from the CNC electrical panel. The Danumerik lathe has two axis of movement. The X axis allows movement in the radial direction of the workpiece and the Z axis allows movement in the axial direction. The currents consumed by the two axis of the machine tool were measured directly by the NI9227 module. For measuring spindle currents, it was necessary to use ITB300S (see Figure 5.2) current transducers to condition the signals because the NI9227 module does not allow high currents. In the encoder signals, Motrona SV210 and GV210 splitters (see Figure 5.2) were used to avoid interfering with the machine tool.

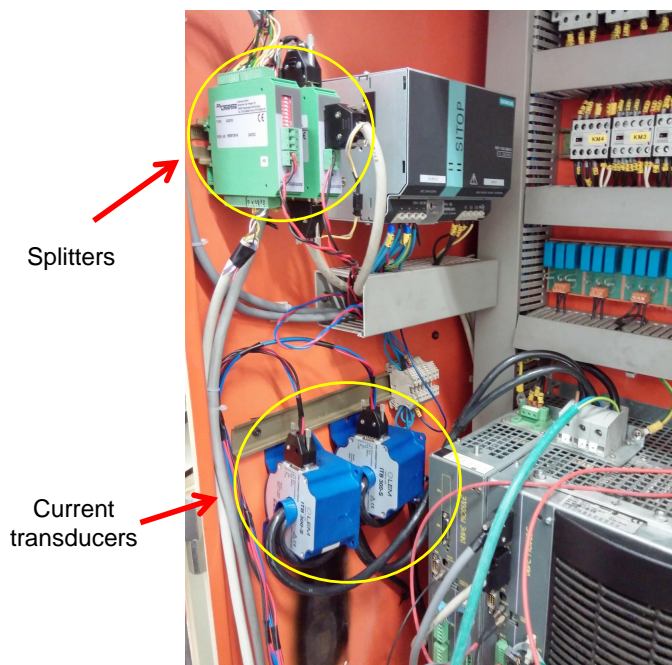


FIGURE 5.2: Electrical panel installed signal conditioners

Considering that chatter vibration occur at the frequency of the most dominant mode of the system, the first natural frequency of the system was identified using

a Montronix WLAN BoxNG Kit monitoring system. This device serves as a mobile diagnostic and monitoring instrument for machine tools using a wireless triaxial accelerometer. Figure 5.3 shows the impact test response of X-Y-Z axis (green, yellow and red respectively) in the time domain (above) and the frequency domain (below). The first natural frequency was identified in 498 Hz.

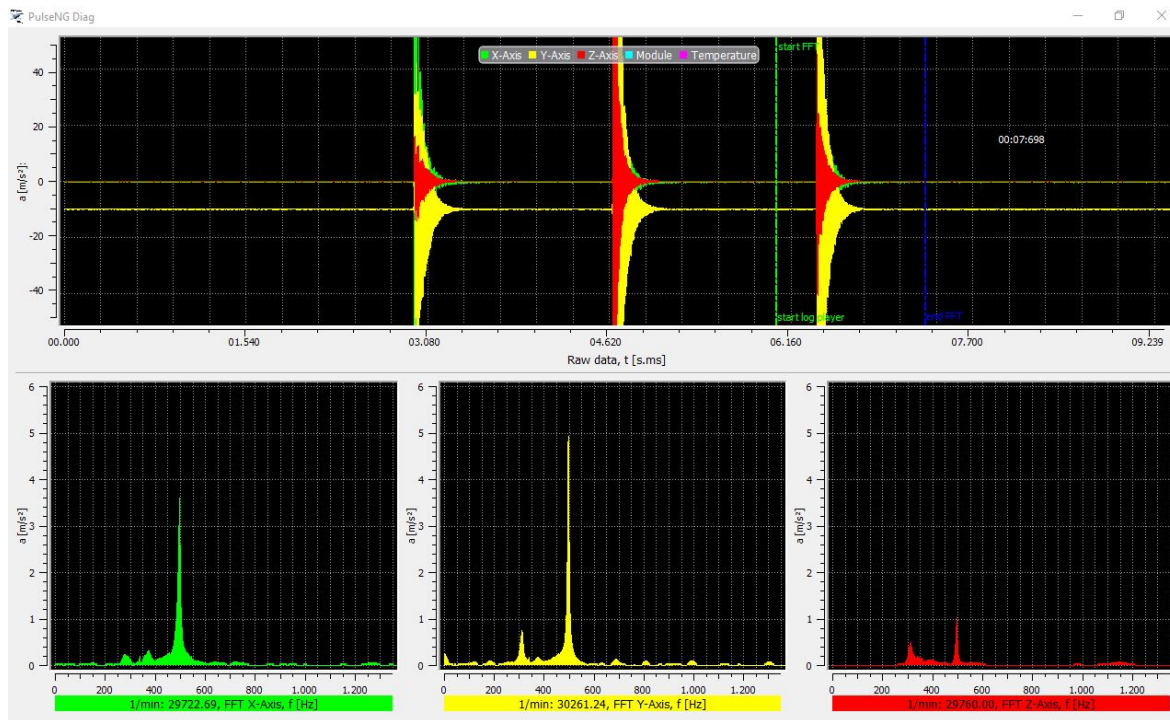


FIGURE 5.3: Natural frequency identification with Montronix WLAN BoxNG Kit.

The following figures show different the measurements of turning tests in the frequency domain. Figure 5.4 and Figure 5.5 show the Fast Fourier Transform (FFT) of spindle acceleration and cutting force raw signals respectively. The natural frequency of 498.3 Hz and its first harmonic at 996.6 Hz can be seen in both figures. However, in Figure 5.5, several frequency components are also observed. Therefore, according to the results, it can be said that the accelerations signals provides clearer information about chatter vibration than cutting forces and they are more suitable for chatter monitoring.

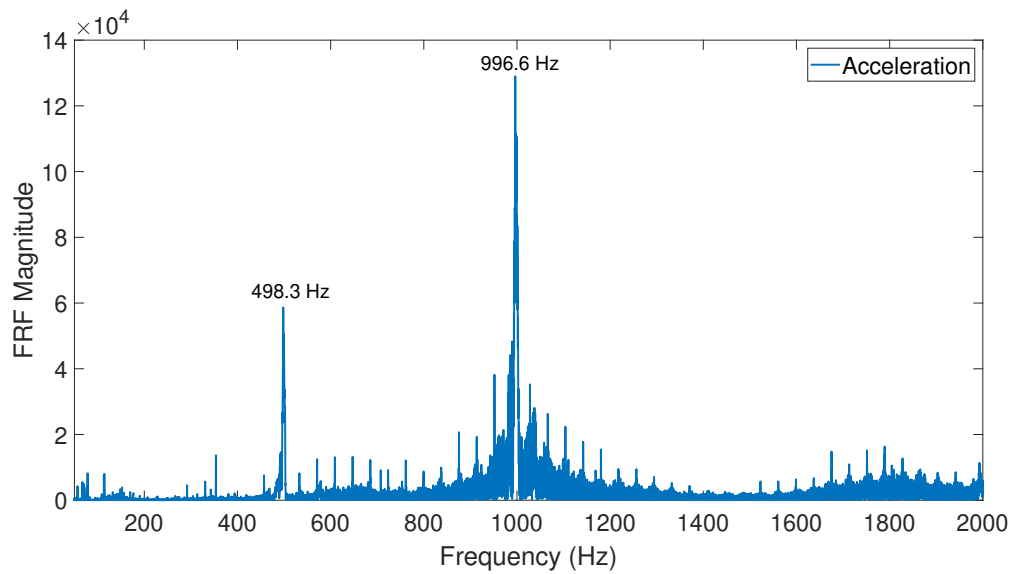


FIGURE 5.4: Acceleration signal in frequency domain.

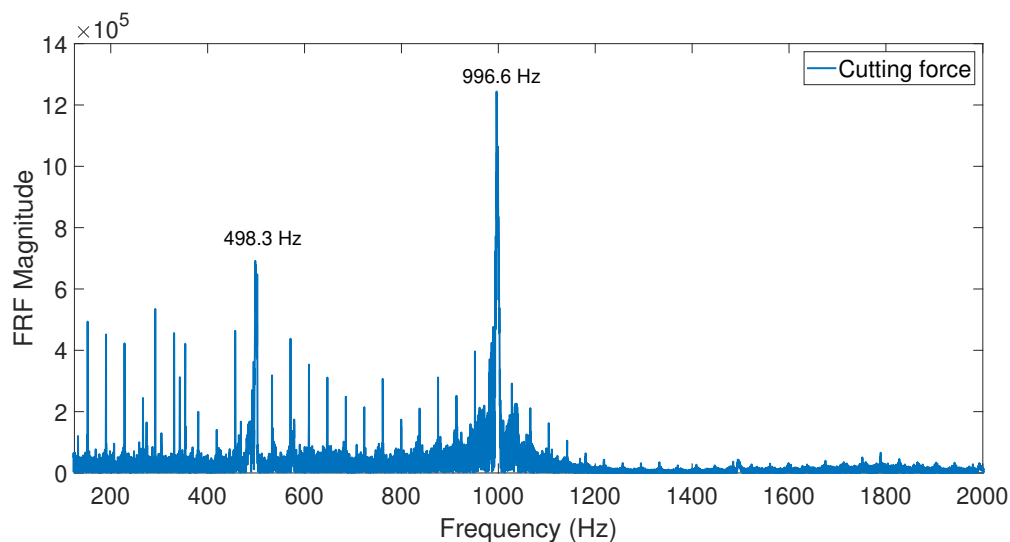


FIGURE 5.5: Cutting force signal in frequency domain.

Regarding measured internal signals, spindle and axis currents, voltages and encoder signals were analysed. Due to the high inertia of the spindle, no chatter vibrations were detected in its signals. Nevertheless, axis signals show evidence of chatter vibration. It is worth highlighting that the X axis measurements show more information about chatter. This is because the workpiece vibrates mostly in the radial direction, as shown in the turning simulation in Chapter 2. Figure 5.6 shows the raw current signal of the X axis in the frequency domain. The evidence of chatter

can be clearly seen in the signal spectrum. Strong component of 498.3 Hz can be seen in the figure. Current signals appear to be suitable for chatter monitoring.

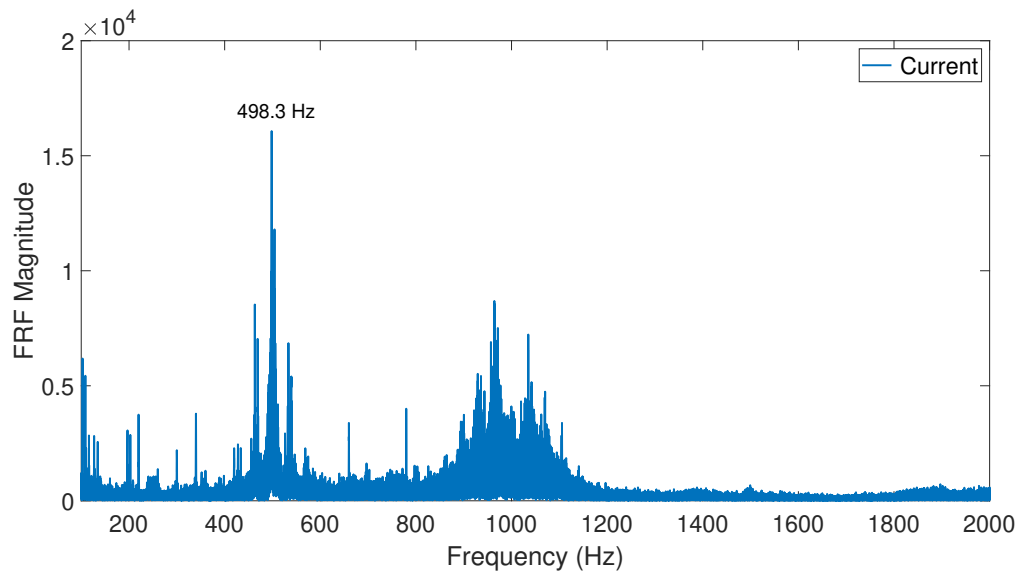


FIGURE 5.6: X axis current signal in frequency domain.

The following Figure 5.7 presents raw voltage measurement of lathe X axis in the frequency domain. Although a slight manifestation of the frequency of 498.3 Hz can be observed, the presence of other more significant frequency components is evident. Therefore, the possibility of monitoring chatter using axis voltages was discarded.

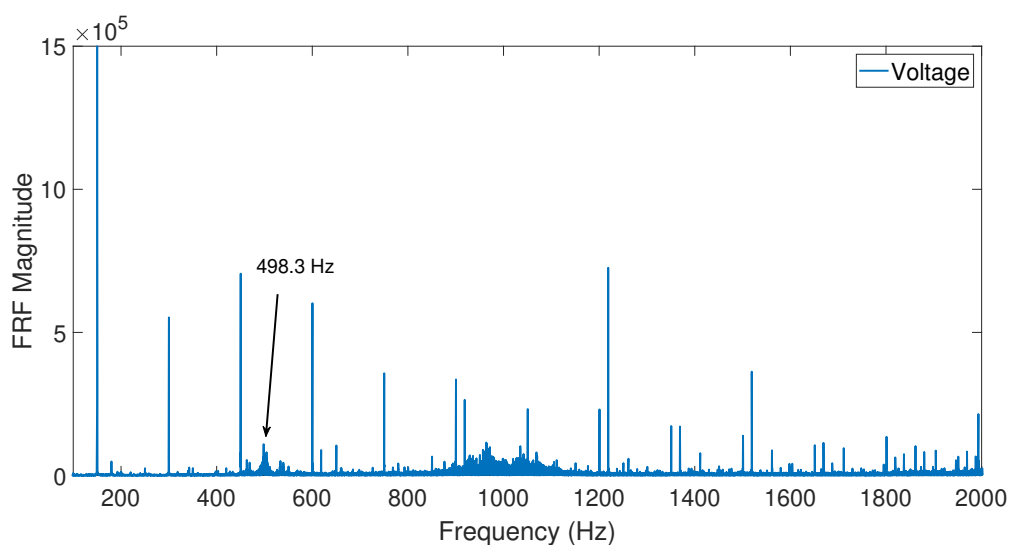


FIGURE 5.7: X axis voltage signal in frequency domain.

Regarding encoder signals, the Danumerik lathe has Sin-Cos encoders for both axis. The measured encoder signals were processed to obtain valuable information. Figure 5.8 shows the processing performed to the encoder signals. The output signals are two sinusoidal signals, A and B . Using $\text{atan}(A/B)$ function, the phase is obtained. Then, the phase angle is unwrapped. Whenever the jump between consecutive angles is greater than or equal to π radians, unwrap function shifts the angles by adding multiples of $\pm 2\pi$ until the jump is less than π . Finally, the phase angle is derivated.

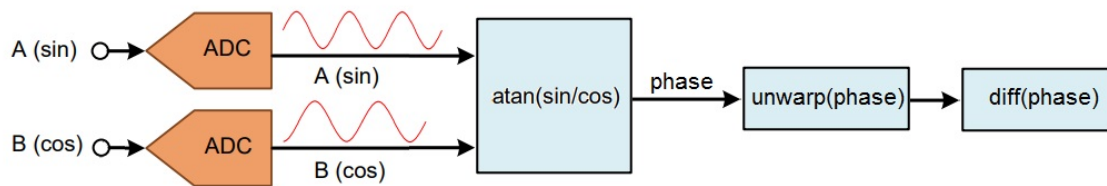


FIGURE 5.8: Sin-Cos encoder signal processing.

Figure 5.9 shows the signal obtained after processing in the frequency domain. Interestingly, the chatter frequency of 498.3 Hz can be observed in the figure. Similarly to current signals, chatter monitoring is apparently achievable using encoder signals.

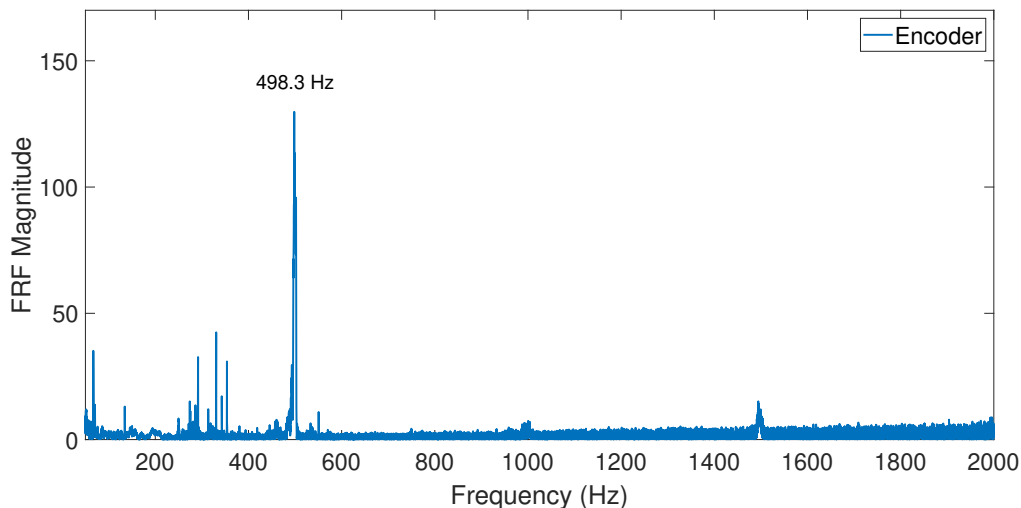


FIGURE 5.9: Encoder signal in frequency domain.

The results obtained from the preliminary test suggest that turning process stability can be monitored using internal signals. The currents and encoder signals seem

to be feasible to carry out the monitoring of the process. Encoder signals require a more complex signal processing and there are also several types of encoders. Although the current signals can be more sensitive to the noise and disturbances, it was decided to develop the monitoring system based on current signals. It is worth highlighting that using both signals would be the most effective solution.

5.4 Internal signals based chatter monitoring and control system development

A monitoring system for supervising the machining process based on currents was developed. All warnings and configuration controls are managed by an Human Machine Interface (HMI) developed in Labview. In addition, the monitoring system communicates with the CNC to act in case of chatter detection. Figure 5.10 shows the monitoring system architecture.

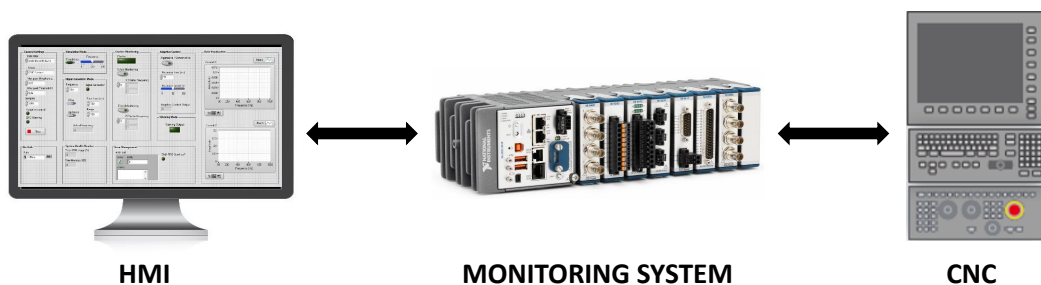


FIGURE 5.10: Monitoring system architecture.

5.4.1 Monitoring system hardware

The monitoring system has been implemented on a cRIO-9039 of National Instruments. It is an embedded controller for control and monitoring applications. This controller has a Field-Programmable Gate Array (FPGA) and a real-time processor running a Real Time (RT) Operating System (OS). This controller offers a variety of

connectivity ports and lets to add a HMI) to show process information and control the monitoring system options. In addition, several input and output modules are available for both analog and digital signals. In this case, the following modules have been used:

- NI9227: Analog current input module. 5 Arms. 4 channels. Up to 50 kS/s
- NI9263: Analog voltage output module. ± 10 V. 4 channels. Up to 100 kS/s



FIGURE 5.11: cRIO-9039 and I/O modules.

5.4.2 Monitoring system software

The monitoring system was developed by Labview. The monitoring software has three main parts: acquisition, detection and control. The acquisition and control loops were implemented on the FPGA. The detection algorithm and other secondary functions as communication, data logging and visualization were implemented on the real-time processor.

Acquisition

The acquisition part of the monitoring system was implemented on the FPGA as the sample rate limit for the RT processor is 1000 Hz. The FPGA allows higher sampling

frequencies, depending on the module used (up to MHz). The default sampling frequency of the X and Z axis currents is 5.12 KHz. The maximum sampling frequency is 50 KHz which is limited by the NI9227 input module. Once current signals are measured, the data is transferred to the real-time processor for signal processing.

Detection

Chatter detection is based on current signals from both axis of the lathe. The detection algorithm follows the next sequence:

1. The currents on the X and Z axes are measured.
2. A high-pass filter with a cut-off frequency of 75 Hz is applied to filter out lower frequencies.
3. FFT-based spectral measurement is performed (default number of samples 5120). The spectrum is obtained and the peak amplitudes are displayed.
4. Peak detection is performed based on the preset maximum threshold. The sensitivity of the system is adjusted with this threshold.
5. In case of detecting peaks that exceed the threshold, the chatter warning is activated and the monitoring system executes the selected control mode.

Figure 5.12 shows the flow diagram of the detection algorithm.

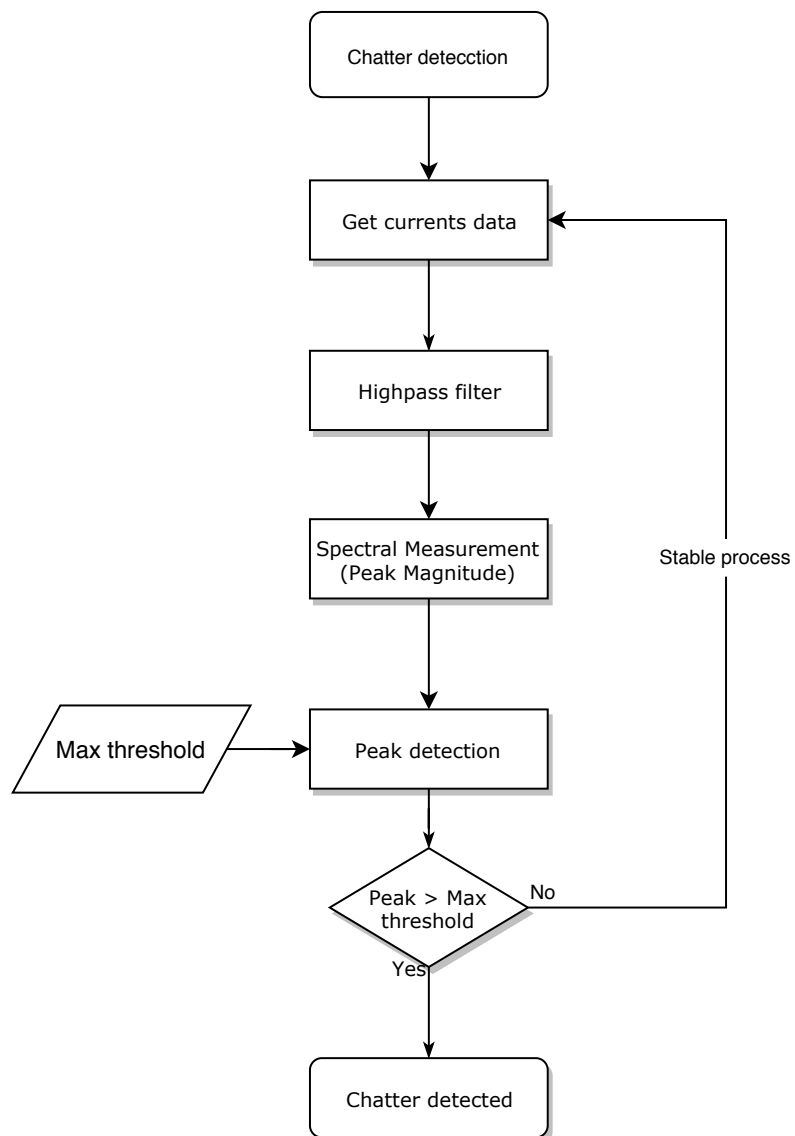


FIGURE 5.12: Detection algorithm flow diagram.

Control

The most extended and effective chatter suppression method for turning is SSV. Due to the dynamic limitations of the Danumerik lathe, it is not possible to implement SSV method. The actual lathe configuration does not allow speed variations required by the SSV method without overheating. For this reason, the following two control modes were implemented to act in case of chatter detection:

- **CNC control mode:** In this mode the system only monitors the process. When chatter is detected, the monitoring system enables an output that alerts the CNC. The response to the chatter is managed at the CNC according to its capabilities.
- **Adaptive control mode:** The monitoring system not only alerts the CNC, but also adapts the cutting conditions. The adaptive control algorithm can adopt an aggressive or conservative strategy. Depending on this, it will increase or decrease the cutting conditions in the range defined by the user. The control outputs a setpoint that is handled at the CNC.

Figure 5.13 shows the flow diagram of the control algorithm.

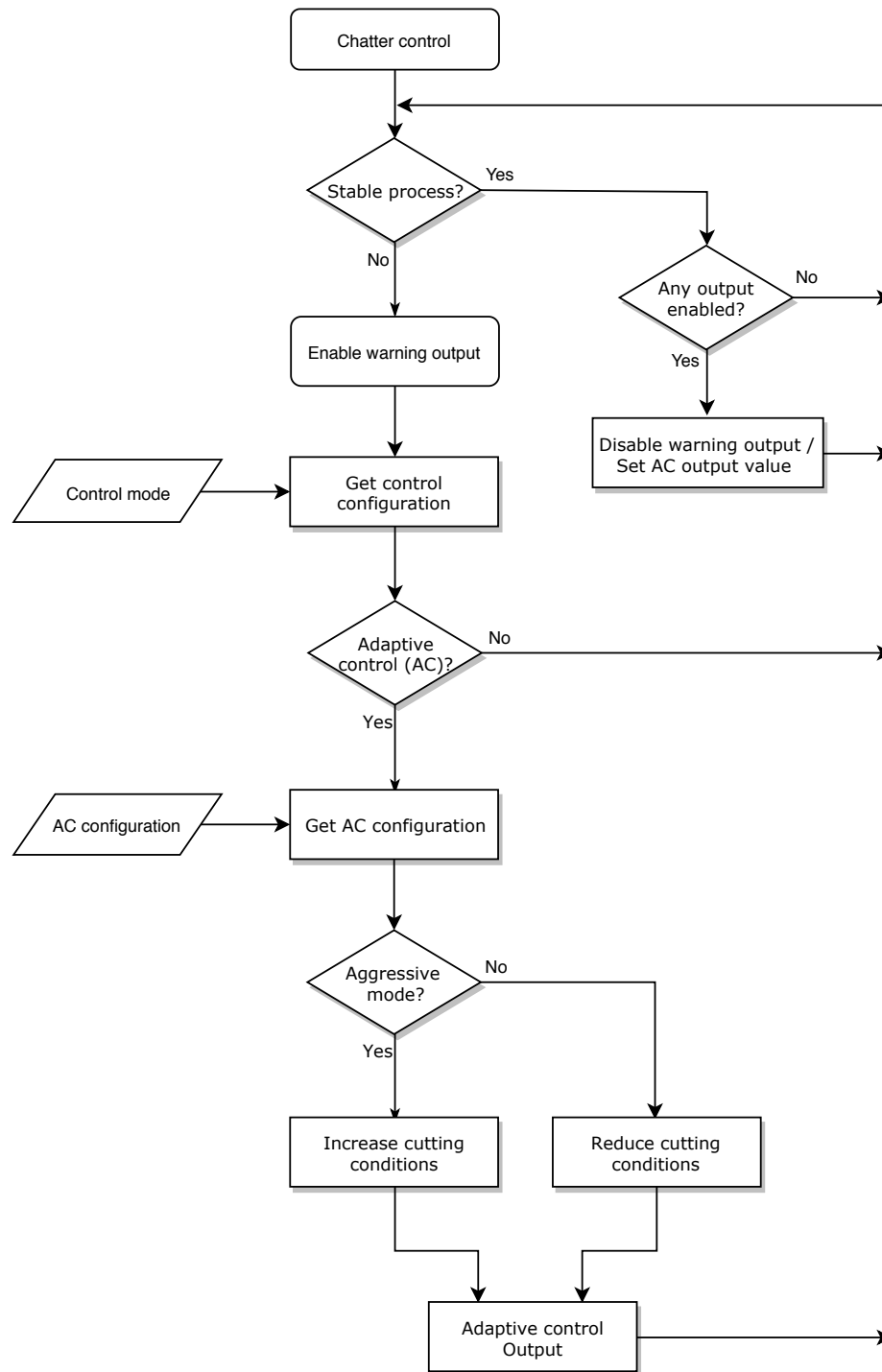


FIGURE 5.13: Control algorithm flow diagram.

Secondary functions

Other secondary functions were implemented in the cRIO.

- **Signal generator:** Excitation signal generation function for piezo-actuator prototype developed in Chapter 2 was implemented. The algorithm allows you to select a specific frequency or generate a frequency chirp in a selected range and duration. This function allows the automation of the system identification process.
- **Simulation Mode:** This mode generates a signal with a certain frequency that is used as input for the detection algorithm. Allows to activate the control loop and test its response.
- **System health:** Monitors the use of the resources of the monitoring system.
- **Data logging:** Saves current measurements when chatter is detected.
- **Error management:** Manages and reports errors that occur while running the monitoring system
- **Communications:** Data flow between FPGA, Real-Time OS and HMI

5.4.3 HMI

An HMI was developed in Labview to select operation mode and settings, data visualization and alarm notification. The HMI can be run on a integrated touch screen in the machine or on a remote computer. Figure 5.14 shows the HMI front panel which is composed of the following 10 sections:

1. **General Settings:** The main parameters of the monitoring system are defined here. The data rate, the monitoring system control mode and the sensitivity threshold of both axes are configured in this section. There are also two indicators related to the control mode and a stop button.
2. **Simulation Mode:** The simulation mode of the monitoring system is controlled from here. It is comprised of the activation button and a frequency selector.

3. Signal Generator Mode: The excitation input signal for piezo-actuator prototype is controlled from here. The initial frequency, the step time and the range of the chirp can be adjusted. The chirp can be performed with ascending or descending frequency. It also has an indicator that shows the frequency of excitation at every instant.
4. Chatter Monitoring: There are two buttons to select the axis to be used for monitoring. In addition, the frequencies detected above the threshold (chatter frequency and harmonics) are shown. There is also an indicator that is activated when the chatter occurs.
5. Adaptive Control: When the adaptive control mode is selected, the control response is configured here. The strategy of increasing or reducing the cutting conditions and the response time is defined. The range allowed to modify the cutting conditions by the control is defined also here.
6. Warning Mode: An indicator notifies the presence of chatter when warning mode is activated.
7. File Path: The path where the measurement signals are logged when chatter is detected is defined here.
8. System Health Monitor: This section shows the load status of the processor and the remaining available memory of the monitoring system.
9. Error Management: Errors that have occurred during the operation of the monitoring system are reported here.
10. Data Visualization: The spectra of the measured current signals of X and Z axis are shown here.

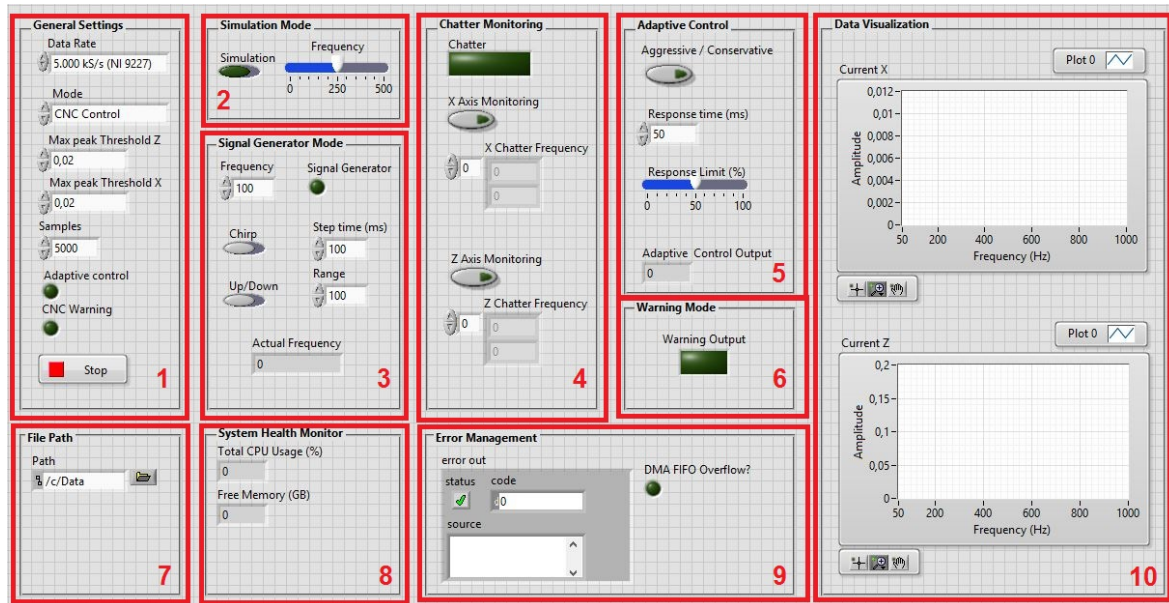


FIGURE 5.14: Monitoring system HMI.

5.5 Monitoring system experimental validation

5.5.1 Setup

The experimental setup used in the study is depicted in Figure 5.15. The tests were performed in a Danumerik CNC Lathe. A workpiece with a length diameter ratio of 8.5 was machined to emerge the chatter easily. The workpiece specifications are shown in Table 5.1. In order to detect chatter, the monitoring system developed was employed measuring one current phase of each axis.

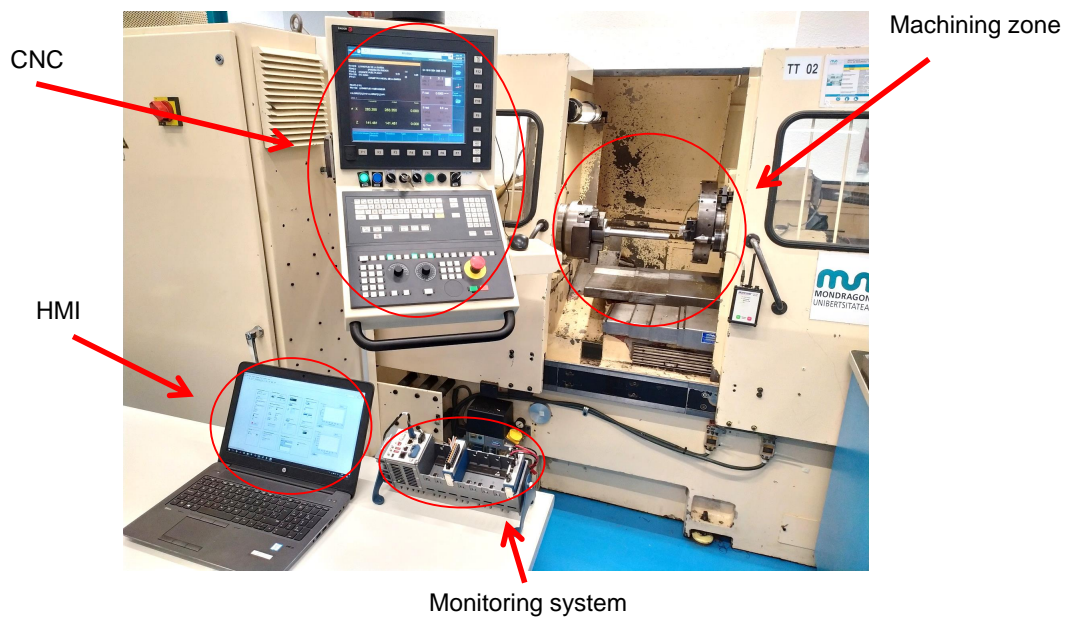


FIGURE 5.15: Monitoring system validation experimental setup.

TABLE 5.1: Workpiece specifications

Parameter	Values
Workpiece material	Steel C45
Material density (ρ)	7800 Kg/m ³
Workpiece length (l)	255 mm
Workpiece diameter (d)	30 mm

5.5.2 Experimental validation test

Before the machining test, the most dominant modes were identified by hammer impact test using a Bruel & Kjaer 8206-003 impact hammer and PCB356A16 triaxial accelerometer. As shown in Figure 5.16, two main modes of 259.6 Hz and 320.5 Hz were identified. So, during the machining, chatter is expected to occur around those frequencies.

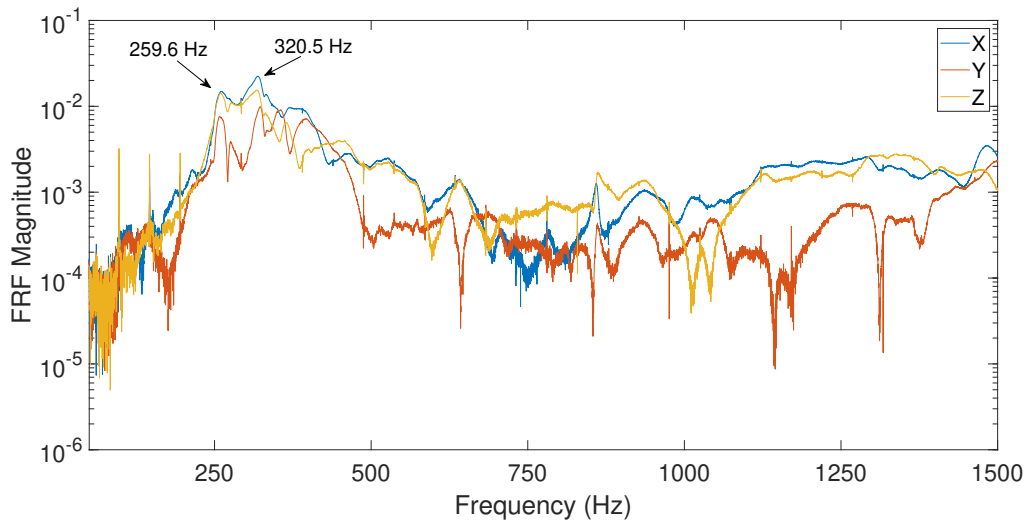


FIGURE 5.16: FRF of the experimental set up.

In order to validate the developed monitoring system machining tests were carried out under chatter conditions. Table 5.2 describes the monitoring system configuration in the test. During the test, due to the high length-diameter ratio, the workpiece began to vibrate right away.

TABLE 5.2: Monitoring system configuration

General Settings	Values
Data Rate	5120 S/s
Control mode	CNC Control
Max peak threshold X	0.02
Max peak threshold Z	0.02
FFT Samples	5120 S
Chatter Monitoring	Values
X axis monitoring	Activated
Z axis monitoring	Deactivated

Figure 5.17 shows the surface of the machined workpiece. It can be clearly seen that there are chatter marks in zones A (beginning), B (40mm) and C (100mm). Zone D (160mm), on the other hand, shows a good finishing.



FIGURE 5.17: Surface of the workpiece after the test.

In the following figures it can be seen that the monitoring system detects the instability of the process and identifies the vibration frequency during the machining. In the graphs shown in the HMI for the X axis currents, strong peaks with a magnitude above the threshold can be observed in zones A, B and C (see Figure 5.18, Figure 5.19 and Figure 5.20). Interestingly, the chatter frequency varies as the bar is machined because the system changes with the position of the tool (see Figure 5.18, Figure 5.19 and Figure 5.20). The closer the tool is to the spindle, the stiffer is the system. The natural frequency of the system increases little by little until it stops vibrating and the cutting process is stabilized (see Figure 5.21).

Figure 5.18 shows a screenshot of the monitoring system HMI in zone A, at the beginning of the machining test. It can be observed that the chatter indicator light is activated and the chatter frequency indicator shows a value of 283.97 Hz. In the graph of the current signal spectrum, a strong peak about 2.5 times larger than the maximum threshold is observed.

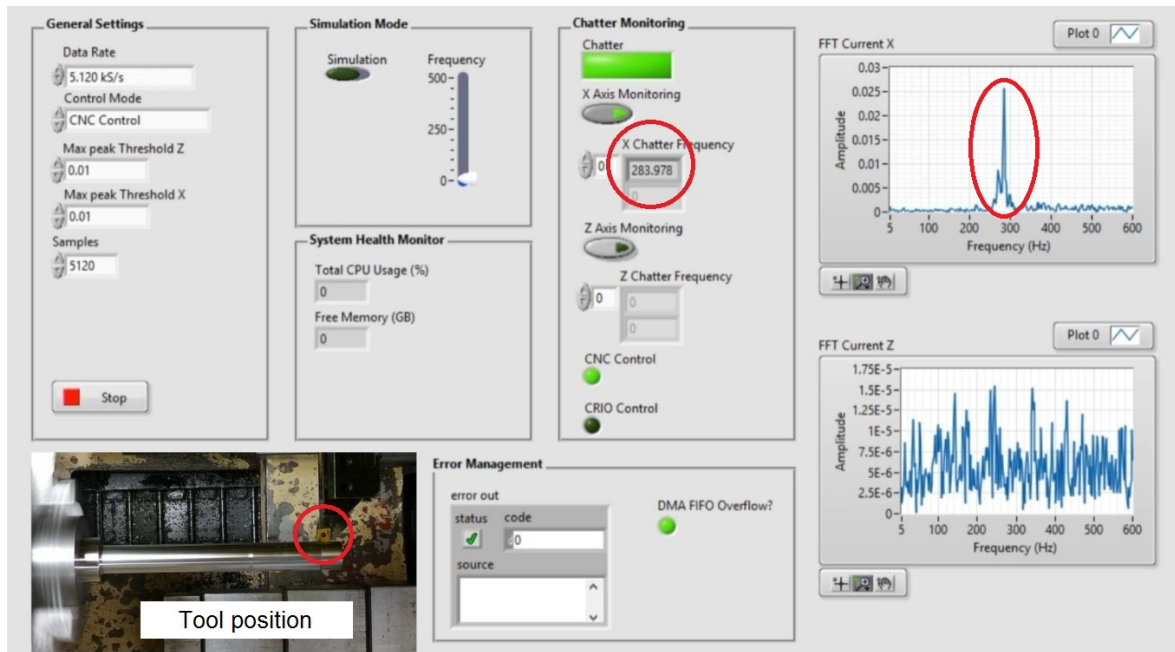


FIGURE 5.18: Monitoring system validation test. Area . Chatter frequency detected at 283.97 Hz, unstable machining.

Figure 5.19 shows another screenshot of the monitoring system HMI in zone B, after machining 40 mm. Here also the chatter indicator light is activated and the chatter frequency indicator shows a value slightly higher than the previous one, 286.84 Hz. In the graph of the current signal spectrum, a strong peak about two times larger than the maximum threshold is observed.

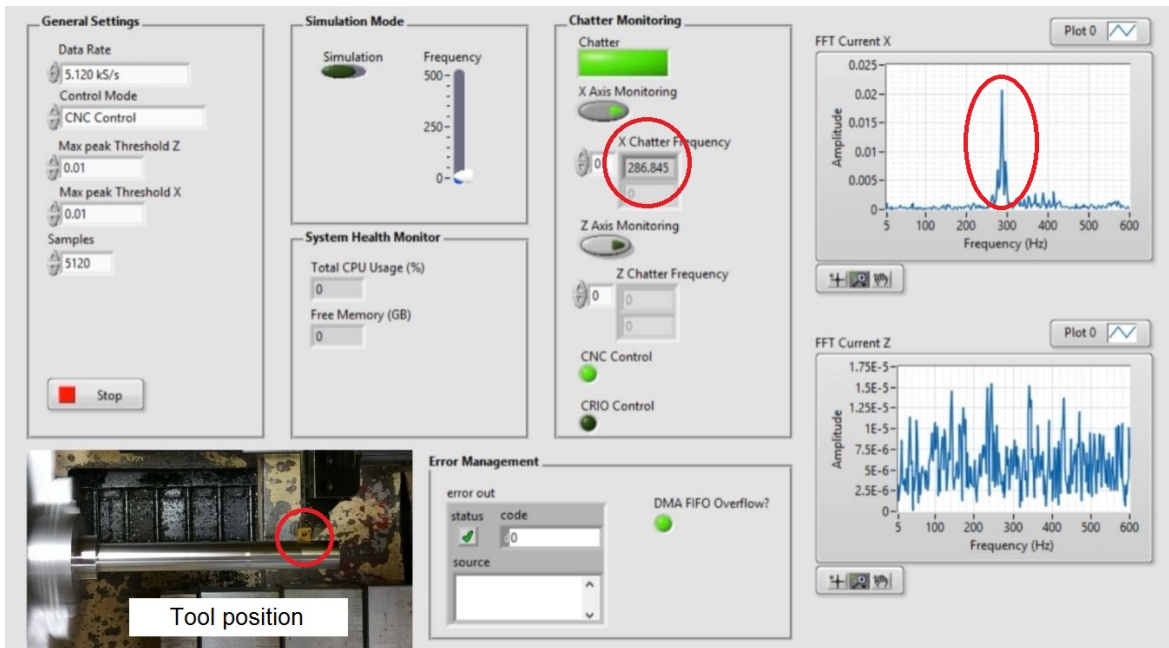


FIGURE 5.19: Monitoring system validation test. Area B. Chatter frequency detected at 286.84 Hz, unstable machining.

Figure 5.20 shows the monitoring system HMI in zone C, after machining 100 mm. It can be observed that the vibration frequency continues increasing slightly, showing 290.47 Hz. Interestingly, the spectrum of the current signal shows a stronger peak than the previous one, about eight times larger than the maximum threshold.

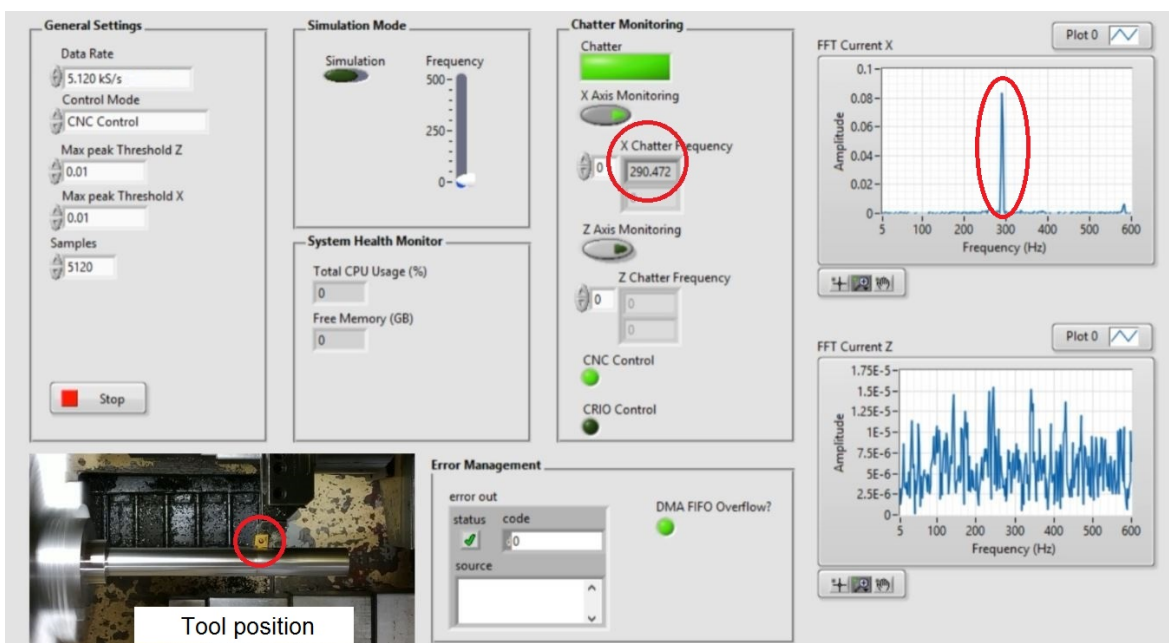


FIGURE 5.20: Monitoring system validation test. Area C. Chatter frequency detected at 290,47 Hz, unstable machining.

Figure 5.21 shows the monitoring system HMI in zone D, after machining 160 mm. No chatter is identified in this position. It can be observed that the chatter indicator light is deactivated and the chatter frequency indicator does not show any value. In the graph of the current signal spectrum, a peak about three times lower than the maximum threshold is observed.

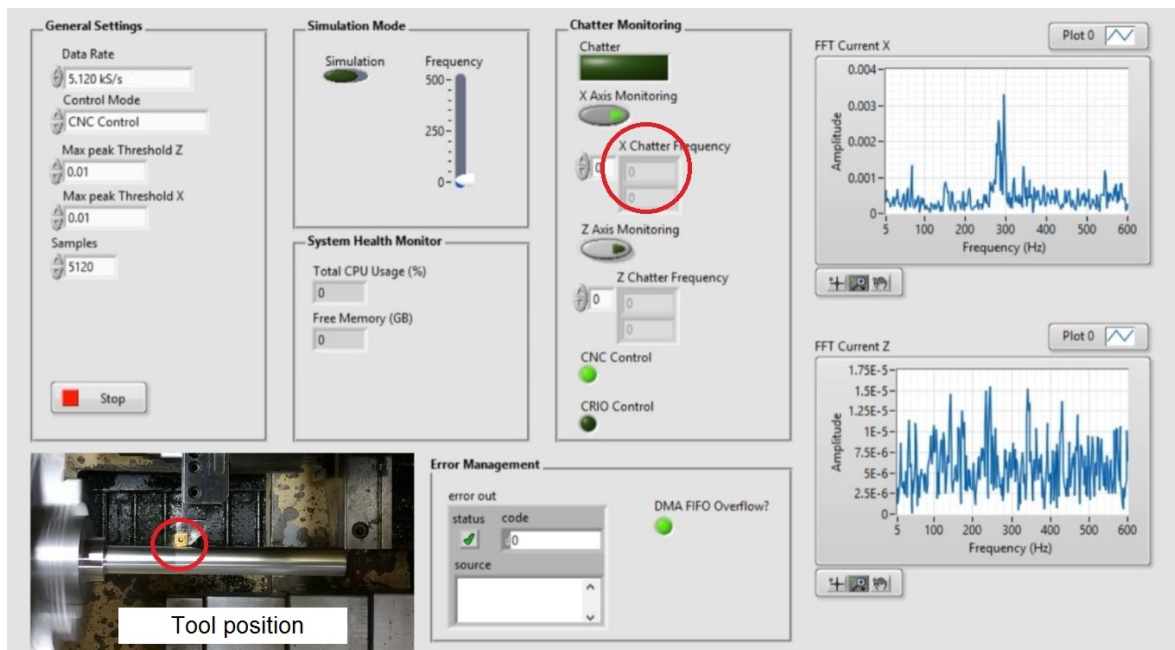


FIGURE 5.21: Monitoring system validation test. Area D. No chatter frequency detected, stable machining.

Results suggest that the developed system is able to monitor the machining process in real time successfully.

Chapter 6

Conclusions

6.1 Conclusions of the dissertation

The main conclusion of this dissertation is that slender workpieces cutting process stability can be (I) predicted by a model and (II) monitored based on available internal signals from the regulator.

These are other conclusions obtained in this dissertation:

- For a slender workpiece clamped to the spindle through a self-centering chuck with hard or soft jaws, classical boundaries are not enough. Natural frequencies are usually lower because (I) the clamping is not completely rigid and (II) the influence of the spindle. More realistic boundary conditions are identified including translational and rotational springs in the model. Results suggest that unknown system parameters can be identified employing a piezo actuator tool. It allows to excite the joint system by frequency sweeps.
- The modal coupling effect and the regenerative effect are two phenomena that coexist and can cause instability in the cutting process. According to the results, although the system is unstable at some intervals due to the modal coupling effect and it is stable for most of the cycle, the system tends to turn unstable due to wave regeneration. The vibration that arises from the modal coupling effect is amplified by the regenerative effect. The system stability can be determined by monitoring the evolution of the natural frequencies.

- LTP models best describe slender rotary systems such as slender workpieces or milling tools. It contributes to existing knowledge of chatter by providing a more detailed description of the workpiece and cutting process coupling phenomenon. Floquet theory can be employed to determine the dynamics of an LTP system. Results suggest that chatter-free cutting conditions can be accurately determined employing a LTP model. Considering both the rotation speed and the cutting speed a precise 3D SLD is obtained.
- Chatter can be detected using available internal signals from the regulator. Experimental tests suggest that current and encoder signals are the most suitable for chatter detection. Currents require less signal processing but are more sensitive to noise and disturbances. On the other hand, encoder signals require a more complex signal processing. According to the experimental tests, it can be concluded that chatter can be monitored by currents signals.

6.2 Suggestions for future research

A more detailed model that also contemplates the flexibility of the tool together with the workpiece could be developed. Although the workpiece is the least rigid component in slender parts turning, it would be interesting to take into account the influence of the tool.

Another future guideline is a in-depth study of the possibilities of exciter tools focused on (I) the dynamics of the actuator, (II) automation of the excitation and parameter identification process and (III) chatter suppression using the actuator tool.

The monitoring system should be tested on a lathe that supports SSV. The monitoring system performance should be evaluated by analysing the detection and stabilization times against different types of workpieces and scenarios. Presented control method should be validated experimentally.

The monitoring system should be implemented in other machining operations to analyse its viability in other processes such as milling. Several internal signals could

be combined to improve the robustness of the monitoring system and avoid false warnings. More advanced algorithms could be implemented to monitor the process and compare the robustness of algorithms.

Once the validation of the monitoring system has been carried out and the requirements for its implementation have been defined, the integration into the CNC should be carried out.

Chapter 7

Main contributions and publications

The main contribution in **Chapter 1** is the review of the state of the art about cutting process stability. Different strategies for chatter prediction, detection and suppression are discussed.

The main contribution in **Chapter 2** is a method for machining system identification. The method is patented and accepted for a conference:

- X. Badiola, P.J. Arrazola and A. Iturrospe. *Patent No ES2711000 B2*, 2019.
- X. Badiola, P.J. Arrazola, A. Iturrospe and J.M. Abete. Identificación de sistemas de mecanizado. In the *22th Congreso máquina herramienta, San Sebastian, Spain*, 2019.

The main contribution in **Chapter 3** is the mode coupling model for slender workpiece cutting process. This model has already been published in the following journal:

- X. Badiola, A. Iturrospe, J.M. Abete, and P.J. Arrazola. State–space analysis of mode-coupling workpiece chatter. *The International Journal of Advanced Manufacturing Technology*, 1-9, 2019.

The main contribution in **Chapter 4** is the LTP model for determine the chatter-free cutting conditions in slender workpiece machining. This research is under revision in the following journal:

- X. Badiola, A. Iturrospe, J.M. Abete, and P.J. Arrazola. Chatter stability prediction of slender workpieces with linear time periodic dynamics. *Mechanical Systems and Signal Processing*, 2019.

The main contribution in **Chapter 5** is a process monitoring system to detect chatter using available internal signals from the regulator.

Bibliography

- Ahmadi, K. and Y. Altintas (2014). "Identification of Machining Process Damping Using Output-Only Modal Analysis". In: *Journal of Manufacturing Science and Engineering* 136.5.
- Ahmadi, K. and F. Ismail (2011). "Analytical stability lobes including nonlinear process damping effect on machining chatter". In: *International Journal of Machine Tools and Manufacture* 51.4, pp. 296–308.
- (2012a). "Modeling chatter in peripheral milling using the Semi Discretization Method". In: *CIRP Journal of Manufacturing Science and Technology* 5.2, pp. 77–86.
 - (2012b). "Stability lobes in milling including process damping and utilizing Multi-Frequency and Semi-Discretization Methods". In: *International Journal of Machine Tools and Manufacture* 54-55, pp. 46–54.
- Al-Regib, Emad, Jun Ni, and Soo Hun Lee (2003). "Programming spindle speed variation for machine tool chatter suppression". In: *International Journal of Machine Tools and Manufacture* 43.12, pp. 1229–1240.
- Albertelli, P. et al. (2015). "Model-based broadband estimation of cutting forces and tool vibration in milling through in-process indirect multiple-sensors measurements". In: *The International Journal of Advanced Manufacturing Technology*.
- Altintas, Y. and M. Weck (2004). "Chatter Stability of Metal Cutting and Grinding". In: *CIRP Annals - Manufacturing Technology* 53.2, pp. 619–642.
- Altintas, Y. et al. (2008a). "Chatter stability of milling in frequency and discrete time domain". In: *CIRP Journal of Manufacturing Science and Technology* 1.1, pp. 35–44.
- Altintas, Y., M. Eynian, and H. Onozuka (2008b). "Identification of dynamic cutting force coefficients and chatter stability with process damping". In: *CIRP Annals - Manufacturing Technology* 57.1, pp. 371–374.
- Altintas, Yusuf (2012). *Manufacturing Automation Futures*. Second Edi.

- Artis (2019a). *Artis Marposs*.
- (2019b). *CTM Tool and Process Monitoring*.
- Aslan, Deniz and Yusuf Altintas (2018). “On-line chatter detection in milling using drive motor current commands extracted from CNC”. In: *International Journal of Machine Tools and Manufacture* 132, pp. 64–80.
- Balaji, A.K. et al. (2006). “Performance-Based Predictive Models and Optimization Methods for Turning Operations and Applications : Part 1 — Tool Wear / Tool Life in Turning with”. In: *Journal of Manufacturing Processes* 8.2, pp. 54–66.
- Bayly, P. V. et al. (2003). “Stability of Interrupted Cutting by Temporal Finite Element Analysis”. In: *Journal of Manufacturing Science and Engineering* 125.2, p. 220.
- Benardos, P. G., S. Mosialos, and G. C. Vosniakos (2006). “Prediction of workpiece elastic deflections under cutting forces in turning”. In: *Robotics and Computer-Integrated Manufacturing* 22.5-6, pp. 505–514.
- Bhuiyan, M.S.H., I.A. Choudhury, and Y. Nukman (2012). “An innovative approach to monitor the chip formation effect on tool state using acoustic emission in turning”. In: *International Journal of Machine Tools and Manufacture* 58, pp. 19–28.
- Blevins, Robert D (2015). *Formulas for dynamics, acoustics and vibration*. John Wiley & Sons.
- Budak, E. and Y. Altintas (1998). “Analytical Prediction of Chatter Stability in Milling—Part I: General Formulation”. In: *Journal of Dynamic Systems, Measurement, and Control* 120.1, p. 22.
- Budak, E. and E. Ozlu (2007). “Analytical modeling of chatter stability in turning and boring operations: A multi-dimensional approach”. In: *CIRP Annals - Manufacturing Technology* 56.1, pp. 401–404.
- Budak, E. and L. T. Tunc (2010). “Identification and modeling of process damping in turning and milling using a new approach”. In: *CIRP Annals - Manufacturing Technology* 59.1, pp. 403–408.
- Budak, Erhan et al. (2012). “Prediction of workpiece dynamics and its effects on chatter stability in milling”. In: *CIRP Annals - Manufacturing Technology* 61, pp. 339–342.

- Butcher, Eric A. et al. (2004). "Stability of linear time-periodic delay-differential equations via Chebyshev polynomials". In: *International Journal for Numerical Methods in Engineering* 59.7, pp. 895–922.
- Byrne, G. et al. (1995). "Tool Condition Monitoring (TCM) - The Status of Research and Industrial Application". In: *CIRP Annals - Manufacturing Technology* 44.2, pp. 541–567.
- Caliskan, Hakan, Zekai Murat Kilic, and Yusuf Altintas (2018). "On-Line Energy Based Milling Chatter Detection". In: *Journal of Manufacturing Science and Engineering* 140.November, pp. 1–12.
- Cao, Hongrui et al. (2017). "Chatter detection in milling process based on synchrosqueezing transform of sound signals". In: *International Journal of Advanced Manufacturing Technology* 89.9-12, pp. 2747–2755.
- Cen, Lejun et al. (2018). "A Method for Mode Coupling Chatter Detection and Suppression in Robotic Milling". In: *Journal of Manufacturing Science and Engineering* 140.8, p. 081015.
- Chandiramani, N. K. and T. Pothala (2006). "Dynamics of 2-dof regenerative chatter during turning". In: *Journal of Sound and Vibration* 290.1-2, pp. 448–464.
- Chen, C. K. and Y. M. Tsao (2006a). "A stability analysis of regenerative chatter in turning process without using tailstock". In: *International Journal of Advanced Manufacturing Technology* 29.7-8, pp. 648–654.
- (2006b). "A stability analysis of turning a tailstock supported flexible work-piece". In: *International Journal of Machine Tools and Manufacture* 46.1, pp. 18–25.
- Chen, Min and Carl R Knospe (2007). "Control approaches to the suppression of machining chatter using active magnetic bearings". In: *IEEE Transactions on control systems technology* 15.2, pp. 220–232.
- Chiou, Chu Hsiang, Min Sung Hong, and Kornel F. Ehmann (2003). "The feasibility of eigenstructure assignment for machining chatter control". In: *International Journal of Machine Tools and Manufacture* 43.15, pp. 1603–1620.
- Chiou, Richard Y. and Steven Y. Liang (1998). "Chatter stability of a slender cutting tool in turning with tool wear effect". In: *International Journal of Machine Tools and Manufacture* 38.4, pp. 315–327.

- Chiou, Richard Y. and Steven Y. Liang (2000). "Analysis of acoustic emission in chatter vibration with tool wear effect in turning". In: *International Journal of Machine Tools and Manufacture* 40.7, pp. 927–941.
- Clancy, Bason E. and Yung C. Shin (2002). "A comprehensive chatter prediction model for face turning operation including tool wear effect". In: *International Journal of Machine Tools and Manufacture* 42.9, pp. 1035–1044.
- Dassanayake, Achala V. and C. Steve Suh (2008). "On nonlinear cutting response and tool chatter in turning operation". In: *Communications in Nonlinear Science and Numerical Simulation* 13.5, pp. 979–1001.
- Dimla, D.E and P.M Lister (2000). "On-line metal cutting tool condition monitoring." In: *International Journal of Machine Tools and Manufacture* 40.5, pp. 769–781.
- Ding, Ye et al. (2010). "A full-discretization method for prediction of milling stability". In: *International Journal of Machine Tools and Manufacture* 50, pp. 502–509. arXiv: /dx.doi.org/10.1016/j.ijmachtools.2010.01.003 [http:].
- Dombovari, Zoltan et al. (2011). "On the global dynamics of chatter in the orthogonal cutting model". In: *International Journal of Non-Linear Mechanics* 46.1, pp. 330–338.
- Elbestawi, M. a. et al. (1994). "Modelling Machining Dynamics Including Damping in the Tool-Workpiece Interface". In: *Journal of Engineering for Industry* 116.4, p. 435.
- Eynian, M. and Y. Altintas (2009). "Chatter stability of general turning operations with process damping". In: *Journal of Manufacturing Science and Engineering* 131.2.
- Floquet, G. (1883). "Sur les Equations Differentielles Lineaires a Coefficients Periodiques". In: *Annales scientifiques de E.N.S.* 12, pp. 47–88.
- Fofana, M. S., K. C. Ee, and I. S. Jawahir (2003). "Machining stability in turning operation when cutting with a progressively worn tool insert". In: *Wear* 255.7-12, pp. 1395–1403.
- Frumusanu, Gabriel R. et al. (2013). "Development of a stability intelligent control system for turning". In: *International Journal of Advanced Manufacturing Technology* 64.5-8, pp. 643–657.
- Gallina, P. and A. Trevisani (2003). "On the stabilizing and destabilizing effects of damping in wood cutting machines". In: *International Journal of Machine Tools and Manufacture* 43.9, pp. 955–964.

- Ganguli, A., A. Deraemaeker, and A. Preumont (2007). "Regenerative chatter reduction by active damping control". In: *Journal of Sound and Vibration* 300.3-5, pp. 847–862.
- Ganguli, Abhijit et al. (2005). "Active damping of chatter in machine tools - Demonstration with a " Hardware in the Loop " simulator". In: *Journal of Systems and Control Engineering* 219.2, pp. 359–369.
- Gasparetto, A. (2001). "Eigenvalue Analysis of Mode-Coupling Chatter for Machine-Tool Stabilization". In: *Journal of Vibration and Control* 7.2, pp. 181–197.
- Guckenheimer, John and Philip Holmes (1983). "Local bifurcations". In: *Nonlinear oscillations, dynamical systems, and bifurcations of vector fields*. Springer, pp. 117–165.
- Guo, Qiang et al. (2014). "Prediction of stability limit for multi-regenerative chatter in high performance milling". In: *International Journal of Dynamics and Control* 2, pp. 35–45.
- Han, X. et al. (2012). "Self-excited vibration of workpieces in a turning process". In: *Proceedings of the Institution of Mechanical Engineers, Part C: Journal of Mechanical Engineering Science* 226.8, pp. 1958–1970.
- Hanna, N H and S a Tobias (1974). "A Theory of Nonlinear Regenerative Chatter". In: *Journal of Manufacturing Science and Engineering* 96.1, pp. 247–255.
- Heyns, P S (2007). "Tool condition monitoring using vibration measurements a review". In: *Insight-Non-Destructive Testing and Condition Monitoring* 49.8, pp. 447–450.
- Hynynen, Katja M. et al. (2014). "Chatter Detection in Turning Processes Using Coherence of Acceleration and Audio Signals". In: *Journal of Manufacturing Science and Engineering* 136.August 2014, p. 044503.
- Inspurger, T and G Stepen (2011). *Semi-Discretization for Time-Delay Systems: Stability and Engineering Applications*. Vol. 178. Springer-Verlag New York.
- Inspurger, T. et al. (2003). "Stability of up-milling and down-milling, Part 1: Alternative analytical methods". In: *International Journal of Machine Tools and Manufacture* 43.1, pp. 25–34.
- Inspurger, Tamás and Gábor Stépán (2002). "Semi-discretization method for delayed systems". In: *International Journal for Numerical Methods in Engineering* 55.5, pp. 503–518. arXiv: 1411.2664.

- Iturrospe, Aitzol, Vicente Atxa, and Jose Manuel Abete (2007). "State-space analysis of mode-coupling in orthogonal metal cutting under wave regeneration". In: *International Journal of Machine Tools and Manufacture* 47.10, pp. 1583–1592.
- Iturrospe, Aitzol et al. (2012). "Health monitoring strategy for electromechanical actuator systems and components. Screw backlash and fatigue estimation". In: Jalali, Ali a, Craig S Sims, and Parviz Famouri (2006). *Nonlinear observers and applications*, p. 199.
- Ji, Yongjian et al. (2018). "Milling stability prediction with simultaneously considering the multiple factors coupling effects — regenerative effect , mode coupling , and process damping". In: *The International Journal of Advanced Manufacturing Technology*.
- Jin, Xiaoliang and Yusuf Altintas (2013). "Chatter Stability Model of Micro-Milling With Process Damping". In: *Journal of Manufacturing Science and Engineering* 135.3, p. 031011.
- Jun, Martin B. et al. (2002). "Evaluation of a spindle-based force sensor for monitoring and fault diagnosis of machining operations". In: *International Journal of Machine Tools and Manufacture* 42.6, pp. 741–751.
- Kakinuma, Y. and T. Kamigochi (2012). "External sensor-less tool contact detection by cutting force observer". In: *Procedia CIRP* 2.1, pp. 44–48.
- Kakinuma, Yasuhiro et al. (2014). "Active chatter suppression in turning by band-limited force control". In: *CIRP Annals - Manufacturing Technology* 63.1, pp. 365–368.
- Kebdani, S et al. (2008). "Analysis of chatter stability in facing". In: *Journal of Applied Sciences* 8.11, pp. 2050–2058.
- Kurata, Yusuke et al. (2010). "Chatter Stability in Turning and Milling with in Process Identified Process Damping". In: *Journal of Advanced Mechanical Design, Systems, and Manufacturing* 4.6, pp. 1107–1118.
- Kurihara, Daisuke, Yasuhiro Kakinuma, and Seiichiro Katsura (2009). "Sensorless Cutting Force Control using Parallel Disturbance Observer". In: *Proceedings of International Conference on Leading Edge Manufacturing in 21st century : LEM21 2009.5*, pp. 191–196.

- Lamraoui, M. et al. (2014). "Indicators for monitoring chatter in milling based on instantaneous angular speeds". In: *Mechanical Systems and Signal Processing* 44.1-2, pp. 72–85.
- Lee, B. Y., Y. S. Tarn, and S. C. Ma (1995). "Modeling of the process damping force in chatter vibration". In: *International Journal of Machine Tools and Manufacture* 35.7, pp. 951–962.
- Li, Zhongyun, Yuwen Sun, and Dongming Guo (2017). "Chatter prediction utilizing stability lobes with process damping in finish milling of titanium alloy thin-walled workpiece". In: *International Journal of Advanced Manufacturing Technology* 89.9-12, pp. 2663–2674.
- Liang, Steven Y, Rogelio L Hecker, and Robert G Landers (2004). "Machining process monitoring and control: The state-of-the-art". In: *Journal of Manufacturing Science and Engineering, Transactions of the ASME* 126, p. 297.
- Lin, S. C. and M. R. Hu (1992). "Low vibration control system in turning". In: *International Journal of Machine Tools and Manufacture* 32.5, pp. 629–640.
- Liu, Hongqi et al. (2011). "On-line chatter detection using servo motor current signal in turning". In: *Science China Technological Sciences* 54.12, pp. 3119–3129.
- Louarroudi, E. et al. (2012). "Frequency domain, parametric estimation of the evolution of the time-varying dynamics of periodically time-varying systems from noisy input-output observations". In: *Mechanical Systems and Signal Processing* 47.1-2, pp. 151–174.
- Lu, Chen and Tieying Li (2013). "Online Milling Tool Wear Monitoring Based on Continuous". In: pp. 65–69.
- Lu, Kaibo et al. (2018). "Model-based chatter stability prediction and detection for the turning of a flexible workpiece". In: *Mechanical Systems and Signal Processing* 100, pp. 814–826.
- Lv, Binglin, Wanyou Li, and Huajiang Ouyang (2015). "Moving Force-Induced Vibration of a Rotating Beam with Elastic Boundary Conditions". In: *International Journal of Structural Stability and Dynamics* 15.01, p. 1450035.
- Magnus, W and S Winkler (1976). *Hills Equation. Tracts Pure Appl Math.*
- Merritt, HE (1965). "Theory of Self-Excited Machine-Tool Chatter". In: *Journal of engineering for industry* 87, pp. 447–454.

- Minis, I and R Yanushevsky (1993). "A new theoretical approach for the prediction of machine tool chatter in milling". In: *Journal of Engineering for Industry* 115.1, pp. 1–8.
- Mohammadi, Y. and K. Ahmadi (2019). "Frequency domain analysis of regenerative chatter in machine tools with Linear Time Periodic dynamics". In: *Mechanical Systems and Signal Processing* 120, pp. 378–391.
- Montronix (2019a). *Montronix Monitoring Solutions*.
- (2019b). *PulseNG Kit*.
 - (2019c). *Spectra Monitoring System*.
- Munoa, Jokin et al. (2015). "Active suppression of structural chatter vibrations using machine drives and accelerometers". In: *CIRP Annals - Manufacturing Technology*, pp. 1–4.
- Okuma (2015). *Machining Navi*.
- (2019). *Okuma Company*.
- Omatic (2019a). *Adaptive Control & Vibration Monitoring*.
- (2019b). *Condition Monitoring For Predictive Maintenance*.
 - (2019c). *Omatic Company*.
- Ouyang, Huajiang and Minjie Wang (2007). "Dynamics of a Rotating Shaft Subject to a Three-Directional Moving Load". In: *Journal of Vibration and Acoustics* 129.3, p. 386.
- Ozlu, Emre and Erhan Budak (2007). "Comparison of one-dimensional and multi-dimensional models in stability analysis of turning operations". In: *International Journal of Machine Tools and Manufacture* 47.12-13, pp. 1875–1883.
- Pan, Jingchuan and Chun-Yi Su (2001). "Chatter suppression with adaptive control in turning metal via application of piezoactuator". In: *Decision and Control, 2001. Proceedings of the 40th IEEE Conference on*. Vol. 3. IEEE, pp. 2436–2441.
- Pan, Zengxi et al. (2006). "Chatter analysis of robotic machining process". In: *Journal of Materials Processing Technology* 173.3, pp. 301–309.
- Quintana, Guillem and Joaquim Ciurana (2011). "Chatter in machining processes: A review". In: *International Journal of Machine Tools and Manufacture* 51.5, pp. 363–376.

- Rivin, Eugene I and Hongling Kang (1989). "Improvement of machining conditions for slender parts by tuned dynamic stiffness of tool". In: *International Journal of Machine Tools and Manufacture* 29.3, pp. 361–376.
- Schmitz, Tony L and Kevin S Smith (2008). *Machining Dynamics - Frequency Response to Improved Productivity*. Springer. arXiv: arXiv:1011.1669v3.
- Sekar, M. et al. (2009). "Stability analysis of turning process with tailstock-supported workpiece". In: *International Journal of Advanced Manufacturing Technology* 43.9-10, pp. 862–871.
- Shinno, H., H. Hashizume, and H. Yoshloka (2003). "Sensor-less Monitoring of Cutting Force during Ultraprecision Machining". In: *CIRP Annals - Manufacturing Technology* 52.1, pp. 303–306.
- Siddhpura, A. and R. Paurobally (2013). "A review of flank wear prediction methods for tool condition monitoring in a turning process". In: *International Journal of Advanced Manufacturing Technology* 65.1-4, pp. 371–393.
- Siddhpura, M. and R. Paurobally (2012). "A review of chatter vibration research in turning". In: *International Journal of Machine Tools and Manufacture* 61, pp. 27–47.
- Siddhpura, M., A. Siddhpura, and R. Paurobally (2017). "Chatter stability prediction for a flexible tool-workpiece system in a turning process". In: *International Journal of Advanced Manufacturing Technology* 92.1-4, pp. 881–896.
- Sisson, T.R. (1969). "An Explanation of Low-Speed Chatter Effects". In: *Journal Of Engineering For Industry* November, pp. 951–958.
- Soliman, E. and F. Ismail (1997). "Chatter detection by monitoring spindle drive current". In: *International Journal of Advanced Manufacturing Technology* 13.1, pp. 27–34.
- Suzuki, Norikazu et al. (2010). "Effect of Cross Transfer Function on Chatter Stability in Plunge Cutting". In: *Journal of Advanced Mechanical Design, Systems, and Manufacturing* 4.5, pp. 883–891.
- Taylor, Fred W (1907). "The art of cutting metals". In: *Scientific American* 63.312, pp. 25942–25944.
- Thusty, J (1986). "Dynamics of high-speed milling". In: *Journal of Engineering for industry* 108.2, pp. 59–67.
- Thusty, J. (2000). *Manufacturing Processes and Equipment*. Prentice Hall, p. 928.

- Thusty, J. and G. C. Andrews (1983). "A Critical Review of Sensors for Unmanned Machining". In: *CIRP Annals - Manufacturing Technology* 32.2, pp. 563–572.
- Thusty, J and M Polacek (1963). "The stability of machine tools against self-excited vibrations in machining". In: *International research in production engineering* 1, pp. 465–474.
- Thusty, Jiri and Franz Koenigsberger (2016). *Machine tool structures*. Elsevier.
- Tobias, SA (1961). "Machine tool vibration research". In: *International Journal of Machine Tool Design and Research* 1, pp. 1–14.
- Tobias, S.A. and W. Fishwick (1958). "The chatter of lathe tools under orthogonal cutting conditions". In: *Transactions of ASME* 80 1079–1088.
- Tunc, L. T. and E. Budak (2012). "Effect of cutting conditions and tool geometry on process damping in machining". In: *International Journal of Machine Tools and Manufacture* 57, pp. 10–19.
- Tyler, Christopher T. and Tony L. Schmitz (2013). "Analytical process damping stability prediction". In: *Journal of Manufacturing Processes* 15.1, pp. 121–126.
- Urbikain, G, D Olvera, and L N Lopez De Lacalle (2015). "Stability and vibrational behaviour in turning processes with low rotational speeds". In:
- Vela-Martinez, Luciano et al. (2008). "Analysis of compliance between the cutting tool and the workpiece on the stability of a turning process". In: *International Journal of Machine Tools and Manufacture* 48.9, pp. 1054–1062.
- Wan, Min et al. (2015). "Study on the construction mechanism of stability lobes in milling process with multiple modes". In: *International Journal of Advanced Manufacturing Technology* 79.1-4, pp. 589–603.
- Wang, Min et al. (2010). "Design and implementation of nonlinear TMD for chatter suppression: An application in turning processes". In: *International Journal of Machine Tools and Manufacture* 50.5, pp. 474–479.
- Wiercigroch, M. and E. Budak (2001). "Sources of nonlinearities, chatter generation and suppression in metal cutting". In: *Philosophical Transactions of the Royal Society A: Mathematical, Physical and Engineering Sciences* 359.1781, pp. 663–693.
- Wu, D. W. (1989). "A New Approach of Formulating the Transfer Function for Dynamic Cutting Processes". In: *Journal of Engineering for Industry* 111.1, p. 37.

- Wu, Dan, Ken Chen, and Xiankui Wang (2009). "An investigation of practical application of variable spindle speed machining to noncircular turning process". In: *International Journal of Advanced Manufacturing Technology* 44.11-12, pp. 1094–1105.
- Xiao, M. et al. (2002). "Analysis of chatter suppression in vibration cutting". In: *International Journal of Machine Tools and Manufacture* 42.15, pp. 1677–1685.
- Yang, Y., J. Muñoa, and Y. Altintas (2010). "Optimization of multiple tuned mass dampers to suppress machine tool chatter". In: *International Journal of Machine Tools and Manufacture* 50.9, pp. 834–842.
- Yaser, Mohammadi, Tunc Lutfi Taner, and Budak Erhan (2017). "Investigation of Process Damping Effect for Multi-mode Milling Systems". In: *Procedia CIRP* 58, pp. 198–203.
- Yue, Caixu, Xianli Liu, and Steven Y. Liang (2017). "A model for predicting chatter stability considering contact characteristic between milling cutter and workpiece". In: *International Journal of Advanced Manufacturing Technology* 88.5-8, pp. 2345–2354.
- Zadeh, Lotfi A. (1951). "On Stability of Linear Varying-Parameter Systems". In: *Journal of Applied Physics* 22.6, pp. 782–786.
- Zhang, Xiao Jian et al. (2012). "Milling stability analysis with simultaneously considering the structural mode coupling effect and regenerative effect". In: *International Journal of Machine Tools and Manufacture* 53.1, pp. 127–140.
- Zhang, Zhao et al. (2016). "Chatter detection in milling process based on the energy entropy of VMD and WPD". In: *International Journal of Machine Tools and Manufacture* 108, pp. 106–112.
- Zhu, Kunpeng P., Yoke San Wong, and Geok Soon Hong (2009). "Wavelet analysis of sensor signals for tool condition monitoring: A review and some new results". In: *International Journal of Machine Tools and Manufacture* 49, pp. 537–553.